POLITECNICO DI MILANO

School of Industrial and Information Engineering

Master of Science in Materials Engineering and Nanotechnology

---

M.Sc. Thesis

EVALUATION OF TEST METHODOLOGIES AND SELF-CLEANING PERFORMANCES OF TiO_2 CONTAINING CONSTRUCTION MATERIALS

Supervisor: Dr. Maria Vittoria Diamanti

Co-supervisor: Dr. Riccardo Paolini

Aysegul Basak Aslan

ID: 780068

Academic Year 2013-2014

Abstract

The M.Sc. thesis work here presented is dedicated to the study of the surface properties of photocatalytic cementitious materials, specially focusing on mortars modified through the addition of titanium dioxide (TiO_2) an on the definition of a characterization method to evaluate their photocatalytic and self-cleaning performances. This evaluation has been carried out by examining the TiO_2-assisted photodegradation of organic compounds, the variation of hydrophilicity through absorption-evaporation tests, and the real life behavior of the materials through a long-lasting exposure test. In the latter, a correlation between the atmospheric parameters, such as rain, sunlight radiation and pollution, and self-cleaning attitude was sought.

Before discussing the experimental results, a general overview about fundamentals and applications of TiO_2 based photocatalysis and self-cleaning in the field of construction and building materials is presented.

Different setups of degradation of rhodamine B, an organic dye, were tested to develop a characterization method aimed at assessing the self-cleaning performances of materials containing TiO_2. Experimental data on the onset of superhydrophilic performances of TiO_2-containing commercial mortars are discussed in relation to absorption-evaporation trends of the surface. Finally, the actual self-cleaning behavior of the mortars was evaluated through a two-year exposure by collecting color variations of the mortars, as indicative of surface soiling; environmental parameters were collected too, and their trend was compared with color variations in order to identify a possible influence of atmospheric agents on the self-cleaning efficiency.

Keywords: TiO_2; photocatalysis; self-cleaning

Abstract

Il lavoro di tesi magistrale qui presentato è dedicato allo studio delle proprietà superficiali di materiali cementizi fotocatalitici, e si concentra in particolare su malte modificate attraverso l'aggiunta di biossido di titanio (TiO_2) e sulla definizione di un metodo di caratterizzazione per valutarne le prestazioni fotocatalitiche e di autopulizia. Questa valutazione è stata effettuata esaminando la fotodegradazione di composti organici, la variazione di idrofilia in prove di assorbimento-evaporazione, e il comportamento reale dei materiali in un test di esposizione di lunga durata. In quest'ultimo, si è cercata una correlazione tra i parametri atmosferici, quali pioggia, radiazione solare e inquinamento, e l'instaurarsi di meccanismi di autopulizia.

Prima di discutere i risultati sperimentali, la tesi propone una panoramica generale sui principi fondamentali e sulle applicazioni della fotocatalisi e dell'autopulizia indotte dal TiO_2 nel campo dei materiali da costruzione.

Diversi setup di degradazione della rodamina B, un colorante organico, sono stati testati per sviluppare un metodo di valutazione delle prestazioni di autopulizia di materiali contenenti TiO_2. I dati sperimentali relativi alle prestazioni di superidrofilia di malte commerciali contenenti TiO_2 sono stati discussi in relazione all'assorbimento ed evaporazione d'acqua da parte della superficie. Infine, l'effettiva autopulizia delle malte è stata studiata per mezzo di un'esposizione di due anni, in cui la variazione di colore delle malte è stata presa a misura dello sporcamento della superficie; sono stati raccolti anche i parametri ambientali, il cui trend è stato raffrontato con le variazioni di colore al fine di identificare la possibile influenza degli agenti atmosferici sull'efficienza di autopulizia.

Parole chiave: TiO_2; fotocatalisi; autopulizia

TABLE OF CONTENTS

LIST OF FIGURES

LIST OF TABLES

Introduction

Since Fujishima and Honda discovered the phenomenon of the photocatalytic splitting of water on a titanium dioxide (TiO_2) electrode under ultraviolet light in 1972[1], TiO_2 became one of the mostly used innovative photocatalytic material. Over the years, extensive research has been performed on fundamentals of photocatalytic oxidation reaction mechanism and the applications of TiO_2 as photocatalytic material in various fields.

The application of building materials modified with TiO_2 photocatalyst began towards the end of the 1980s and is constantly growing. The major applications of TiO_2 based photocatalytic building materials consist of cement, mortars, exterior tiles, paving blocks, glass, paints, finishing coatings, road-blocks and concrete pavements[2-4], and the effects that can be achieved are environmental purification, self-cleaning and self-disinfecting surfaces.

The mechanism only requires photonic energy to activate the reaction, which can take place even in weak solar irradiation; moreover TiO_2 is a cheap, nontoxic and chemically stable semiconductor photocatalyst, which has been also used as a white pigment with traditional construction materials[5]. Therefore using TiO_2 modified construction and building materials, especially cementitious materials due to their extensive range of application in the construction field, can give great

advantages in terms of decreasing energy consumption, improving environmental conditions and urban surfaces.

The two fundamental photochemical phenomena that occur simultaneously on the surface of a photocatalyst under ultraviolet irradiation are the foundation of its applications[6]: one is the photoinduced redox reaction of both inorganic polluting substances, such as nitrogen oxides in gas and liquid phase, and organic ones, such as volatile organic compounds (VOCs) emitted by exhausts, combustion gases, paints, cigarette smoke and many other sources, absorbed or deposited on photoactive surfaces[7]; and the other is the photoinduced superhydrophilicity.

In the construction field, the synergy of these two photoinduced properties (photocatalysis and superhydrophilicity) and the advantage of solar light as the natural light source with humidity and/or rainwater create self-cleaning surfaces, thus providing a unique way to retard the natural surface ageing, as a result reducing the need for cleaning maintenance.

The work here presented focuses on the self-cleaning effect of cementitious surfaces, especially mortars modified through the addition of TiO_2 nanoparticles through characterization tests. Different experimental setups were applied in laboratory testing, depending on the material and property to be tested. The laboratory tests performed are: rhodamine B test, which is the impregnation of the organic dye and evaluation the surface ability to discolor the dye; water capillary absorption-evaporation tests to evaluate possible changes of wettability of the treated surface. An extended exposure test was also performed to establish a relationship between the self-cleaning effect and environmental variables: that was achieved by monitoring the evaluation of chromatic changes of the samples that were subjected to the external environment.

Chapter 1

TiO_2 as Semiconductor Photocatalyst

1.1 Structure and Properties of TiO_2

The main crystalline structures of TiO_2 are rutile, brookite and anatase. Rutile is employed mostly as pigment. Brookite is more difficult to produce and its potential applications are not fully explored[8]. A third form, the anatase type, is more widely used in engineered applications because it has higher photocatalytic abilities than the other types of TiO_2[9]. Unit cell structures of the rutile and anatase TiO_2 can be described in terms of chains of TiO_6 octahedra, where each Ti^{4+} ion is surrounded by an octahedron of six O^{2-} ions (fig. 1.1).

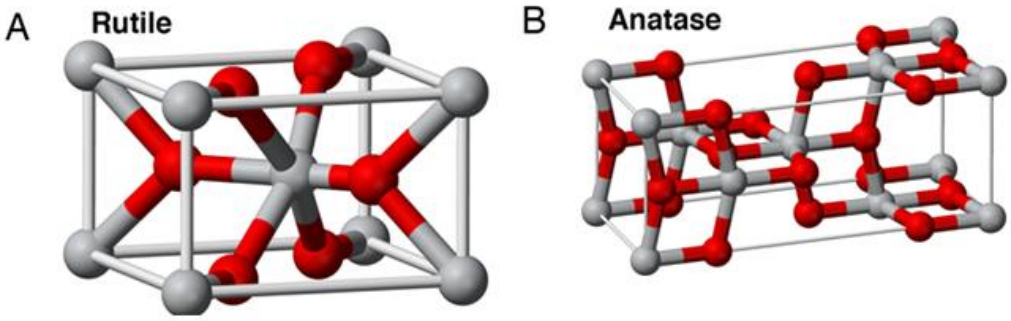

Figure 1.1 - Crystal structures of the two forms of titanium dioxide - (*A*) Rutile unit cell, (*B*) Anatase unit cell[11].

The two crystal structures differ in the distortion of each octahedron and by the assembly pattern of the octahedra chains. In anatase the Ti-Ti distances is larger and each octahedron is in contact with eight neighbors, whereas in rutile the Ti-O distances is larger than anatase and each octahedron is in contact with ten neighbor octahedrons. Deviations between the two forms of TiO_2 lattice structures cause differences in mass densities and electronic band structures[10].

These structures have different stability. The phase transformation sequence of nanocrystalline aggregates during their growth[12]: anatase to brookite to rutile, brookite to anatase to rutile, anatase to rutile, and brookite to rutile transformations during coarsening accompanied with heat; and thermodynamic phase stability depend on the initial particle size. Rutile is the most stable phase for particles above 35 nm in size, anatase is the most stable phase for nanoparticles below 11 nm, and brookite is the most stable in the 11-35 nm range nanoparticles[13].

The two wide band gap semiconductors anatase and rutile are the two phases which can be used for practical applications in photocatalysis and in self-cleaning due to their high photoactivity and higher stability compared to brookite. The variation of the photoactivation extent as a function of the irradiation wavelength follows the absorption spectrum of the catalyst, with a threshold corresponding to its band gap energy, E_g. The E_g value for rutile phase is 3.0 eV and for anatase phase is 3.2 eV, which corresponds to a wavelength of 384 nm. The threshold energy required from the irradiating source should be higher than the band gap energy, that is in the near-UV region, UV-A, which is only a small fraction of the sun's energy (<10%)[10] (fig. 1.2), while visible light is not sufficiently energetic to induce photoactivity in this material[14].

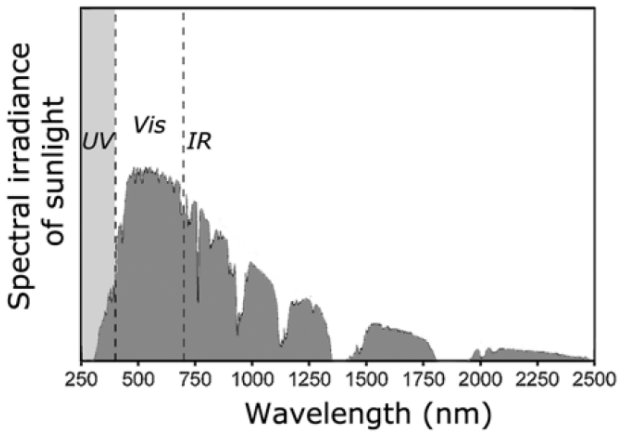

Figure 1.2 - Solar spectral irradiance as a function of wavelength, highlighting the ultraviolet (UV), visible (Vis) and infrared (IR) fractions[15].

1.2 Photoinduced Properties of TiO_2

Two important photoactivated phenomena originate from the absorption of light by the TiO_2 band gap, which causes an electron to be promoted to the conduction band leaving a hole in the valence band: one is the heterogeneous photocatalysis, and the other is the photoinduced superhydrophilicity. The composition and processing of TiO_2 can change the surface characteristics, as it can exhibit higher photocatalytic activity while being less superhydrophilic, or low photocatalytic activity and enhanced superhydrophilic character[16].

1.2.1 Heterogeneous Photocatalysis

Photocatalytic activity depends on the photocatalysts ability to create electron-hole pairs, which can drive chemical redox reactions that lead to the synthesis or degradation of inorganic or organic compounds, is named heterogeneous photocatalysis. This can be performed in various media: gas phase, liquid phase or solid phase[17].

The overall process under irradiation can be decomposed into four steps[18,39]:

1. absorption of light, followed by the separation of the electron–hole couple,
2. adsorption of the reagents,
3. redox reaction between electron-hole couple and adsorbed species,
4. desorption of the reaction products.

1.2.1.1 Mechanism of Photocatalitic Reaction

The principle of heterogeneous photocatalysis has been described in several literature works[1,6,10,12]. Process of semiconductor supported heterogeneous photocatalysis of organic and inorganic compounds is initiated by absorption of photons with energy equal to or greater than the band gap energy of TiO_2 ($h\nu \geq 3.2$ eV or $\lambda \leq 385$ nm for anatase). An electron is excited from the valence band to the unoccupied conduction band, leaving an electron deficiency or hole (h^+) in the valence band, thus creating an electron-hole pair is leading to an electronic disequilibrium. The photoexcitation process converts the photon energy to chemical energy with little loss, and thus the hole (h^+) and the electron (e^-) are powerful oxidizing and reducing agents respectively, (fig. 1.3).

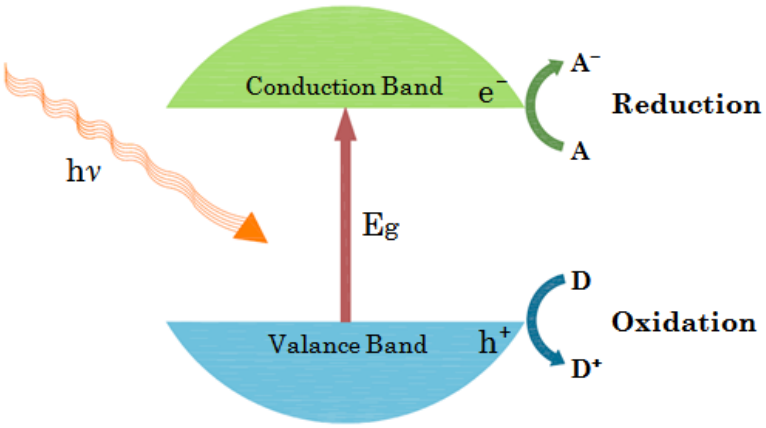

Figure 1.3 - Schematic representation of photoactivation mechanism - hυ: incident radiation energy, E_g: semiconductor bandgap, A: acceptor, D: donor.

Charge carriers can recombine in a short time, nonradiatively or radiatively (dissipating the input energy as heat), or take part in chemical reactions depending on reaction conditions and molecular structure of the semiconductors and leading TiO_2 to recover its electronic equilibrium. The charge transfer process must compete with charge carriers recombination, which can strongly decrease photocatalytic efficiency, i.e., the number of events occurring per absorbed photon. The competition between these processes determines the overall efficiency for various applications of TiO_2 nanoparticles. It is known that rarely organics and inorganics react directly with positive holes and free electrons, but the oxidation reactions on photoactivated TiO_2 surfaces are mainly driven by highly oxidative species, like hydroxyl radicals, ·OH, superoxides, $O_2^{-\bullet}$ (which is almost as effective as the holes and hydroxyl radicals in the chain reactions for the breaking down of organic compounds), peroxides, HO_2^-, etc, all generated by initial interaction of oxygen with conduction band electrons and water and/or surface OH groups with valence band positive holes. These fundamental processes that show the reaction network involving O_2 and H_2O can be expressed as follows[19,20].

The process starts with the generation of electron-hole pairs after irradiation (eq.1).

$$TiO_2 + h\upsilon \rightarrow TiO_2 + e^- + h^+ \qquad \text{(eq.1)}$$

The generated valence band positive holes react with water molecules adsorbed on titanium dioxide particles generating hydroxyl groups (eq.2).

$$3H_2O + 3h^+ \leftrightarrow 3HO^\bullet + 3H^+ \qquad \text{(eq.2)}$$

The electrons of the conduction band, with strong reducing potential, react with oxygen to produce superoxide radicals (eq.3).

$$2O_2 + 2e^- \leftrightarrow 2O_2^{-\bullet} \qquad \text{(eq.3)}$$

From this point, these free radicals may react with the pollutant molecules converting them into other compounds or may create other oxidative species (eq.4-8).

$O_2^{-\bullet} + H^+ \leftrightarrow H_2O^\bullet$ (eq.4)

$H_2O^\bullet + e^- \leftrightarrow HO_2^-$ (eq.5)

$HO_2^- + H^+ \leftrightarrow H_2O_2$ (eq.6)

$O_2^{-\bullet} + H_2O_2 \leftrightarrow OH^- + HO^\bullet + O_2$ (eq.7)

$H^+ + OH^- \leftrightarrow H_2O$ (eq.8)

which corresponds to the overall reaction given in equation 9:

$H_2O + ½\ O_2 \leftrightarrow 2HO^\bullet$ (eq.9)

In order for TiO_2 not to undergo changes as a catalyst, the two reactions of oxidation from photogenerated holes and reduction from photogenerated electrons must occur simultaneously during photocatalysis to establish the former electronic balance[12].

TiO_2 has high oxidizing and reducing abilities compared to other photocatalysts, almost all kinds of organic materials can be degraded completely to innocuous final products (e.g. CO_2, H_2O and salts) by either the hydroxyl radicals formed by reaction of holes with adsorbed water molecules, or the holes themselves.

1.2.1.2 Depollution Mechanism

The mechanism concerning the degradation of both organic and inorganic pollutants, such as NO, NO_2 and SO_2, is a multi-step series of reactions which includes the production of reaction intermediates. The mechanism of pollution decomposition is illustrated in figure 1.4.

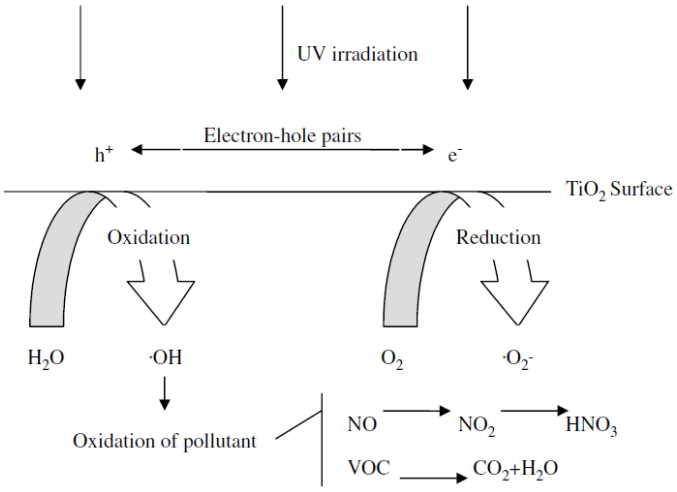

Figure 1.4 - Pollution removal mechanism of TiO_2 photocatalysis[6].

An example of degradation of NO is shown below. Reaction pathway for photocatalytic oxidation of nitrogen monoxide NO to nitric acid (HNO_3) over TiO_2 starts with the formation of the O^{2-} and $OH^{\bullet}$ radicals during the activation process of the photocatalyst, which then react with the pollutant gas producing NO_2 and HNO_3[37,38].

NO diffuses to the surface of TiO_2 and is oxidized to NO_2 by $OH^{\bullet}$ radicals (eq.10-11).

$$NO + OH^{\bullet} \rightarrow NO_2 + H^{+} \quad \text{(eq.10)}$$

$$NO + O_2^{-} \rightarrow NO_3^{-} \quad \text{(eq.11)}$$

Then, the formation of nitric acid, HNO_3, takes place (eq.12).

$$NO_2 + OH^{\bullet} \rightarrow NO_3^{-} + H^{+} \rightarrow HNO_3 \quad \text{(eq.12)}$$

1.2.1.3 Parameters Affecting the Photocatalytic Activity

The photocatalytic activity of a semiconductor is largely controlled by
(i) the light absorption properties, e.g., light absorption spectrum and coefficient,
(ii) reduction and oxidation rates on the surface by the electron and hole,
(iii) and the electron-hole recombination rate[10].

If TiO_2 particles are finely divided and highly dispersed in order to offer the highest surface exposure to the surrounding environment, the fraction of atoms located at the surface will increase providing higher surface area to volume ratios, which can further enhance the catalytic activity. A large surface area with a constant surface density of adsorbents leads to faster surface photocatalytic reaction rates. In this sense, the larger the specific surface area, the higher the photocatalytic activity given by the lager number of active sites. The increase in band gap energy with decreasing nanoparticle size can potentially enhance the redox potential of valence band holes and conduction band electrons, allowing photoredox reactions, which might not otherwise proceed in bulk materials, to occur readily. Moreover, the higher the crystallinity, the fewer the bulk defects, and the higher the photocatalytic activity. Bulk recombination of charge carriers is the dominant process in case of large TiO_2 particles. As particle size is lowered below a certain limit, surface recombination processes become dominant, since most of the electrons and holes are generated close to the surface and surface recombination can be faster than interfacial charge carrier transfer processes[21]. On the other hand, the surface is a defective site and charge carrier trapping can help increasing the photogenerated species lifetime. Localized surface energy states, ascribed to irregularities and surface defects can act as charge traps, and thus reduce recombination effects.

1.2.2 Superhydrophilicity

Photocatalysis is not the only photoinduced property of TiO_2 activated by irradiation of ultraviolet light: another fascinating phenomenon also arises. This effect was actually discovered by accident in work that was being carried out at the laboratories of TOTO Inc., in 1995. It was found that, after UV illumination, the TiO_2 film is experiencing the formation of a highly hydrophilic surface state, defined photoinduced superhydrophilicity[16]. With the discovery of this phenomenon, the application range of TiO_2 coating has been largely widen.

TiO_2 is a moderately hydrophilic material, with a contact angle of water close to 70°. The contact angle, δ, is defined as the angle between the solid surface and the tangent line of the liquid phase at the interface of the solid-liquid-gas phases and is measure of the competing tendencies of a drop to spread so as to cover a solid surface or to round up[47]. When a TiO_2 is subjected to UV irradiation, very small water contact angle, close to zero, is observed. Through the decrease in contact angle, surface experiences a formation of a highly hydrophilic state, thus a creation of uniform water film on photoactive surfaces[22] (fig. 1.5).

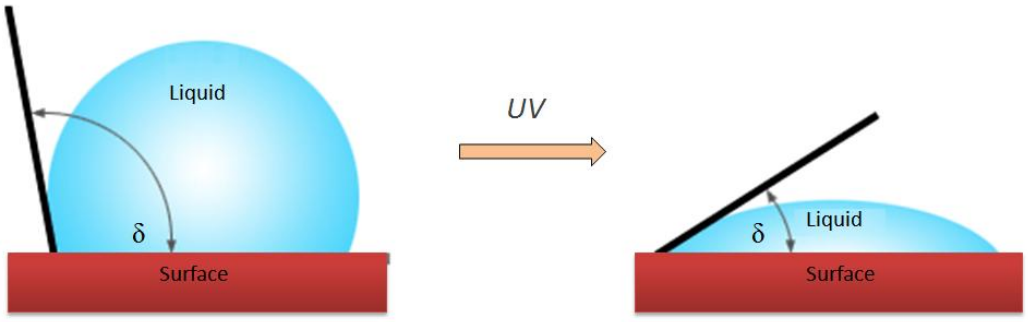

Figure 1.5 - Mechanism of photoinduced superhydrophilicity.

Contact angle, measures the wetting tendency and can be used to calculate the surface tension of a solid surface and a liquid drop[45].

1.2.2.1 Mechanism

It has been shown that the alternation in the contact angle corresponds to the density of the surface hydroxyl groups reconstructed by UV irradiation[24]. Reduction of Ti^{4+} to Ti^{3+} by electrons and simultaneous holes trapping after the UV irradiation reduces the binding energy between the corresponding titanium atom and the closest oxygen, which is then removed when another water molecule arrives in contact with the surface and adsorbs on it. Therefore, a highly hydroxylated surface layer created, due to hydrogen bonding interactions with water and the creation of a layer of chemisorbed H_2O, which is responsible for consequent increase in hydrophilicity of the surface. Moreover, the chemisorbed H_2O can further adsorb layers of water by Van der Waals forces, thus hydrogen bonds hinder the close contact between surface and adsorbed contaminants[23] (fig. 1.6).

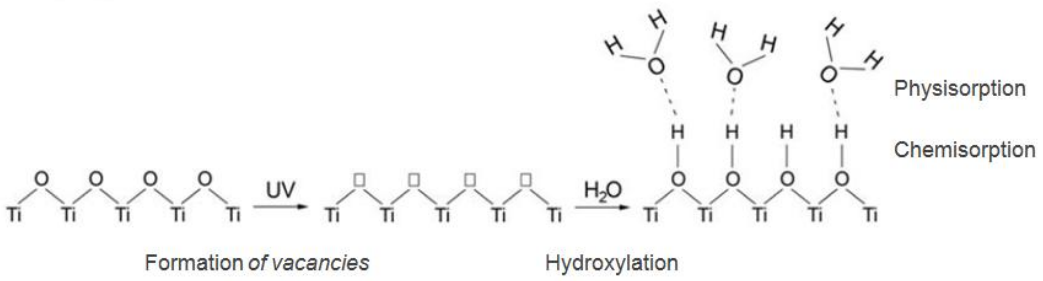

Figure 1.6 - Mechanism of generation of photoinduced superhydrophilicty[15,23].

Indeed, TiO_2 surface is not only hydrophilic, but also it presents an amphiphilic nature after UV irradiation, through hydrophobic and hydrophilic nanometer size zones which are alternating through the surface. This allows both polar and apolar liquids, water and oils, to spread easily on the photoactivated TiO_2 surface[22].

1.3 Applications of TiO_2 in Building Materials Connected with TiO_2 Photoactivity

Since Fujishima et al.[1] found water can be split into H_2 and O_2 by TiO_2 in 1972, the fundamentals of the properties specially heterogeneous photocatalysis and the photoinduced superhydrophilicity, and the effects of these properties were widely investigated. In 1977 the first use of TiO_2 to decompose pollution[25] was reported. After that, in 1985, Matsunaga[26] et al. used TiO_2 as microbiocide in photokilling and in 1997, Wang[22] et al. obtained highly hydrophilic TiO_2 surfaces with anti-fogging and self-cleaning properties.

The progress in academic research on these two properties and the synergetic effect of them significantly promote their practical applications in many fields, in particular building and construction materials showing such behaviour gained much interest. Nowadays, many researchers combine TiO_2 with construction materials by mixing or coating methods to produce novel TiO_2-based building materials with photoactive functions such as environmental pollution remediation, self-cleaning, self-disinfecting, building cooling and anti-fogging[28] (fig. 1.7).

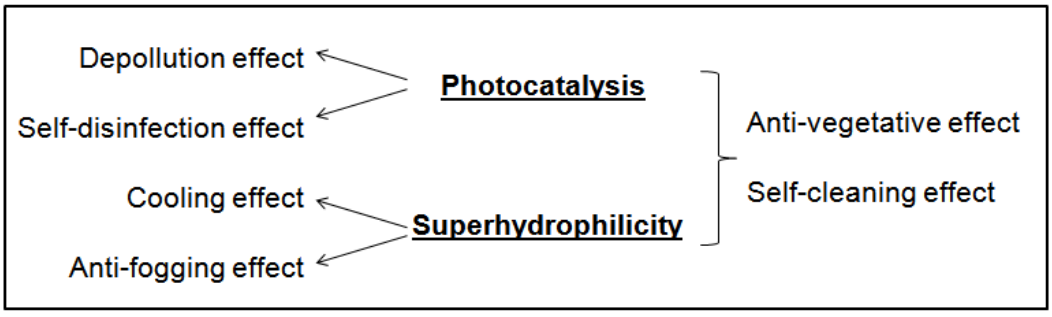

Figure 1.7 - Main effects connected with TiO_2 photoactivity.

The versatile functions of TiO_2 significantly promote its application in building envelope (paints, tiles, glass, plastics, and panels), interior furnishing (paints, tiles,

wall paper, window blinds and finishing coatings), and road construction (paints, concrete pavements, soundproof walls, tunnel walls, road-blocks)[28,29] (Table 1.1).

Table 1.1 - Classification of TiO_2-based photocatalytic construction and building materials.

Materials	Products	Function
Building Envelope	Paints, Tiles, Glass, Plastic films, Panels	Self-cleaning, Depollution, Anti-vegetative, Cooling
Interior Furnishing	Paints, Tiles, Wall papers, Window blinds, Finishing coatings	Self-cleaning, Depollution, Self-disinfection
Road Construction	Paints, Concrete Pavements, Soundproof walls, Tunnel walls, Road blocks	Self-cleaning, Depollution

1.3.1 Depollution Effect

TiO_2 photocatalytic process is considered as an efficient technique for photodegradation of environmentally relevant outdoor and indoor air pollutants, derived from several sources such as industrial implants, heating systems, road traffic and cigarette smoke[30,31]. TiO_2 can decompose many kinds of air pollutants: all natural organic matter (NOM) including hardly oxidizable organic compounds and volatile organic compounds (VOCs) such as benzene, aldehydes and toluene; and variety of inorganic compounds, such as NO_x, SO_x and NH_3, at relative low concentrations. Volatile organic compounds (VOCs) and nitric oxides (NO_x) are major causes of concern on outdoor air quality[32,33].

The presence of NO_x in the atmosphere has many damaging effects on human health and environment. In atmospheric chemistry NO_x refers to the sum of nitric oxide, NO, and nitrogen dioxide, NO_2. NO is considered a primary pollutant[34] because mainly introduced in the atmosphere directly from a source (high temperature combustions in transport and industrial activities). NO_2, is considered as a secondary pollutant because mainly formed in the atmosphere by interaction of a primary pollutant (NO) with O_2 (or O_3) and/or sunlight[35]. Compared with all other technologies, TiO_2 as a photocatalyst provides the great advantage to

decrease NO_x levels in the atmosphere since it only requires UV exposure, atmospheric oxygen and water[36].

In the air-purifying sense for outdoor application, the chemical process is particularly effective only in large scale applications. Considering the difficulty of decreasing NO_x levels in congested urban areas with certain characteristics (lack of wind or rain, intense road traffic, proximity to industrial zone, etc.), using the architectural elements of the city (roadways and building fronts) built with de-polluting building materials, such as photocatalytic glass, tiles, paints, cement pastes, mortars, concrete[15,28], can be one of the most serious attempts to control the air quality.

1.3.2 Self-cleaning Effect

The mechanisms of superhydrophilicity and photocatalysis are independent, but since both of them take place under ultraviolet irradiation, they are generally simultaneous[31]. The simultaneity of these properties is very important to obtain self-cleaning surface, which is a consequence of photocatalytic degradation of deposits accumulating on the surface and subsequent washing away of reaction products by water in contact with the hydroxylated surface layer[16].

In the built environment, it is a common phenomenon that the aesthetic and luster of the surface of ordinary buildings are gradually lost in time due to aging of the material. The building surface could be soiled by greasy and sticky deposits, which results in a strong adherence of ambient dusts. As a result, dirt built up on the surface alters the visual appearance and the reflectance properties of the it, which influences also heat gain on account of a higher heat absorption in darker materials. Without constant and proper maintenance, it is difficult to restore the buildings aesthetic properties[40].

Besides self-cleaning cementitious materials which are studied in this work and explained in detail in Chapter 2, TiO_2-based self-cleaning building products

include paints, tiles and glass have been widely investigated. The representative products as white ceramic tiles for exterior walls and home environments are commercially available. In 1995, the Japanese company, TOTO Ltd, started the manufacturing of antibacterial Cu- or Ag-containing TiO_2 tiles, mainly for operating rooms[7]. Another important example among the photocatalytic building materials is TiO_2-based self-cleaning glass[6] which developed by Pilkington Glass in 2001.

1.3.3 Self-disinfecting Effect

The photocatalytic properties of TiO_2 can also be used for destruction of wide spectrum of microorganisms including viruses, fungi and many species of bacteria which cause the triggering of undesired chemical and aesthetical changes, and control of the biological growth depositing on surfaces[41,42]. The lightinduced bactericidal activity (photocatalytic killing) of TiO_2 is often referred to as photosterilization, and is an effective way to decrease bacteria counts to negligible levels. Applying antibacterial TiO_2 building materials to indoor furnishing, mainly in microbiologically sensitive environments, such as medical facilities and food industries, where biological contamination must be prevented, have been proved to be an effective way for sterilization[43]. For instance, Fujishima et al.[44] found that the bacterial counts on the walls decreased to negligible levels and the bacterial counts in the surrounding air also decreased significantly in 1 h after installing antibacterial tiles.

1.3.4. Cooling Effect

Surface wettability of TiO_2 increase under UV exposure related to the decrase in water contact angle, thus TiO_2 as a superhydrophilic material allows water to spread completely on the surface rather than forming droplets. This phenomenon could increase the amonunt of heat consumed as a consequence of liquid-vapor phase transition, thus dissipiating heat coming from sunlight, and absorbed by the building. It was suggested that sprinkling water onto the surfaces of buildings

with a TiO_2 photocatalyst may be used as a novel building cooling method, with the intent to decrease the urban heat island problem for major cities, which occurs when built-up areas are warmer than the surrounding environment, and to reduce the electricity consumption by air conditioners in summer[45,53] (fig. 1.8).

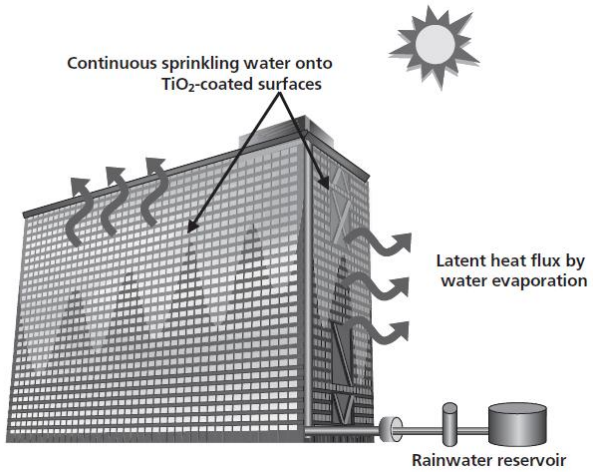

Figure 1.8 - Energy-saving system using solar light and stored rainwater[45].

Under UV exposure, the surface of the photoactive material becomes highly hydrophilic, thus it minimizes the amount of sprinkling water required to form a water film. Continuously supplied small quantities of water, with a layer thickness of approximately 0.1 mm, can cover the whole building surface, and then while evaporates it subtracts heat from the surface. Thus, the building and surrounding can be cooled by the heat consumption that accompanies water evaporation. Moreover, natural rainwater can be collected and stored in specially designed reservoirs for this purpose so that the cost of the water can be reduced. The water film also helps in maintaining the building surface clean by the self-cleaning effect.

The cooling of the building surfaces is expected to result in the reduction of electricity consumption by 10% to several tens of percentage. Therefore, photocatalytic materials could contribute to the development of energy saving technologies.[12].

Chapter 2

Self-cleaning Effect in Cementitious Materials

2.1 TiO_2 in Cement Based Materials

Applying the concepts of photocatalysis to building materials has allowed obtaining functional properties, which are combined with the classical mechanical resistance and durability[46]. At present the preferred photocatalyst added to building materials is TiO_2 in account of its main features: high photocatalytic efficiency, low cost, nontoxicity, chemical stability, and compatibility with traditional construction materials[5]. One of the main effects of the properties of TiO_2 is the self-cleaning attitude conferred by the simultaneous occurring of the contaminant degradation on their surface and a state of photoinduced superhydrophilicity.

Photoactivated properties and the consequent self-cleaning functionality well combine with the use in construction materials for building envelopes, since these materials are exposed to sunlight and rainfall as natural sources of UV and water[44,45], have the widest surface area possible with relatively flat configurations and can gain the maximum efficiency within a limited increase in materials costs. In particular, cementitious materials present an easy source of TiO_2 incorporation due to the nature of matrix represented by cement paste that is suitable for adding

TiO_2 particles as well as for the wide usage of these materials in the construction field.

The applications of these materials concern horizontal and vertical structures such as tiles, pavings, asphalt coatings, concrete structures, plaster, cementitious paintings, and concrete panels[15].

There are two possible ways to attribute photocatalytic properties to building materials: TiO_2 can be added to the mixture proportion of cement-based materials or applied as a surface coating. Many works pay attention to the use of TiO_2 as a surface coating to exploit the whole quantity of TiO_2 employed, as only the surface layers can be activated by UV light[48]. If TiO_2 is added in mass in the mix proportion of concrete, only the small percentage of it contained in the outer layers exposed to the external environment will exert photoactivity, and this approach ends up in wasting potentially active material. Although the best photoefficiency and the highest exploitation of the photoactive admixture are exhibited by a mortar containing TiO_2 as surface covering[49], there are severe durability problems on the surface layer, in particular the removal of the photoactive component due to wind (erosion), rain (leakage) and in general all environmental agents. On the other hand, bulk admixtures exhibit greatest stability, since erosive phenomena only have the effect of exposing fresh photocatalyst surface. TiO_2 addition to finishing layers of mortar or plaster can be a good compromise to avoid durability problems on surface coattings and accessive usage of photoactive material in bulk admixtures[50]. For this reason, attention hereon will be focused on mortars containing TiO_2.

2.1.1 Interactions between Cementitious Matrix and TiO_2 Nanoparticles

The interactions of TiO_2 nanoparticles with cementitious materials were investigated by several research groups, usually by performing the addition of TiO_2 nanopowders or suspensions, with varying particle size, to cement pastes, plasters, mortars and concretes, generally characterized by a low water-to-cement ratio[51]. It has been found that TiO_2 itself may lead to changes of the material characteristics. The strength, sensitivity and ageing processes might be directly affected by TiO_2 additives. Additionally, organic compounds could undergo photoassisted decomposition which are necessary for many building materials.

Concerning fresh concrete, the addition of TiO_2 nanopowders to mortar or concrete causes a decrease in workability due to their high specific surface area, which increase the amount of water adsorbed and changes the rheological behavior of the mix by increasing the viscosity[52]. A rapid consumption of free water indicating that the hydration reactions are accelerated: as a result, dosing nanopowders of TiO_2 into cement pastes has an impact on the solidification, causing a decrease in the setting time[29]. TiO_2 in cementitious materials also modifies the pore size distribution and the total pore volume. TiO_2 is a effective filler of voids due to its nanometric size, and tends to fill up the pore space around them gradually resulting in a reduction of pore volume mainly occurring within the capillary pore range. In parallel, the water content must rise with the increasing amount of nanoparticles to ensure adequeate workability, which contributes to a higher porosity: therefore there is a joint effect of pore size reduction and increased porosity in compositions with high amounts of TiO_2[9].

In the case of hardened concrete, there is an improvement in the compressive strength, due to filler effect of the nanoparticles: TiO_2 is a non-reactive nano-filler and the increase in mechanical resistance can be attributed to its wide surface for nucleation or clinging of hydration products[52,54]. On the other hand, some experimenal tests showed that there is a slight decrease in mechanical resistance,

in spite of its filling action which is likely to depend on a disuniform dispertion of nanoparticles or to their agglomeration[51]. This issue is open for discussion.

Furthermore, there are some changes occurring in the microstructure of concrete and mortar, during the service life of the structure[56]. Due to photocatalytic decomposition reactions, the use of organic admixtures in TiO_2-containing concrete and other cementitious materials, may result in the organic component degradation with possible reduction of performances from the durability and photoactivity point of views. Therefore, the use of organic binders and admixtures with cementitious materials must be minimized[6,50]. Moreover, it was reported that the incorporation of TiO_2 nanoparticles might accelerate the carbonation process associated with CO_2 release[9,57], which has a negative consequence of inducing corrosion of embedded steel reinforcements if present, and also leads to changes in the microstructure of cement paste and composition of pore solution[56]. Furthermore, carbonation induced modifications can influence the photoactivity of the TiO_2 admixture by decreasing its efficiency[6,50].

2.2 Self-cleaning Effect

As previously cited, although the photoinduced processes of TiO_2 photocatalytic degradation of contaminants and superhydrophilicity are different mechanisms, the simultaneous effect of the two processes results in sustaining the self-cleaning effect[6,23]. The surface can have less photocatalytic character and more superhydrophilic character, or vice versa, depend on the composition and the processing[60]. And also it is difficult to distinguish which mechanism is more important for self-cleaning effect[23]. Through the property of self cleaning, surface contaminants are partly photomineralized, and afterwards particles which are loosely adherent are removed from the surface by water which is in direct contact with the surface[15]. Moreover, stains on the surface due to drop formation caused by slow water evaporation can be avoided[16] (fig. 2.1).

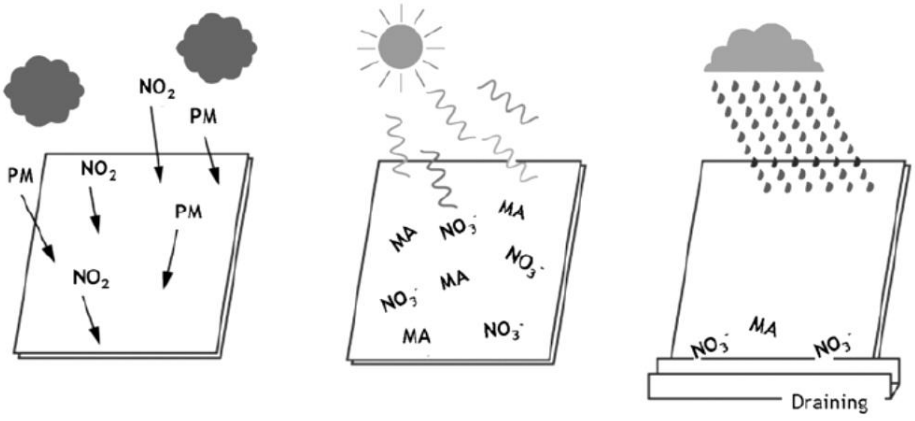

Figure 2.1 - Schematic representation of self-cleaning on TiO_2-containing surfaces - PM: particulate matter, MA: mineral acids.[15].

In buildings facades, soiling causes objectionable stains and change in color which can originate from the deposition of organic and mineral particles, accumulation of fly ash, hydrocarbons and soot from combustion of fossil fuels and biomass, as well as the biological growth (e.g., cyanobacteria, fungi, algae)[15,58].

The main advantage of TiO_2 self cleaning ability is economical considering that only solar light and rainfall are required as driving forces, its application could reduce the need for maintenance, particularly for tall buildings where it can be very difficult and costly[59].

2.2.1 Mechanism

Two main mechanisms have been hypothesized as responsible for self-cleaning.

(1) Photocatalysis enhanced by superhydrophilicity: Small particles and greasy deposits adhere to building surface by organic binders such as hydrocarbons and fatty acids[61,62]. Taking fatty acid molecules as example, their carboxylic groups (–COOH) enable them to stick on building surface via chemical binding with calcium ions present in concrete; on the other hand, their long chains link with

other hydrophobic molecules perpendicularly to the surface, resulting in fatty stains which can trap many atmospheric particles and dusts. The great redox power of the UV induced electron–hole pair of photocatalyst can decompose the soiling compounds into H_2O, CO_2, and organic compounds. Hydrophilicity plays a very important role in that point: if more hydroxyl groups can occur on the surface of TiO_2 due to superhydrophilicity, the efficiency of photocatalytic activity is amplified.

Furthermore, Wang et al.[22] observed that the self-cleaning effect of TiO_2 surfaces could be enhanced when water flow, such as natural rainfall, was applied to the surface. They attributed this enhancing phenomenon of water flow to the superhydrophilic property of TiO_2, i.e., water soaking the molecular level space between the stain and the superhydrophilic TiO_2 surface. In other words, even though the number of sunlight photons captured by TiO_2 may be insufficient to decompose the adsorbed stain, the surface can be maintained clean when water is supplied, since TiO_2 photocatalysis breaks the fatty acid chains binding dirth to the surface, and water carries away the detached soiling agents. On clear days, contaminants accumulate on the whole surface, but during rain, these are washed off the TiO_2-coated surface.

(2) Superhydrophilicity enhanced by photocatalysis: The adsorption of organic compounds on the surface may lead to a conversion of hydrophilic surface to hydrophobic surface; however, photocatalysis can decompose the organic compounds on the surface resulting in the restoration of hydrophilicity. From this point, photocatalytic decomposition of these organic contaminants can restore the superhydrophilic property that will be maintained for a long time[23].

The efficacy of self-cleaning surfaces was found to be dependent on the relative rates of decontamination vs. contamination. The TiO_2 photocatalyst can maintain the surface clean only when the photocatalytic decontamination rate is greater than that of contamination[12].

2.2.2 Problems and Limitations

Although the self cleaning ability of TiO_2-based cementitious materials is evident, there are still unresolved problems about the actual behavior of the photocatalyst in case of complex environmental exposure and the evolution of the material during its lifetime. The interactions between TiO_2 and the hosting material, and the factors affecting the photocatalytic process need further investigation. Up to now, studies show that the mutual interactions between the photocatalyst and its environment have negative effects besides the photocatalyst beneficial usage[63].

One of the important problems regarding such interactions can be loss of the photocatalytic activity due to immobilization of TiO_2 by the cementitious material. Rachel et al.[64] pointed out that TiO_2-cement mixtures and red bricks containing TiO_2 were significantly less efficient than TiO_2 slurries in decomposing 3-nitrobenzenesulfonic. It is thought that the reduction of active surface, and the presence of ionic species, which contributed to charge recombination, are the reasons for the loss of photocatalytic activity.

Another issue is related to the deactivation of active sites. Principally, the removal rate, which is influenced by numerous parameters such as amount, phase, particle size and surface area of TiO_2[27], surface chemistry, pollutant concentration, light intensity, relative humidity and other environmental conditions, should be higher than the contamination rate to prevent a possible decrease and eventually the loss of functionality[65]. Furthermore, the adsorption of surface species, such as intermediates, by-products or pollutants, which are relatively stable, lowers the removal rate and may cause temporary or permenant deactivation of some of the active sites of the catalyst[12,28] Also the shielding effect of calcium carbonate precipitates caused by carbonation of cement paste, result in accumulation of contaminants on surfaces exposed to the environment, and consequently noticeable loss in catalytic efficiency[2,51,63]. The report published by the Hong Kong Environmental Protection Department claimed that the photocatalytic activity of TiO_2 coated paving blocks decreased significantly after 4 months of

exposure in a downtown area due to carbonation and accumulation of contaminants on the block surface[66].

In addition, the potential impacts of nanomaterials on human health should also be thoroughly searched. During the production, transportation, storage, and use the small particles of nanoscale photocatalysts could enter into the human body and may produce adverse effects on health[67].

2.3 Practical Applications

Actual behavior of materials modified with titanium dioxide in real practice, concerning the interactions between the cementitious materials, nanoparticles and environmental factors, and the efficiency of self-cleaning effect in environmental conditions, are probably better investigated through pilot projects. Pilot projects are mostly exploited in white concrete buildings. Relevant examples are[7,15,36]:

- The Music and Arts City Hall, Chambéry, France, 2001 (fig. 2.2 (a))
- the Church "Dives in Misericordia", Rome, Italy, designed by Richard Meier for the Jubilee, 2003 (fig. 2.2 (b))
- Hotel de Police, Bordeaux, France (fig. 2.2 (c))
- Air France Building, Roissy-Charles de Gaulle Airport, France, designed by Denis Vallode and Jean Pistre, 2006 (fig. 2.2 (d))
- Saint John's Court, Montecarlo, Monaco
- Ciments Maroc Headquarter, Morocco
- Chiesa Matrice, Cittanova, Italy

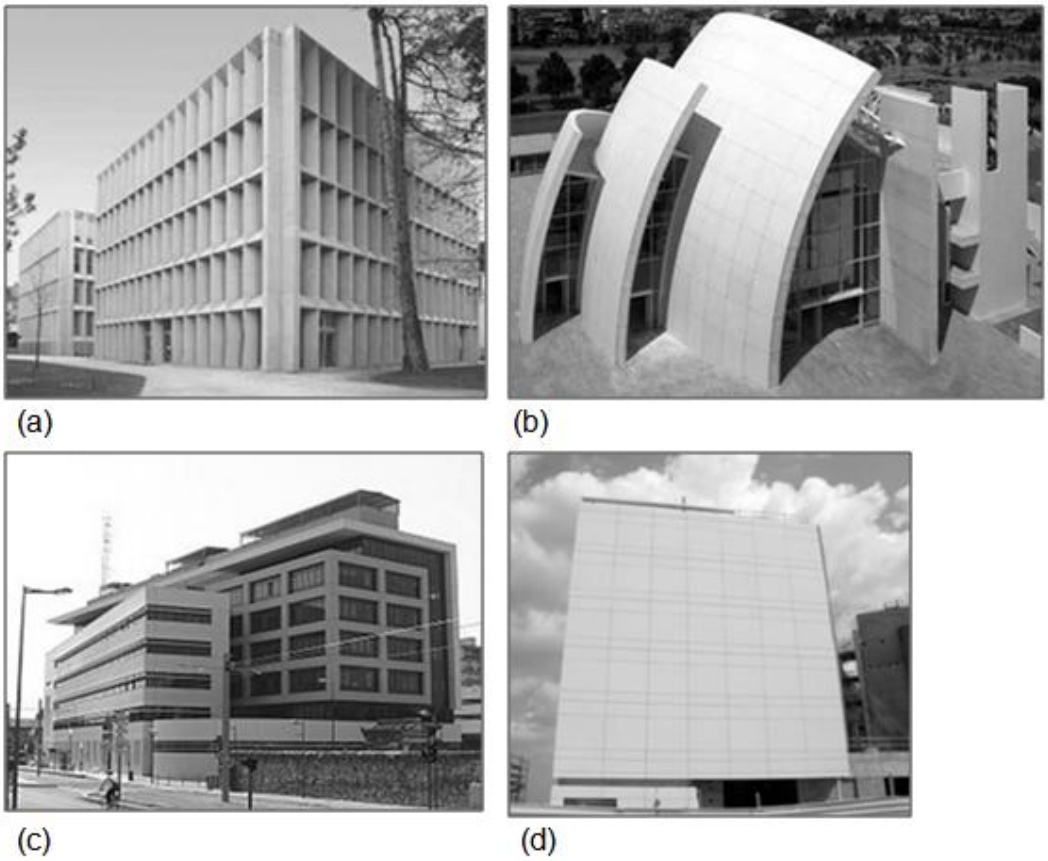

Figure 2.2 - Examples of buildings with TiO_2-containing surfaces - (a) The Music and Arts City Hall, Chambéry, France, (b) Church "Dives in Misericordia", Rome, Italy, (c) Hotel de Police, Bordeaux, France, (d) Air France Building, Roissy-Charles de Gaulle Airport, France.

Chapter 3

Experimental Methodology

The work here presented focuses on the self-cleaning effect on cementitious surfaces, specially mortars, modified through the addition of titanium dioxide nanoparticles. Different experimental setups were applied in laboratory testing, depending on the material and property to be tested to evaluate the self-cleaning performances of TiO_2-containing construction materials. The laboratory tests performed are: rhodamine B degradation test, which consist of an impregnation of the organic dye on the material surface and evaluation of the surface ability to discolor the dye; and water capillary absorption-evaporation tests to evaluate possible changes of wettability of the treated surface. A long term exposure test was also performed to establish a relationship between the self-cleaning effect and environmental variables through the evaluation of chromatic changes of the samples subjected to the external environment.

3.1 Materials Tested

All tests were performed both on anatase-containing glass fiber reinforced commercial mortars and on mortars which do not contain any photoactive component, being the latter considered as reference. Both formulations were characterized by the same mixture proportion with water:cement:sand ratio of

0.56:1:2, as listed in table 3.1. A total of 5% anatase was added to the mixture proportion in the form of 3% of nanometric powder and 2% of an aqueous suspension. It was expected that the different characteristics give rise to different photocatalytic efficiencies[55,66]. TiO_2 powders had particle size ranging from 150 to 400 nm (commercial powders purchased by Precheza), having purity higher than 92% (data were supplied by manufacturers); average diameter of suspended TiO_2 particles (purchased by Degussa) was 88 nm, with a pH of approximately 6. In particular, no pigments were added to the mixture. Specimens were cut in squares with 100 mm side and 10 mm thickness.

Table 3.1 - Mortars mixture proportion.

Mortars mixture proportion (exception made for TiO_2 content) [kg/m^3]		[%] (with respect to cement weight)
Portland cement (CEM I 42.5 R)	555	
Silica sand	1110	
Water	311	
Expansive admixture	33	6%
Waterproof additive	22	4%
Glass fibers	20	3.6%
Antifoaming admixture	1	0.1%

For rhodamine B degradation tests, beside anatase-containing glass fiber reinforced commercial mortars, siloxane coating and clay tile samples with different anatase content were also examined as representative porous materials.

In the case of bulk siloxane coating, anatase was added in the percentages by weight and four specimens of each material were prepared. Also, two kinds of clay bricks examined: the one with TiO_2 contain in mass and the one with sol-gel coating which was applied on the fired tile, with no subsequent consolidation treatment.

3.2 Experimental Tests

3.2.1 Rhodamine B Method

In order to verify self-cleaning performances of photocatalytic cementitious building materials several tests, involving discoloration analysis of the dyes through colorimetric measurements, have been set up. The degradation of organic dyes, which are very soluble in water and can therefore be spread uniformly on a given surface, are considered as liquid pollutants: their drying on the material surface is equivalent to staining the surface itself. Therefore, tests based on dyes discoloration can be considered to be a quick way to test photocatalytic activity as a part of the self-cleaning mechanism, and are suitable to investigate the self-cleaning attitude of materials[51]. One of the first studies on the self-cleaning attitude of photoactive materials was proposed in 2004[68]: white cement disks were impregnated with a yellow dye (phenanthroquinone), and the subsequent restoration of the initial white color was observed in specimens containing TiO_2. Similar tests to evaluate the self-cleaning performance of cement based materials containing TiO_2 were carried out with other organic dyes too; including azo and anthraquinone dyes. Among these dyes rhodamine B is one of the most widely applied one, since it is relatively stable under UV illumination, and showing higher UV resistance among the other dyes used in self-cleaning experimental analyses such as Methylene Blue (MB)[70,71]. In rhodamine B degradation test, the photocatalytic efficiency of materials is evaluated through the degradation of dye deposited on the cementitious material surface subject to artificial light. A semiquantitative measurement of its degradation can be achieved by measuring the loss of color intensity by light absorption as a function of time[36].

3.2.1.1 Degradation Mechanism of Rhodamine B

Rhodamine B, indicated as Rh B ([9-(2-carboxyphenyl)-6-diethylamino-3-xanthenylidene]-diethylammonium chloride) (fig. 3.1), which is a kind of xanthene dye with molecular mass 479.01 g/mol, exhibits a strong magenta color due to its highly delocalized π-electron system.

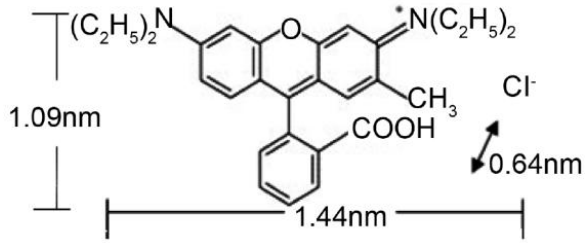

Figure 3.1 - Chemical structure of rhodamine B, $C_{28}H_{31}ClN_2O_3$[71].

Discoloration of Rh B in presence of TiO_2 involves not only photocatalysis (TiO_2-sensitized photoreaction) but also a direct photolysis of the dye (dye-sensitized photoreaction) [36]. In the first mechanism light activates TiO_2 through promotion of electrons from the valence band to the conduction band. Adsorbed water and oxygen play a fundamental role, as they react with valence band positive holes and conductance band electrons respectively, to generate hydroxyl radicals, $HO^{\bullet}$, which are responsible for the mineralization of Rh B adsorbed on TiO_2 (fig. 1.3).

In the second mechanism the organic molecule absorbs visible light photons which can only promote electrons from the highest occupied molecular orbital (HOMO) to the lowest unoccupied molecular orbital (LUMO) in the organic molecule: this occurs when photon energy is insufficient to induce photoactivation of TiO_2 (band gap in the near UV). These electrons are further injected from the Rh B LUMO to the conduction band of TiO_2, leading to the formation of Rh $B^{+\bullet}$ molecular ion radicals on the TiO_2 surface. The transfer of the conduction band electron to adsorbed oxygen on the TiO_2 surface produces $O^{2-\bullet}$. Both radical

species arising from this process are highly reactive and ultimately leading to mineralization of the organic molecule (fig. 3.2) [72,55].

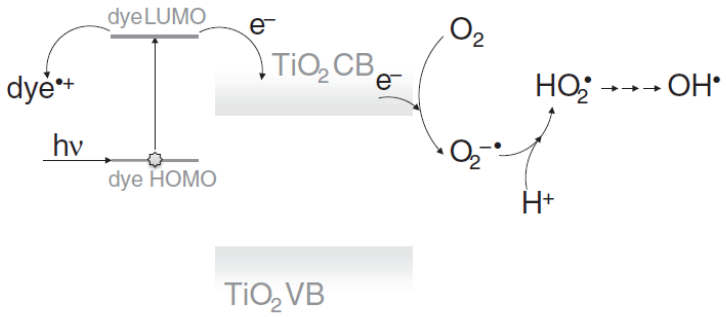

Figure 3.2 - RhB-TiO_2 system under UV irradiation - dye-sensitized photoreaction[36].

The loss of color by photolytic degradation of the dye is quite common and does not mean necessarily complete degradation, it only gives an indication on the partial breakup of the molecule, and the organic molecule can still be partially integer even after the color has disappeared. The chemical mechanism of this process involves four methyl groups at either side of the xanthene ring removal which is called demethylation. Demethylation mechanism causes an important source of misrepresentation of catalyst efficiency when examining the discoloration where controls are not used. However, even by taking into account this effect, it can be shown that enhanced color loss takes place once rhodamine B is exposed under artificial sun light in the presence of TiO_2[36,73]. For a full understanding of photodegradation kinetics total organic carbon (TOC) or mass spectrometry tests should be performed, which assess the real extent of molecule degradation[49].

In this work, photocatalytic efficiency was evaluated by colorimetry following two routes: monitoring the discoloration of Rh B applied to the surface of the materials by reflectance spectrophotometry, and monitoring the degradation of the aqueous solution of Rh B by transmittance spectrophotometry. For all tests, control samples were used to avoid misrepresentation of photocatalyst efficiency.

3.2.1.2 Colorimetry

3.2.1.2.1 Reflectance Spectrophotometry

Reflectance Spectrophotometry was used in rhodamine B degradation tests to analyze the discoloration of Rh B in time. Rh B was first deposited on the surface of the material, allowed to dry and then exposed to artificial light. During the irradiation color analyses are performed by spectrophotometer. In this experiment a Konica Minolta CM-2600d spectrophotometer (fig 3.3), with D65 light source was used, which measures the spectral reflectance of the surface every 10 nm in the range 360– 740 nm.

Figure 3.3 - Konica Minolta CM-2600d spectrophotometer.

From reflectance data it is then possible to express the results in the CIELab color space, which provides the chromatic coordinates of the measured color, as defined by the *International Commission on Illumination* - CIE Standard S004/E-2001, L* - lightness, a* - hues from red to green, and b* - hues from yellow to blue (fig. 3.4).

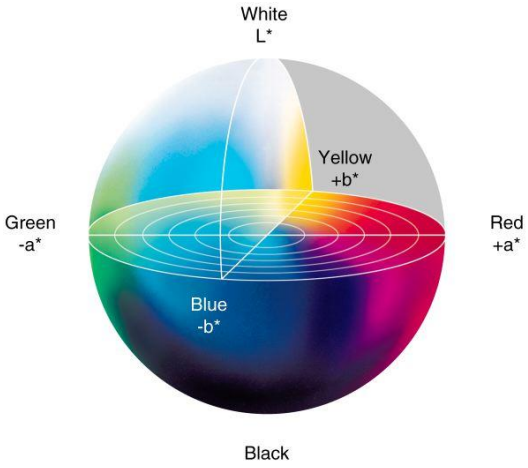

Figure 3.4 - CIELab color space.

In this space, color changes can be measured as geometric distance between two points and it is possible to calculate the color variation in time, ΔE, which corresponds respectively to the color at the time t to the initial color at t=0 (eq.13):

$$\Delta E = \sqrt{\Delta L^{*2} + \Delta a^{*2} + \Delta b^{*2}} \quad \text{(eq.13)}$$

$$\Delta L^* = L_t^* - L_0^* , \Delta a^* = a_t^* - a_0^* , \Delta b^* = b_t^* - b_0^*$$

In the case of Rh B, which exhibits a strong magenta hue, the a* coordinate is generally considered. A decreased intensity of color, resulting in a decrease of the coordinate a*which is related to the red component of color, indicates that the dye is being degraded. Therefore, the relevant parameter considered is its percent variation of a*, $\Delta a_{\%}^*$, calculated as in equation 14.

$$\Delta a_{\%}^* = \frac{a_t^* - a_0^*}{a_0^*} \times 100 \quad \text{(eq.14)}$$

where a_0^* is the value of the chromatic coordinate right after soiling with Rh B and a_t^* its value after a time t of UV irradiation.

Also the lightness parameter can be used (eq.15), whose decrease corresponds to degradation of dye, thus whitening of the surface.

$$\Delta L^*_{\%} = \frac{L^*_t - L^*_0}{L^*_0} \times 100 \qquad \text{(eq.15)}$$

3.2.1.2.2 Transmittance Spectrophotometry

The photocatalytic activity of porous samples is difficult to evaluate with the formerly described method, since Rh B could be absorbed in depth and be degraded only partially on account of the small thickness of material activated by UV light, especially in the case of opaque materials. Another experimental methodology evaluates the degradation of aqueous solution of Rh B by monitoring its concentration in liquid phase. The measurement of the Rh B concentration can be performed by transmittance spectrometry. In this experiment a Jasco/7800 spectrophotometer (fig. 3.5) was used to read the solution absorption, at wavelength 550 nm where Rh B gives a peak of absorption.

Figure 3.5 - Jasco/7800 spectrophotometer.

The basis for using spectrophotometric measurements to quantitatively analyze light absorbing chemical species, (analytes) in solution is the Beer-Lambert equation (eq.16):

$$A_\lambda = \varepsilon_\lambda b c \qquad \text{(eq.16)}$$

Where A_λ is the absorbance at a given wavelength; ε_λ, molar extinction coefficient, which is the molar absorptivity at that wavelength; b, the pathlength, which is the distance light travels through the solution, is defined by the sample compartment; and c is the concentration of the analyte in solution (fig. 3.6).

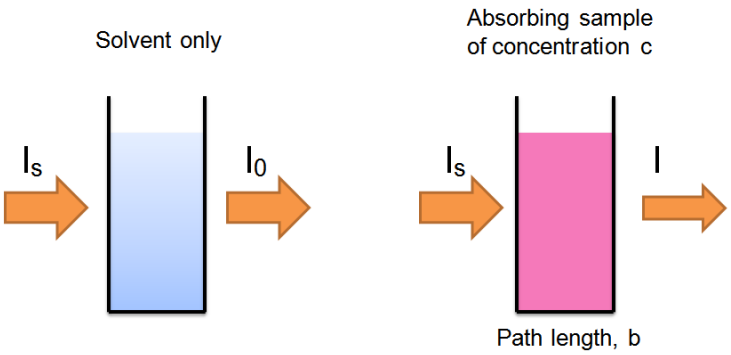

Figure 3.6 - Absorption of light by a sample.

The Beer-Lambert equation states that absorbance is directly proportional to the concentration of analyte in the sample. If A_λ is experimentally known, the concentration of the absorbing species in solution can be determined since (eq.17):

$$c = \frac{A_\lambda}{\varepsilon_\lambda b} \qquad \text{(eq.17)}$$

The extent of Rh B photocatalytic degradation is therefore evaluated through the decrease in concentration of the dye in solution (eq.18):

$$c_{\%} = \frac{c_t - c_0}{c_0} \times 100 \qquad \text{(eq.18)}$$

where c_0 is the concentration of Rh B solution at t = 0, c_t is the concentration of the Rh B after the irradiation.

3.2.1.3 Experimental Setup for Photocatalytic Process

The photocatalytic activities of mortars, roofing tiles and siloxane coatings containing various amounts of titanium dioxide in the anatase form were compared, by applying different test methods and concentrations of Rh B, in order to identify the optimal test conditions to highlight differences in photoactivity. The photocatalytic efficiency of photoactive glass fiber reinforced commercial mortars was further investigated after this methodology pre-screening. Experimental tests were first aimed at finding the best dye concentration to perform reliable photocatalysis test with the application of different concentrations of Rh B. To identify the most efficient method for Rh B degradation evaluation immersion test, immersing-drying test, ring test and stain test were performed on different materials that are showing different properties and various amounts of titanium dioxide in anatase form. All tests were also performed on standard samples which did not contain any photoactive component, considered as reference.

3.2.1.3.1 Stain Test

The experimental method defined as stain test is based on reflectance spectrophotometry; and involves the monitoring of the discoloration of Rh B applied and dried on the surface of the materials. To perform the test, first 1 ml of Rh B solution prepared with tap water was deposited on three different spots of the surface, and then samples were allowed to dry in a dark environment at room temperature and humidity for 24 hours (fig. 3.7).

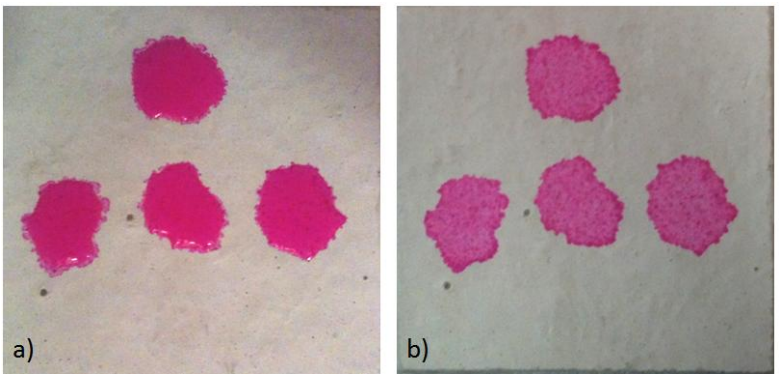

Figure 3.7 - Rhodamine B solution on mortar surface - a) application of the dye, b) 24 hours after the application.

After drop deposition, samples were irradiated with a UV-Vis light source, with UV intensity range dependent on material and Rh B concentration, adjusted with a Konica Minolta UM-10 radiometer. Surface color variations were monitored during irradiation with a Konica Minolta CM-2600d reflectance spectrophotometer, for 4 hours at regular time intervals, less frequently with increasing irradiation time. After the measurements the areas of the stains were calculated to correct the initial dye concentration by the area on which the dye was dispersed. The percent variation of lightness, $\Delta L^*_{\%}$, or percent variation of a*, $\Delta a^*_{\%}$, were then calculated to evaluate discoloration and thus change in concentration of the applied Rh B dye.

3.2.1.3.2 Immersion Test

In immersion tests, the photocatalytic activity of samples was evaluated, under UV irradiation, by monitoring the degradation of a Rh B solution in liquid phase. The test procedure was adapted from ISO 10678[74].

The samples were prepared in the form of coating on a 2.5×1 cm^2 substrate. In this particular case a TiO_2-containing siloxane coating was used, which required a curing period of 2 weeks under a UV light source (300 W Ultra-Vitalux Osram

lamp which is composed of a mercury discharge lamp, whose radiation is similar to that of sun light) with UV intensity range 1000±50 μW/cm^2 (fig. 3.8).

Figure 3.8 - Siloxane coating samples with substrate.

After the treatment, samples were immersed in 15 ml of test solution and irradiated with a blacklight blue lamp light source with an intensity range 2000±50 μW/cm^2. One important parameter is the volume of test solution, which should be at least ten times greater than the volume of the solution required for the spectrophotometric measurement. The test cells were covered with quartz during the whole test, to avoid potential concentration change in the solution of Rh B due to water evaporation while ensuring UV transmission (fig. 3.9).

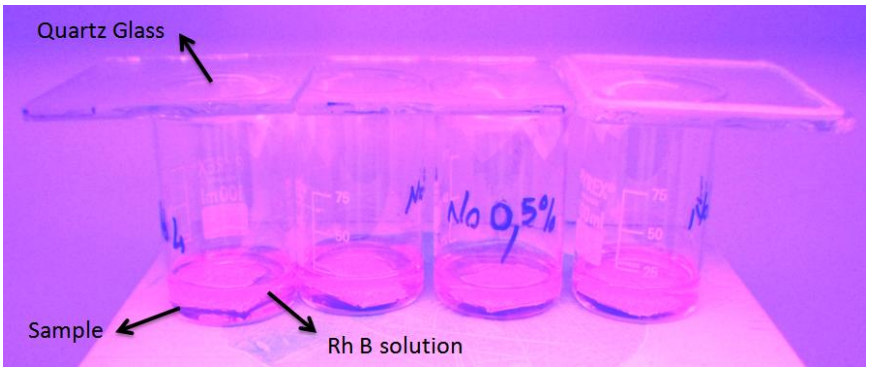

Figure 3.9 - Siloxane coating samples under UV irradiation.

The absorbance A_λ was monitored during irradiation at progressively increasing time intervals for 4 hour. From absorbance, the concentration and therefore the degradation of Rh B, indicative of the material photocatalytic efficiency was evaluated.

3.2.1.3.3 Immersion-drying Test

The test procedure of immersion-drying tests started with immersing samples in Rh B test solution for 24 hour in order to allow the adsorption of dye until surface saturation, and then let the samples dry for another 24 hour in a dark environment at room temperature and humidity (fig. 3.10).

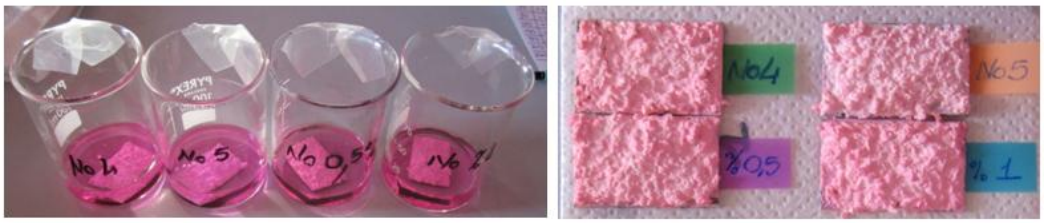

(a) (b)

Figure 3.10 - Immersion-drying test siloxane coating samples - a) immersion, b) drying.

Analogously to the stain test, also in immersion-drying test the stain decolorization was monitored by reflectance measurements during UV irradiation for 4 hour. For each characterization, the mean values of a series of at least 3 measurements were calculated and the percent variation of lightness, $\Delta L^*_{\%}$, and percent variation of a*, $\Delta a^*_{\%}$, were calculated to evaluate the photocatalytic activities.

3.2.1.3.4 Ring Test

In ring tests, a metal ring was first glued to the sample surface, and then stored 24 hours to ensure adherence. The metal ring can be directly covered with silicon sealant (fig. 3.11 (b)), or first covered with silicon ring and then fixed with silicon sealant (fig. 3.11 (a)) to improve sealing.

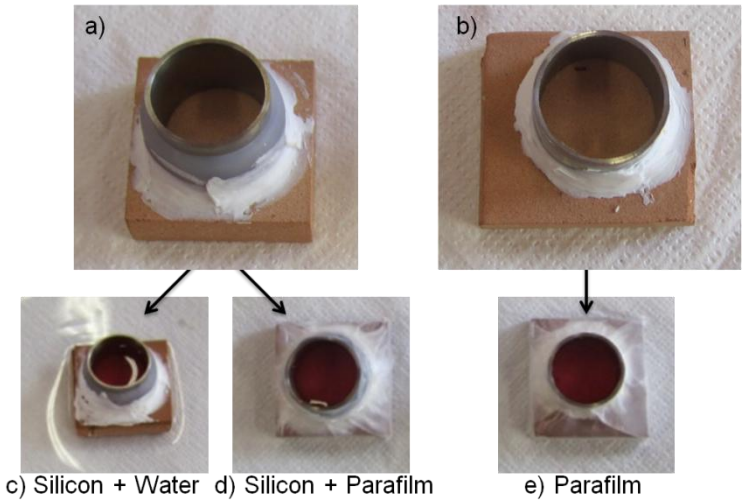

Figure 3.11 - Ring test performed on brick samples - a) with silicon ring, b) without silicon ring, c) with silicon ring and water immersion, d) with silicon ring and parafilm, e) without silicon ring and with parafilm.

Then the samples were dipped in a conditioning solution for one hour and allowed to absorb the solution again in a dark environment at room temperature and humidity; this pre-conditioning step serves to prevent the sample from adsorbing further test solution during the test. Samples were then kept immersed in conditioning solution (fig. 3.11 (c)) or covered with parafilm to avoid water evaporation which is also lead to further absorption during tests (fig. 3.11 (d), (e)). The ring was then filled with 2 ml test solution and sealed with quartz while the samples were submitted to UV light, for 4 hour.

As for immersion tests, the extent of Rh B degradation is calculated through the variations in solution concentration.

3.2.2 Absorption-Evaporation Tests

In order to assess how the wettability of the mortar surface is modified by the addition of TiO_2 nanoparticles, capillary water absorption and evaporation analyses were carried out on both photoactive and standard glass fiber reinforced mortar samples.

In fact, with the addition of TiO_2 nanoparticles the wettability of mortars is expected to increase due to photoinduced hydrophilicity. High wettability may lead to an increase in water absorption and evaporation. Water absorption is also very important to predict the service life of cementitious materials, since capillary action is one of the main mechanisms to transport aggressive species into the bulk material[76]. On the other hand, an increase in evaporation rate is fundamental to produce a cooling effect, on account of the energy consumed by the evaporation latent heat.

3.2.2.1 Capillary Action

Capillary absorption takes place in fine pores (10 nm–10 μm) where forces arising from surface tension are in the same range as gravity forces present in the liquid. It is the primary mechanism when the material is only partially wetted, and is usually described by the Lucas–Washburn equation[78] (eq.19):

$$h = k\sqrt{t} \qquad \text{(eq.19)}$$

where h is height of the liquid front (m), t is the wetting time (s) and k is the capillary absorption coefficient (m $s^{-1/2}$). In the Lucas–Washburn equation, this coefficient is defined as (eq.20):

$$k = \sqrt{\frac{\gamma r \cos\theta}{2\eta}} \qquad \text{(eq.20)}$$

where γ is surface tension (N m^{-1}) which is the driving force for capillary absorption, r the capillary radius (m), θ the contact angle (^{o}) and η the dynamic viscosity (Pa s).

The capillary absorption coefficient is influenced by the relationship between solid and liquid phases, as well as by the pore structure inside the solid phase, and should be determined experimentally. The lack of an adequate method for the determination of liquid height at a given time requires an alternative measurement, sorptivity, S, which is a function of viscosity, density and surface tension of the liquid and also of pore structure such as radius, tortuosity and continuity of capillaries. Sorptivity can be calculated according to the relationship (eq.21):

$$i = S\sqrt{t} \qquad \text{(eq.21)}$$

where i is the volume of liquid absorbed per unit cross section in time t.

There is a linear relationship between height of the liquid front and sorptivity (eq.22), therefore the parameters affecting k also correlate to S.

$$h = k\sqrt{t} \equiv S\sqrt{t} \qquad \text{(eq.22)}$$

The relationship between height of the liquid front (depth of penetration), h and square root of the time (t) is bi- or trilinear, (fig. 3.12), with a period of rapid absorption in which larger pores are filled followed by more gradual absorption[81].

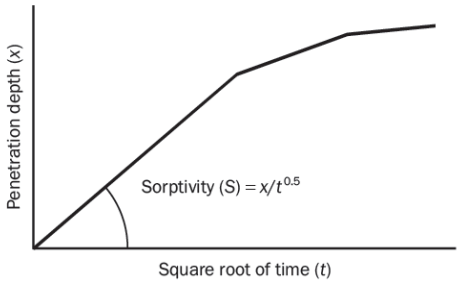

Figure 3.12 - Typical form of result from absorption test[81].

3.2.2.2 Experimental Setup

All analyzes were carried out on both standard and anatase-containing mortars with the application of the standard ISO 15148[77], which specifies a method for determining the short-term liquid water absorption coefficient by partial immersion with no temperature gradient.

First 10 cm × 10 cm specimens with 1 cm thick were sealed with silicon sealant except one surface in order to obtain a directional flux of water. After the silicon hardened at room temperature and humidity for sufficient time, every sample was weighed and then the bottom surface (non-sealed one) was partially immersed to a depth of 5 ± 1 mm in distilled water, on point supports to keep the specimen 1.5 cm clear of the base (fig. 3.13).

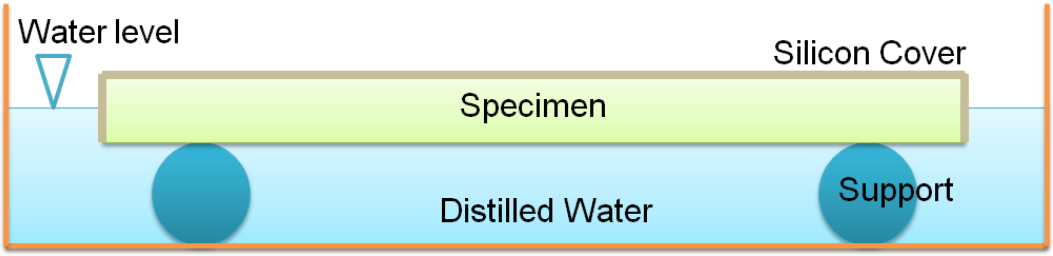

Figure 3.13 - Example of capillary absorption testing apparatus.

During the experiment specimens were weighed with an accuracy of 0.01 g, after 5 min, 20 min, 40 min, 1 h, 1.5 h, 2 h, 3 h, 4 h, 8 h, and 24 h of immersion, as defined by the standard, to determine the increase in mass and consequently the capillary absorption extent. Before every measurement the excess water, adhering to the surface but not absorbed by the sample, was removed by lightly blotting with absorbent paper. After absorption, evaporation tests were carried out at room temperature by holding samples vertically and weighing them at same time intervals as described for absorption test.

For absorption tests water absorption coefficient A_{wt} (kg m^{-2} $s^{-0.5}$) was derived from the linear relation between mass of water absorbed by a test specimen per surface area and per square root of time (eq.23).

$$A_{wt} = \frac{\Delta m_t}{\sqrt{t}} \qquad \text{(eq.23)}$$

where is $\Delta m_t = \Delta m_t - \Delta m_0$, and Δm_t (kg m^{-2}) is the mass gain per surface area after time t (s). The same equation used for evaporation experiments too.

The analysis of water absorption was also carried out by spray technique: water was sprayed on the surface by means of nozzle. As for the absorption test also for spray test mortars were made impermeable with silicon sealant to prevent water suction or evaporation from other surfaces. Specimens were placed on a vertically inclined support (fig. 3.14), and then sprayed with distilled water, from a 10 cm distance, for 4 minutes with mass flow rate 2 g/min, which is equivalent to 12 mm rainfall.

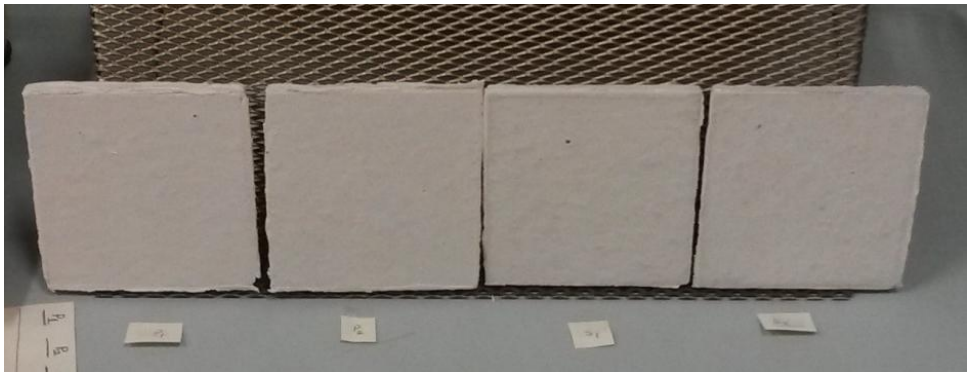

Figure 3.14 - Spray technique - vertically inclined samples.

Every sample was weighed before spraying and after spraying at times, 0, 5 min, 10 min, 15 min, 20 min, 30 min, 40 min, 60 min, 80 min, 100 min, 2 h, 3 h, 4 h, 6 h and 8 h, to determine the decrease in mass. In this method the samples used for absorption test were also reused to evaluate possible changes after the first exposure to water compared to pristine samples.

In order to establish possible differences in water absorption arising from photoinduced hydrophilicity due to TiO_2 addition, absorption and spray technique tests also were carried out under UV irradiation with intensity 2000 mW/cm^2. For water absorption tests performed with UV, a quartz container was used to allow the irradiation of the surface of the samples exposed to contact with water, i.e. the bottom surface (fig. 3.15). In order to ensure the maintaining of the correct water level, since evaporation constantly decreases the level, a measuring cylinder was used to stabilize it. Concerning the spray technique, samples were irradiated before the experiment for one hour and during evaporation for eight hours. Two different UV light sources, black light blue lamp and 300 W Ultra-Vitalux Osram lamp, were used to assess the possible effects of only UV irradiation and UV irradiation combined with source such as consequently heating provided by the osram lamp.

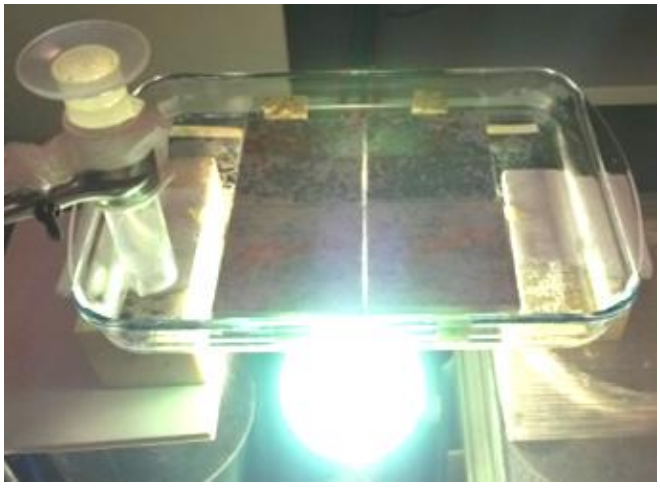

Figure 3.15 - Absorption test under UV irradiation.

3.2.3 Exposure Test

Self-cleaning behavior does not depend on only the material composition, but also atmospheric conditions, including UV radiation, atmospheric pollutants, rain, moisture, temperature variations, snow, wind, affect the performance[6,9]. However, the extent of these factors contribution to self cleaning performance is still a controversial issue.

Considering the mechanism, the most relevant parameters that enhance the self-cleaning effect are expected to be the amount of radiation reaching the surface during the day, and the time of wetness[50]. The correlation between radiation and performance can be divided into three limiting cases: i) for $E \leq 250$ W/m² degradation increases proportional to irradiance linearly, ii) at very low range of irradiance ($E \approx 15$ W/m²) the dependency deviates from this linear relation, iii) for $E > 250$ W/m² the photocatalytic activity grows with the square root of irradiance[83,84]. Rain water is essential for superhydrophilic effect, and in the case of bulk mixtures, it may also help to restore of the initial color of the material by climatic soiling especially along with wind sweeping[85]. Furthermore, temperature and humidity also influence the self-cleaning ability. An increase in temperature results in an increase in photocatalytic activity due to acceleration of the photodecomposition rate[86] and thermal effects, such as evaporation of pollutants[87], consequently causing loss of contaminants. In the case of relative humidity there is a contradiction, some studies argues that high values of relative humidity provide more accentuated hydrophilic effect which results in prevention of pollutants from being absorbed on the surface[19,88],but according to other studies degradation rate decreases linearly with increasing relative humidity starting from 10%, since water competes for free sites at the catalyst surface and can be considered as an additional reactant[89]. It is also important to mention that when a photoactive material is subjected to cycles of deactivation, it still keeps its photocatalytic ability, since its surface is regenerated[9].

In order to establish a relationship between these environmental parameters and the self-cleaning attitude induced by the presence of a photoactive component, atmospheric exposure tests were performed on glass fiber reinforced commercial mortars both anatase-containing and standard ones. Two surface finishing conditions were chosen, sandblasted and smooth, to evaluate the effect of different surface morphology on self-cleaning performance. As can be seen in figure 3.16, sandblasted and smooth samples have different textures: smooth ones have glossy, sandblasted ones have rough surface finishes. Also, in the case of sandblasting, glass fibers are exposed on the surface of the mortars.

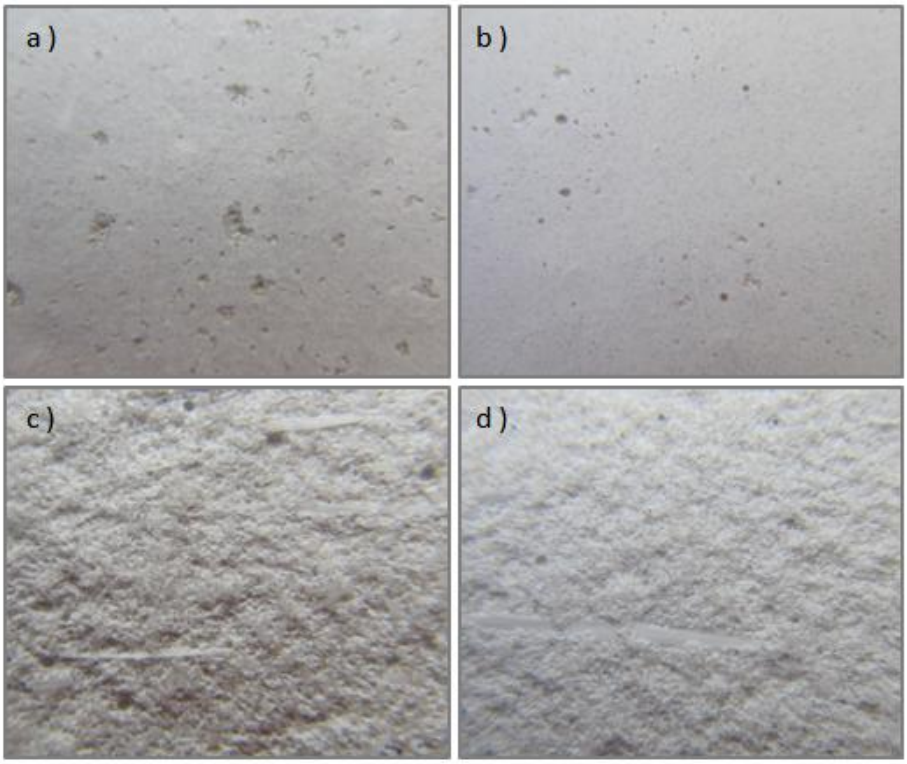

Figure 3.16 - Surface structure of mortar samples - a) standard smooth, b) anatase-containing smooth, c) standard sandblasted, d) anatase-containing sandblasted.

3.2.3.1 Experimental Setup

Samples were exposed in urban environment, on an unshadowed rooftop of a university building, in Milano (Italy), approximately 32 m altitude, for a period of 2 years (October 2011 - October 2013), to obtain valuable information on a large scale change of air quality as well as on the long-term behavior of the materials. They were positioned facing both north and south with multiple inclinations (fig. 3.17) to have a wider understanding of the possible variations of efficiency in different irradiation conditions on vertical surfaces, compared to horizontal, inclined and sheltered ones, which is particularly connected with the wetting extent during rain event.

All samples are labeled with indications referring to their characteristics, respectively:

Sample composition (S: standard, T: with TiO_2)
Finishing (L: smooth, S: sandblasted)
Exposure orientation (N: north, S: south)
Inclination: (H: horizontal, S: sheltered, I: inclined, V: vertical)

There replicates were used for each material and for each exposure orientation. After the first year, for further investigations with laboratory tests, some samples were withdrawn, consequently the experiment continued with a reduced amount of specimens. Figure 3.18 reports a schematic illustration of the positioning of samples, and the indication of which specimens were withdrawn.

Figure 3.17 - Specimens exposed facing south.

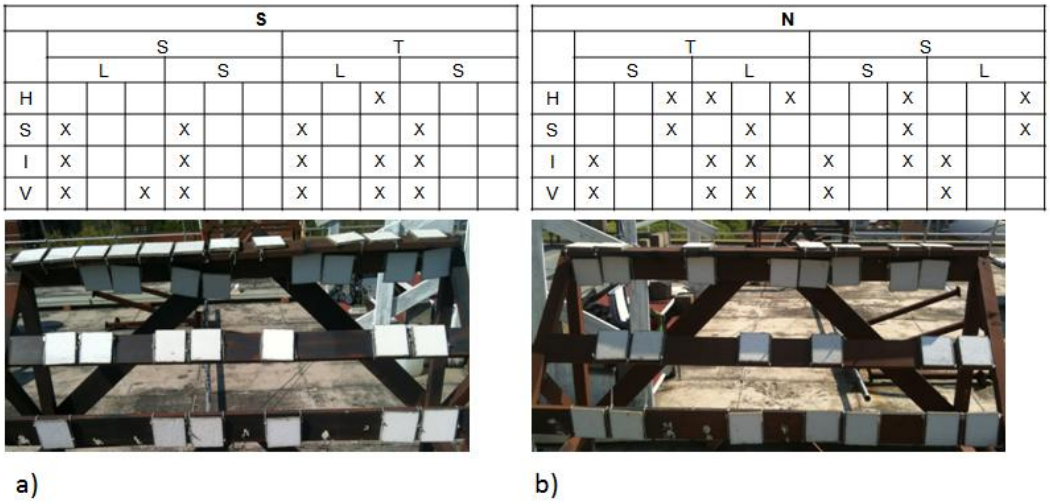

S												
	S						T					
	L			S			L			S		
H									X			
S	X			X			X			X		
I	X			X			X		X	X		
V	X		X	X			X		X	X		

N												
	T						S					
	S			L			S			L		
H			X	X		X			X			X
S			X		X				X			X
I	X			X	X		X		X	X		
V	X			X	X		X			X		

a) b)

Figure 3.18 - Specimens after the first year (X: withdrawn sample) - a) facing south, b) facing north.

3.2.3.2 Evaluation Method

The possible onset of self-cleaning behavior was observed by monitoring the variations in visible light solar reflectance and surface color of the exposed samples with a portable spectrophotometer (Konica Minolta spectrophotometer CM-2600d), which measures the spectral reflectance of the surface every 10 nm in the visible light range (360-740 nm).

Meteorological data were collected by the local environmental agency (ARPA– Regional Agency for Environmental Protection), from an atmospheric station located 0.5 km east from the exposure site. Data include hourly amounts of mean radiation, mean temperature, relative humidity, total precipitation, wind velocity, wind direction and air quality parameters (PM 2.5, PM10, NO_x). Data were then cumulated in daily amounts to establish a relationship between the change in material colorimetric measurements and atmospheric parameters.

Color measurements performed were evaluated by monitoring the variation of color coordinates in the CIELab space as described in Chapter 3.2.1.2.1 as an indicative parameter of the photoactivated self-cleaning attitude of samples. TiO_2 addition increases the materials lightness, which is a typical effect of TiO_2 powders, given their high refractive index[49]. Moreover, different surface finishing gives different initial lightness at the beginning of the test. Thus, instead of overall color change ΔE, single color coordinates were analyzed. Attention was focused on variation of the lightness ΔL*and Δb* as representative of dirt accumulation on the surface.

The visible solar reflectance ρ_v was also calculated. Calculation requires the integration of the spectral reflectance values of each sample with the application of weighting factor for each wavelength (eq.24). Since no specific standard exists for the specific wavelength interval 360-740 nm, the procedure was derived from ISO 9050.

$$\rho_v = \frac{\Sigma_{\lambda=380\ nm}^{780\ nm} \rho(\lambda) D_\lambda V(\lambda) \Delta\lambda}{\Sigma_{\lambda=380\ nm}^{780\ nm} D_\lambda V(\lambda) \Delta\lambda} \qquad \text{(eq.24)}$$

where D_λ is the relative spectral distribution of illuminant D65 (corresponding to the illumination of the spectrophotometer used), $\rho(\lambda)$ is the spectral reflectance, $V(\lambda)$ is the spectral luminous efficiency for photopic vision defining the standard observer for photometry, $\Delta\lambda$ is the wavelength interval.

Chapter 4

Results and Discussion

4.1 Rhodamine B method

The photocatalytic activities of different photoactive construction materials, such as mortars, roofing tiles and siloxane coatings, were evaluated by applying different test methods, in order to identify the optimal test conditions to highlight differences in photoactivity. In fact, photocatalytic tests need development in order to establish more reliable and sensitive methods, specially when analyzing similar materials. This need is particularly stringent in this work, since one of the objectives is to evaluate changes in photocatalytic efficiency in materials that have been exposed to external atmosphere and aged for a long time: the small amount of samples available couldn't allow multiple tests, which makes particularly important the reliability of the test method. The following paragraph discusses the different test methodologies proposed and the early results provided on various materials.

4.1.1 Choice of Rh B Concentration

In order to choose the Rh B concentration that allows the most reliable comparisons among photoactive materials, comparative analyses were performed by stain test method with the application of five different concentrations (1×10^{-6},

5×10^{-6}, 1×10^{-5}, 5×10^{-5}, 1×10^{-4} mol/l) of Rh B solution on photoactive glass fiber reinforced commercial mortar specimens. For each characterization, the mean values of a series of at least 3 measurements were calculated. A UV light source (300 W Ultra-Vitalux Osram lamp) with an intensity range 750±50 μW/cm^2 was used. After measurements a correction factor depending on stain areas was applied, and the percent variation in lightness $\Delta L^*_{\%}$ was evaluated (fig. 4.1).

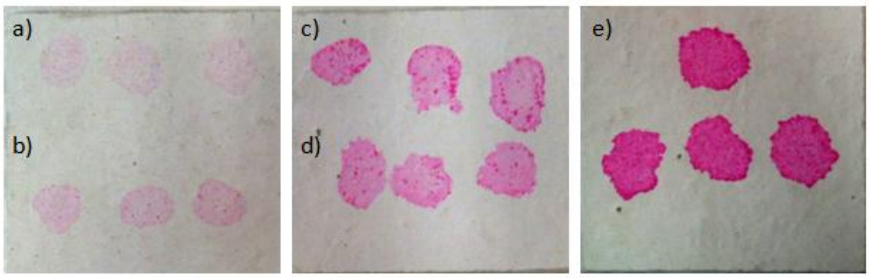

Figure 4.1 - Stain test for 5 different concentrations, [mol/l] - a) 1×10^{-6}, b) 5×10^{-6}, c) 1×10^{-5}, d) 5×10^{-5}, e) 1×10^{-4}.

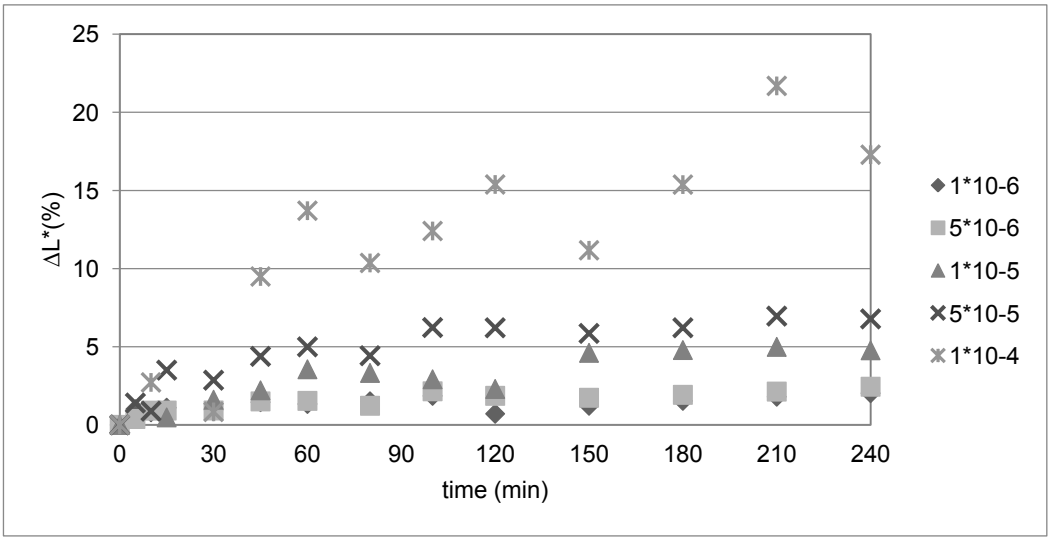

Figure 4.2 - The percent of lightness variation, $\Delta L^*_{\%}$ values - for five different concentration stain test performed on photoactive glass fiber reinforced commercial mortars.

As can be seen from figure 4.2 increasing amount of Rh B in solution, magnify the differences in discoloration. The concentrations lower than 1×10^{-5} mol/l gives

similar trendlines and, those greater than 5×10^{-5} mol/l have more evident fluctuations after the first 2 hour. In the 4th hour decrease in the percent variation in lightness is recovered at concentrations 1×10^{-4} mol/l, which would signify an intensification in dye color. This is clearly an artifact caused by exceeding fluctuations, which makes this concentration reading unreliable.

Although the most commonly applied dye concentration found in literature works is 1×10^{-4} mol/l, which is also selected as critical parameter in the rhodamine B standard test (0.05±0.005 g/l) described in the UNI 11259:2008, in this work 1×10^{-5} mol/l is chosen as best concentration for reliable stain tests performed on white mortars.

4.1.2 Choice of Test Method

To find the best method porous materials were considered first. The stain method revealed to be unstable for both brick and siloxane coating samples. In the case of bricks the red color of the material did not create enough contrast with Rh B to allow quantitative analyses. In fact, in photocatalysis tests, the change in surface color should reach an increase in red hue intensity of at least 12 ($\Delta a^* \geq 12$) compare to initial color, as indicated in UNI 11259. On the other hand, the siloxane coatings had hydrophobic character, which did not allow the formation of uniform stain on the surface (fig. 4.3). A relevant absorption of Rh B solution in both materials further impeded tests performance.

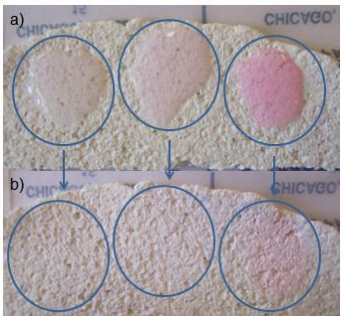

Figure 4.3 - Different concentration of Rh B solution on siloxane coating surface - a) during application of the solution, b) after drying.

Siloxane coatings were then examined with immersion and immersion-drying test methods. The samples were first immersed in a test solution of Rh B with a concentration of 1×10^{-4} mol/l, and either directly subjected to blacklight blue lamp (UV light source) with an intensity range 2000 ± 50 μW/cm^2, or kept in the solution for 24 hour and afterwards let dry. The latter test could only be performed on light colored substrates for the same reasons described in the case of the stain test.

In the presence of photoactive materials the change in Rh B concentration (immersion test) (fig. 4.4) and the percent variation in a* (immersion-drying test) (fig. 4.5) increased with increasing irradiation time. In both tests, a slow decrease in concentration and a* was observed in standard samples and ascribed to photolytic degradation of the dye due to UV irradiation.

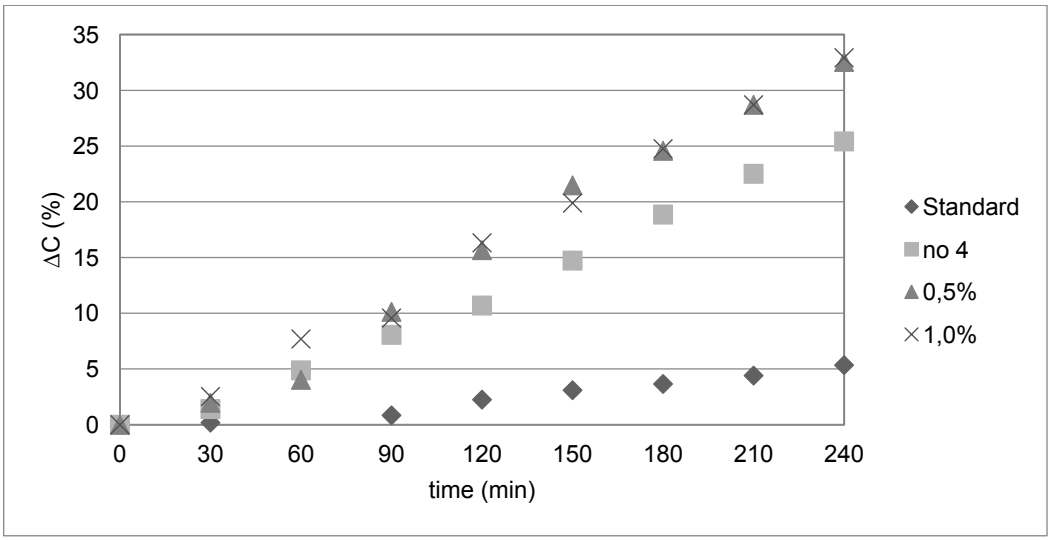

Figure 4.4 - Siloxane coating immersion test - percent variation of concentration, ΔC (%).

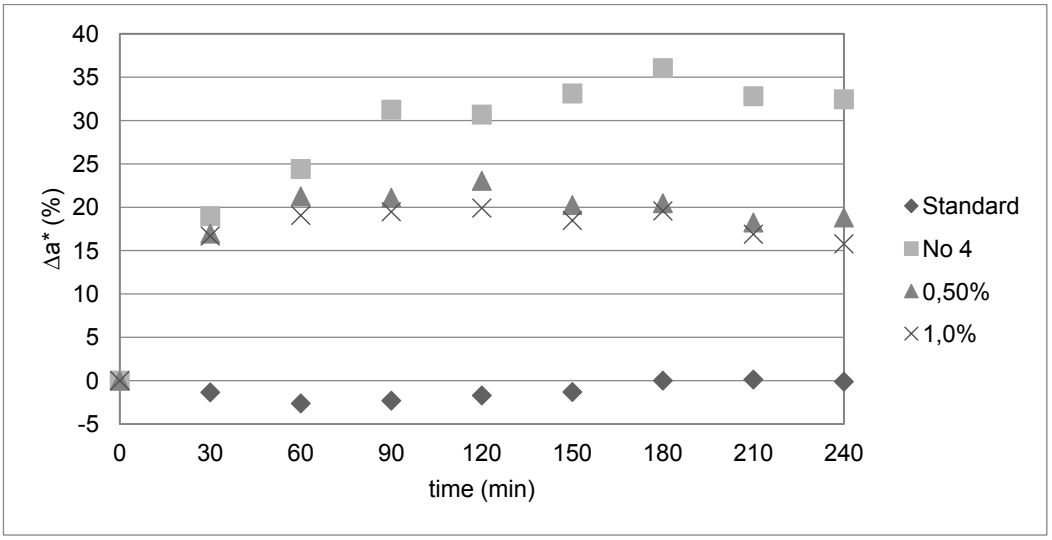

Figure 4.5 - Siloxane coating immersion-drying test - percent variation of a*, Δa*(%).

Although the decrease in concentration in immersion tests is linear, the variation of a* in immersion-drying test is prevalently logarithmic. A particular behavior is shown by sample No 4 in which the amount of TiO_2 is not known. In immersion test sample No 4 exhibited lower photocatalytic efficiency compared with specimens containing 0.5-1% of TiO_2, while in immersion-drying tests the opposite behaviors observed. In spite of this difficulty in judgment, all three materials correctly showed a clear photocatalytic efficiency. Therefore both methods were considered suitable in testing substrates with clear color.

Finally, the ring test method was applied to bricks to understand its reliability. For this substrate, the ring method represented the only choice due to materials high porosity and color. For the ring test different experimental paths were followed, all aimed at avoiding the evaporation of Rh B solution confined in the ring. To obtain the sealing between the surface and the ring, two methods were evaluated: metal ring covered with silicon ring and then fixed with silicon sealant, and metal ring directly covered with silicon sealant. Finally, the brick samples were wrapped with parafilm to avoid lateral evaporation of the pure-conditioning treatment and

consequent absorption of test solution, or immersed in water. Irradiation was set to a UV intensity of 1000 ±50 μW/cm^2 for two hours.

A reduction in solution volume was observed in all conditions, both in the ring and in a side cuvette containing the same volume of liquid (Table 4.1). Therefore, the combination of preconditioning and parafilm avoided the solution absorption by the brick, while certain evaporation occurred towards the environment. Same effect observed without parafilm, keeping the brick immersed in water to maintain it presaturated. The use of a silicon ring, to improve adhesion of metallic ring to the brick, caused decrease in concentration due to suction of dye by the silicon ring, which could mislead the evaporation; this experimental condition was thus discarded.

Table 4.1 - Ring test on brick samples - change in Rh B concentration and volume during 2-hour UV irradiation.

Time (min)	Reference			Silicon ring + Water			Parafilm			Silicon ring + Parafilm		
	Trans.	V (ml)	ΔV %	Trans.	V (ml)	ΔV %	Trans.	V (ml)	ΔV %	Trans.	V (ml)	ΔV %
0	-1,022	5,00	0	-1,022	5,00	0	-1,022	5,00	0	-1,022	5,00	0
60	-1,025	4,75	5	-0,920	4,75	5	-0,984	4,49	10	-0,966	3,68	26
120	-1,023	4,55	9	-0,955	4,55	9	-0,920	4,20	16	-0,946	4,15	17

For this reason further experiments were done without the silicon ring, using parafilm (fig. 4.6 (a,c)), to cover the samples. The immersion step was performed in a pre-conditioning solution with Rh B with concentration 1×10^{-5} mol/l instead of water, to avoid solution contamination and consequent concentration decrease due to release of water in the ring area (fig. 4.6 (b)). Also during the experiments samples were covered with quartz to avoid excessive evaporation (fig. 4.6 (d)).

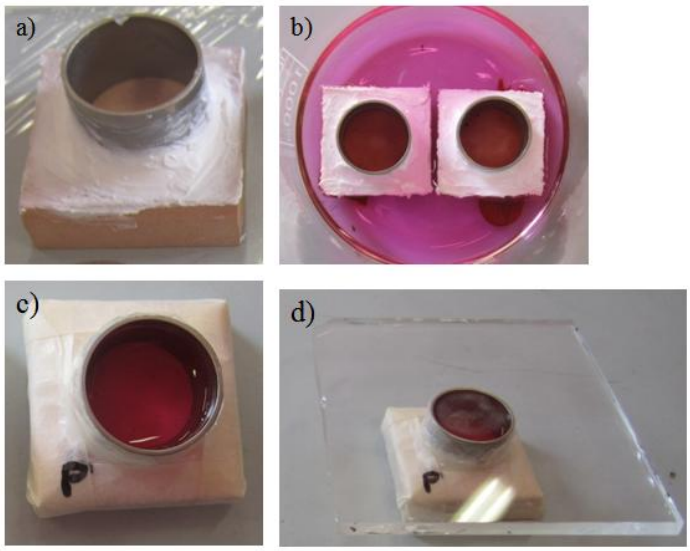

Figure 4.6 - Ring test method - a) with metal ring covered with silicon, b) immersion in pre-conditioning of Rh B solution, c) covering with parafilm, and insertion of Rh B test solution in ring, d) with quartz glass.

It is seen from the figure 4.7 that the concentration change in photoactive samples is 15% higher than that observed in standard samples. Again a linear increase in Rh B degradation is observed in photoactive samples.

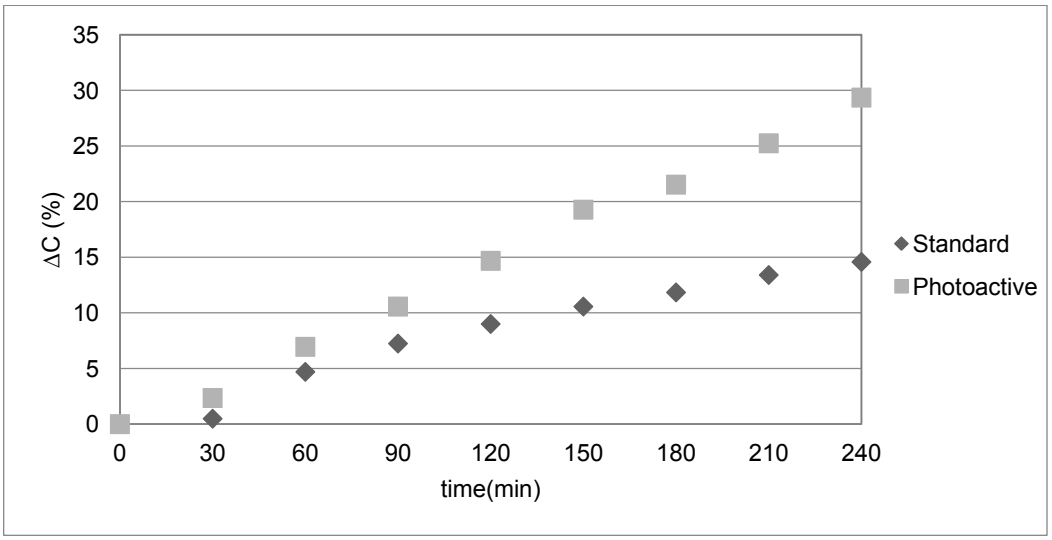

Figure 4.7 - Ring test on photoactive and standard brick samples - percent variation of concentration, ΔC (%).

Another test was performed on the samples with multiple depositions of TiO_2 sol-gel layers (from 2 to 6). The results did not indicate photocatalytic activity, producing results similar to those of the standard sample (fig.4.8). It was conclude that materials were not photoactive. Yet the repeatability of results confirmed the reliability of the ring test method.

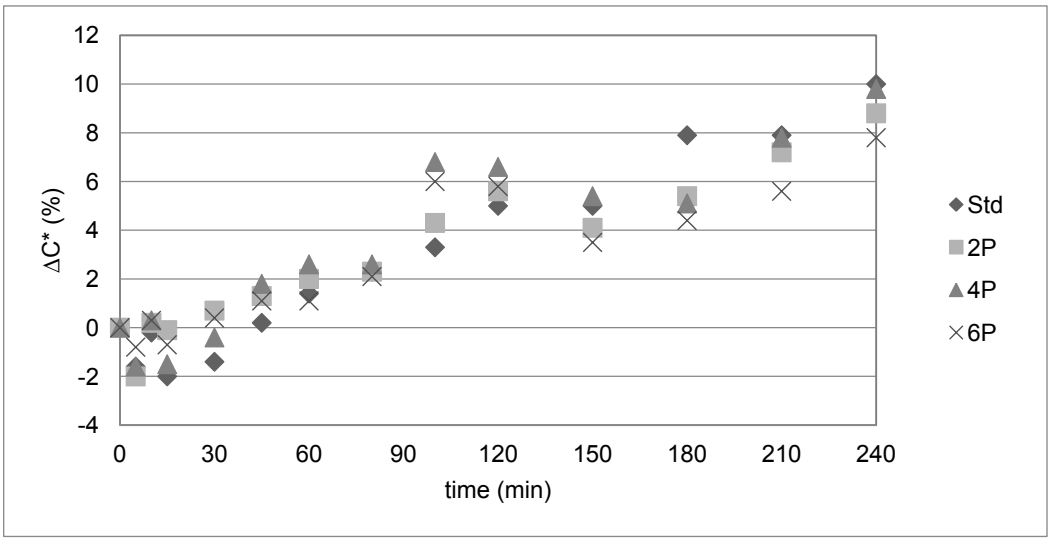

Figure 4.8 - Ring test on brick samples with different amount of TiO_2 - percent variation of concentration, ΔC (%).

4.1.3 Evaluation of Anatase-Containing Glass Fiber Reinforced Mortars

The photocatalytic efficiency of photoactive glass fiber reinforced mortars was evaluated by applying the most effective method among the ones tested, which was found to be the stain test. The reasons for this choice are: the mortars are white, thus there is no issue in using reflectometry, which is more reliable compared to concentration measurements, where evaporation problems might affect the experiment and induce misleading evaluations; moreover, for stain test a standard[69] has already been proposed and approved by Italian committees.

To evaluate the efficiency of the mortar a comparative analysis was performed on photoactive and standard samples. For each characterization, the mean values of a series of at least 3 measurements were calculated (fig. 4.9).

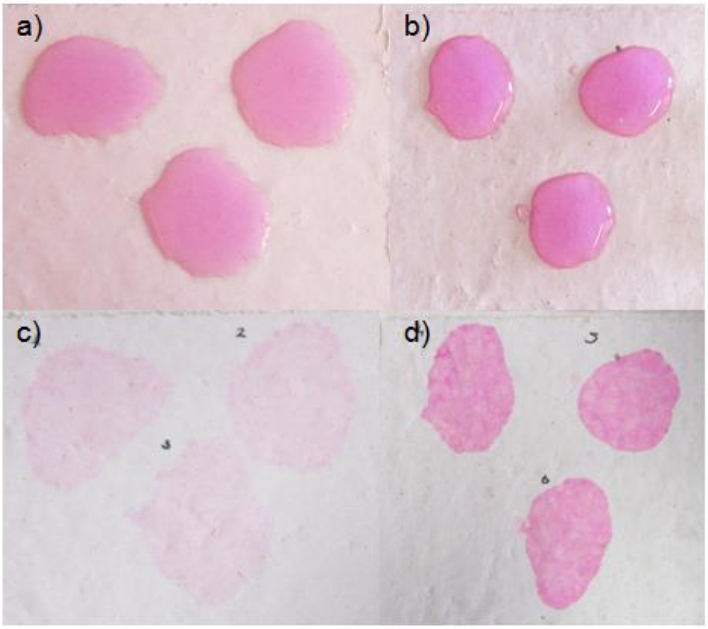

4.9 - Glass fiber reinforced mortars - a) application of dye on anatase-containing sample, b) application of dye on standard sample, c) anatase-containing sample after drying, d) standard sample after drying.

Results are reported in figure 4.10. After 80 min of light exposure the degradation of Rh B on photoactive mortars become very evident compared to standard ones, with a decrease in a* 35% higher than that observed on the untreated one. According to UNI 11259 standard, the tested material is considered photocatalytic if the percentage of decrease in color intensity of the dye is greater than 20% after 4 hours (Δa_4^*>20%). The change in a* was found to be 43% on the photocatalytic sample, and 7% on the standard sample: as a result, the photocatalytic ability of TiO_2-containing mortar allowed the degradation of 36% of the organic contaminant by photocatalytic action, which satisfies the requirement, while the remaining 7% is due to the dye photolysis.

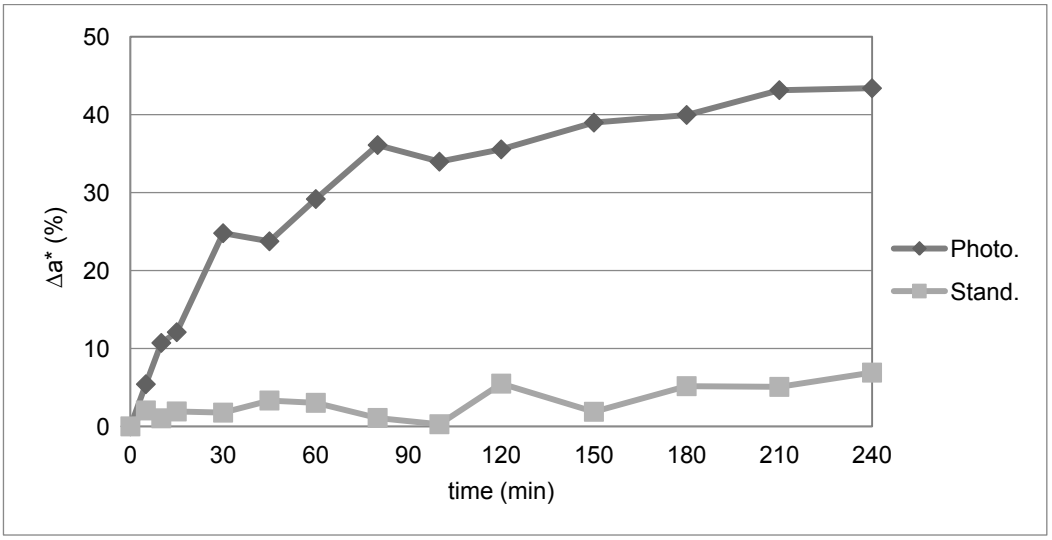

Figure 4.10 - Stain test on glass fiber reinforced mortar - percent variation of a*, $\Delta a^*_{\%}$.

4.2 Absorption-Evaporation Tests

Percentage of water absorption is an evaluation of the pore volume or porosity of material after, which is occupied by water in saturated state and rate of water absorption is a measure of the capillary forces exerted by the pore structure causing fluids to be drawn into the body of the material[52]. For this reason the results of absorption-evaporation tests were compared with the porosity, pore size distribution and permeability of the mortars, which were determined by means of mercury intrusion porosimetry (MIP) and was taken from Department of Structural Engineering, summarized in table 4.2, and figure 4.11.

Table 4.2 - Mercury intrusion porosimetry results for standard and photoactive mortars.

Parameters	Standard	Photoactive
Total Pore Area, [m²/g]	4,303	5,944
Median Pore Radius (Area), [μm]	0,0066	0,0075
Average Pore Radius (2V/A), [μm]	0,0504	0,0529
Bulk Density at 1.52 psia, [g/mL]	1,9947	1,8066
Apparent (skeletal) Density, [g/mL]	2,5458	2,5225
Porosity [%]	21,6473	28,3822
Characteristic Pore length, [μm]	0,7529	0,5592
Tortuosity	26,9153	32,3504

Pores appear as a result of the poor packing of particles of aggregates. These voids will be partly filled by hydration products as the setting process of the cement takes place[65]. As can be seen from table 4.2, pores are larger both in diameter and number in photoactive samples, which is due to formation of lower amounts of hydration products[79]. Adsorption depends on both the capillary pressure, which is related to the pore space in the capillary and gel pores, and effective porosity.

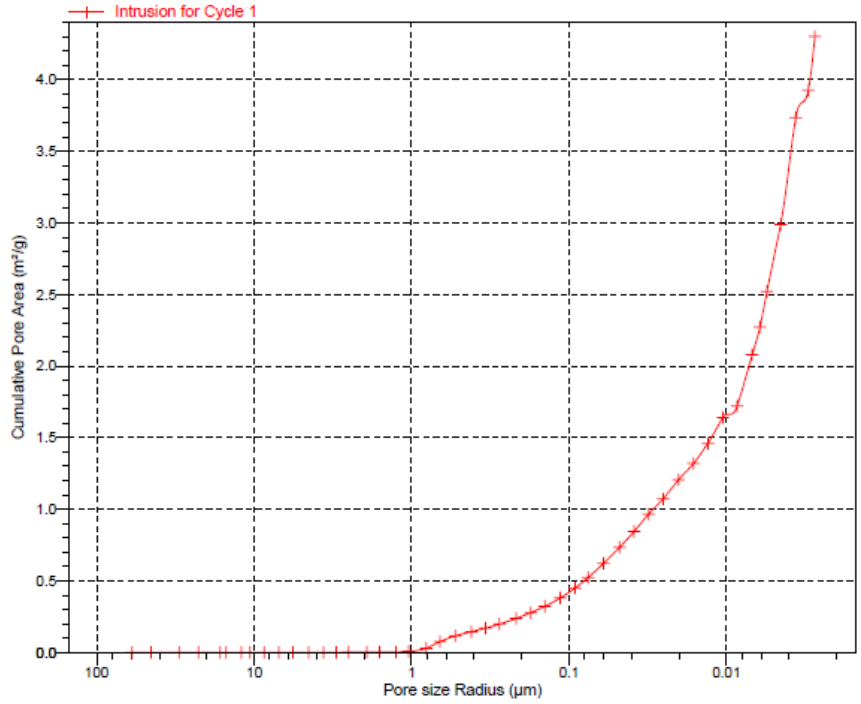

a)

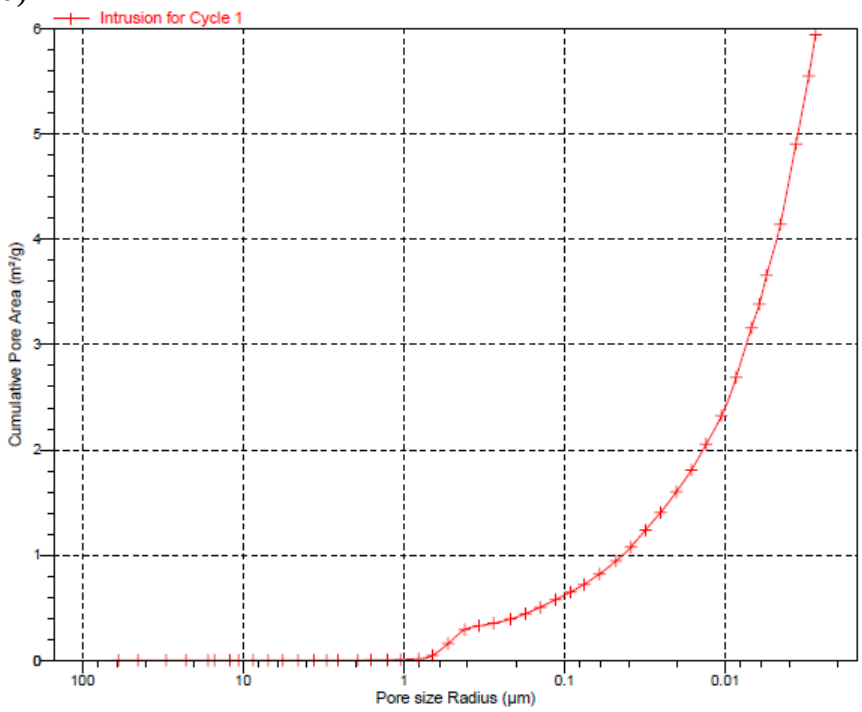

b)

Figure 4.11 - Cumulative pore area vs. pore size - a) standard samples, b) photoactive samples.

Water capillary absorption-evaporation, evaluated through ISO 15148 standard test method, gave significant differences between the photoctive and standard mortars. As can be seen in table 4.3 and 4.4, without UV exposure the mass gain in absorption and consequently water absorption coefficients, after 24 hours, were increased in photoactive samples. The increase in mass which is directly related to the flow of fluids through continuous pores[80] can be explained by the physical and chemical properties of the TiO_2 nanoparticle containing mortar samples, and to an increase in radius, porosity, tortuosity and the continuity of capillaries compare to standard mortar samples as can be seen in table 4.2.

Table 4.3 - Average mass gain after 24-hour of absorption and mass loss after 24-hour of evaporation per surface area, for photoactive and standard samples, with and without UV irradiation.

ΔM_{24} (kg/m^2)	Photoactive	Standard	UV
Absorption	1,29	1,22	no
	0,75	0,40	yes
Evaporation	-0,71	-0,61	no
	-0,66	-0,32	yes

Table 4.4 - Average capillary absorption coefficient after 24-hour of absorption and evaporation coefficient after 24-hour of evaporation, for photoactive and standard samples, with and without UV irradiation.

$A_{w,24}$ (kg/(m^2 s^{0,5}))	Photoactive	Standard	UV
Absorption	$4,4\times10^{-3}$	$4,1\times10^{-3}$	no
	$2,6\times10^{-3}$	$1,4\times10^{-3}$	yes
Evaporation	$-2,4\times10^{-3}$	$-2,1\times10^{-3}$	no
	$-1,5\times10^{-3}$	$-1,1\times10^{-3}$	yes

The increase in mass gain during absorption and its decrease during evaporation under UV irradiation was more evident in photoactive samples compared to standard ones, can be attributed to the onset of super hydrophilicity. On the other hand, under UV light the total amonut of absorbed water was lower compared to non irradiated specimens for both standard and photoactive samples (table 4.4-5, fig. 4.12-13).

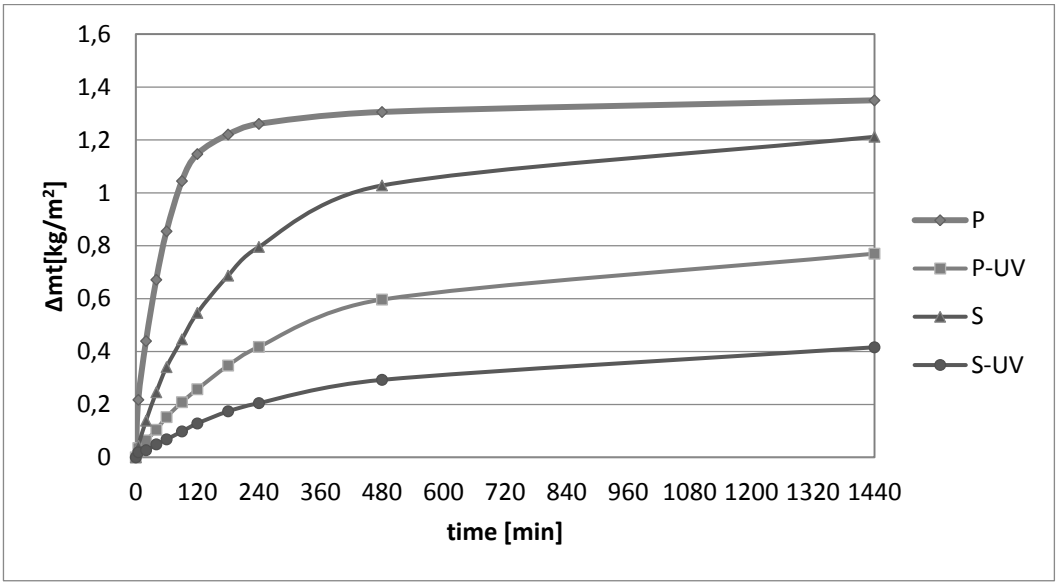

Figure 4.12 - Average mass gain per surface area during 24-hour absorption - P: photoactive, S: standard, UV: irradiation. .

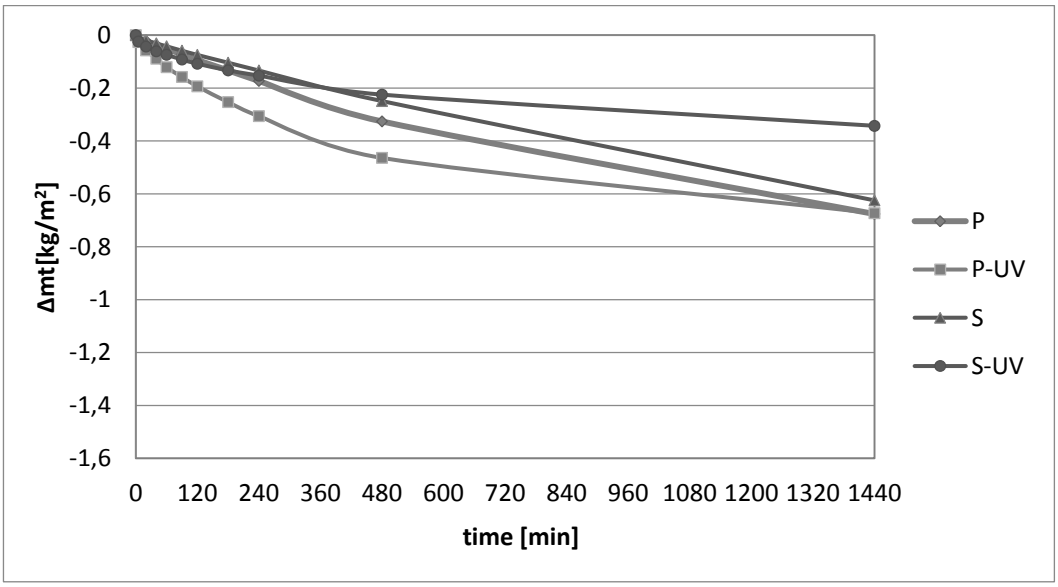

Figure 4.13 - Average mass loss per surface area during 24-hour evaporation - P: photoactive, S: standard, UV: irradiation.

This can be explained by the generation of heat from the UV source, since the increase in temperature causes a decrease in surface tension, which is one of the

parameters for capillary suction. The tests were performed under two different UV sources which generate different amonuts of heat, being that of osram lamp higher than that of blacklight blue lamp to confirm potential influences of the light source on the materials behavior. It was seen that the decrease in the amount of mass gain in the case of osram lamp was higher than that observed tests performed with blacklight blue lamp, confirming the former hypothesis, (fig. 4.14).

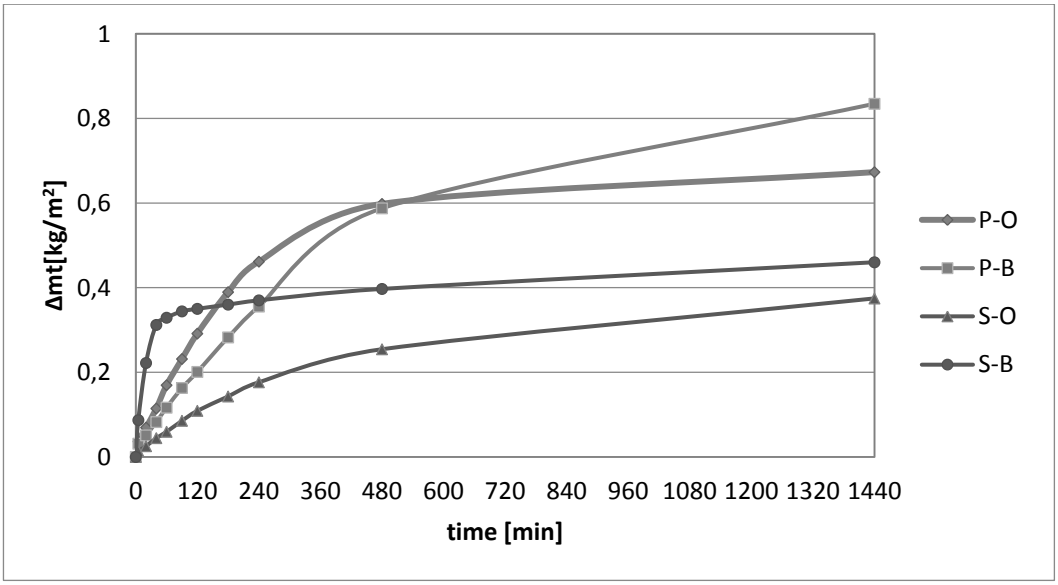

Figure 4.14 - Average mass gain per surface area during 24-hour absorption (with UV) - P: photoactive, S: standard, O: osram lamp, B: blacklight blue lamp.

Without UV irradiation the trend in absorption is different for photoactive and standard samples (fig. 4.15). The water capillary absorption by photoactive samples was rapid in the first two hours, reaching 79% of total mass gain (fig. 4.16); afterwards the trend was almost linear and produced only a slight increase. It is important to find a difference in mass gain trends, since measurements over 24 hours can provide information to model capillary transport over long periods, while the surface effects can be probed with short term measurements.[76] For standard samples a lower absorption rate was observed, with parabolic trend over the first eight hours, during which the suction percentage was 83% of the total. This indicates a difference between the surface structure between the photoactive

and standard samples even in the case of no irradiation, being the former ones more hydrophilic.

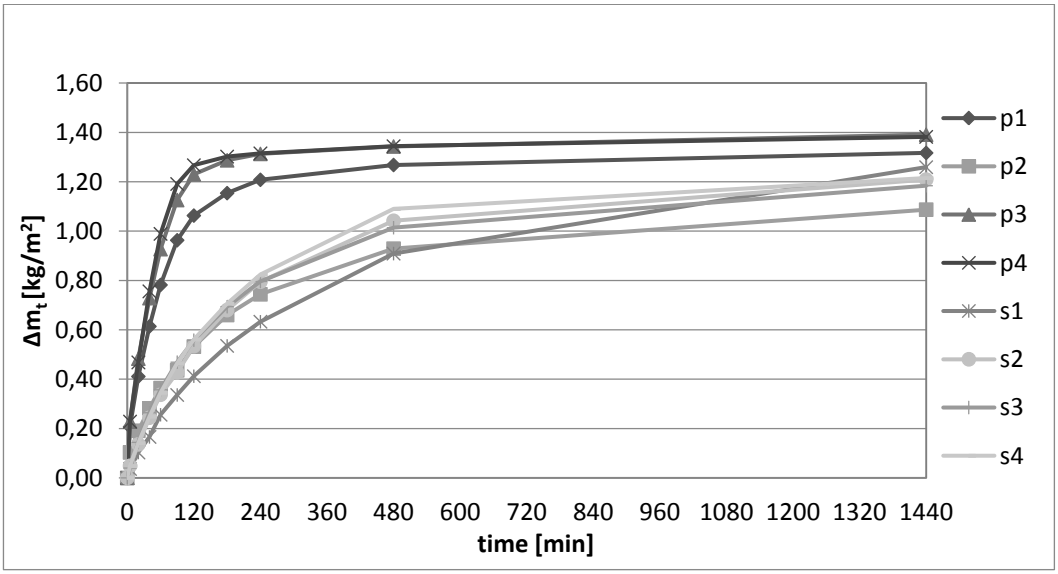

Figure 4.15 - Mass gain per surface area during 24-hour absorption (no UV) - p: photoactive, s: standard.

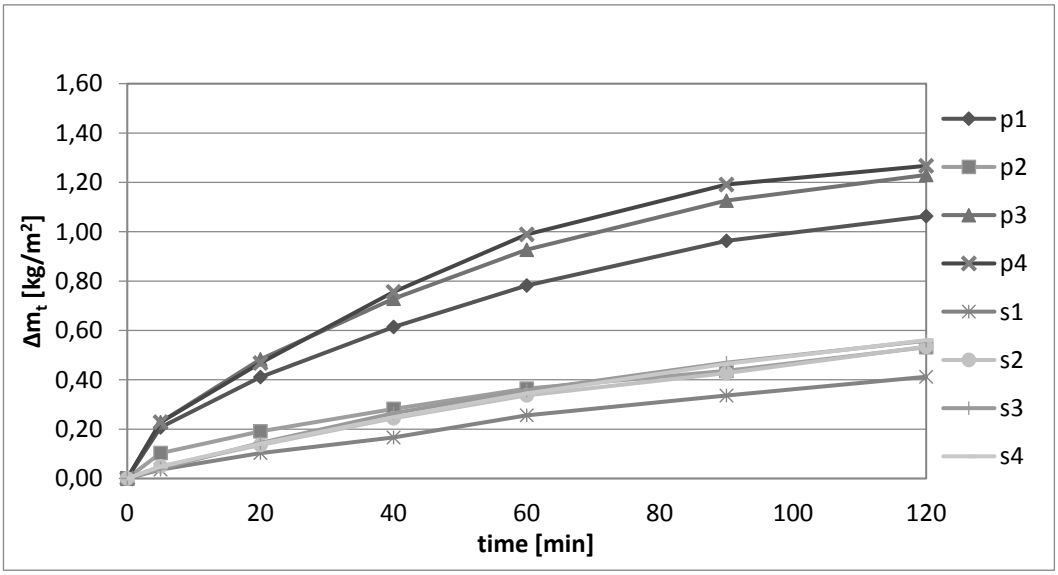

Figure 4.16 - Mass gain per surface area during 2-hour absorption (no UV) - p: photoactive, s: standard.

As already said, UV influences the total amount of absorption due to heat generation. Furthermore, it changes the trend in absorption for photocatalytic samples. Under UV irradiation the photoactive and standard materials presented an identical absorption trends with different overall amounts of water absorption (fig. 4.17). This behavior did not bring any indication of alternation of the surface water absorption due to UV illumination in an evident way.

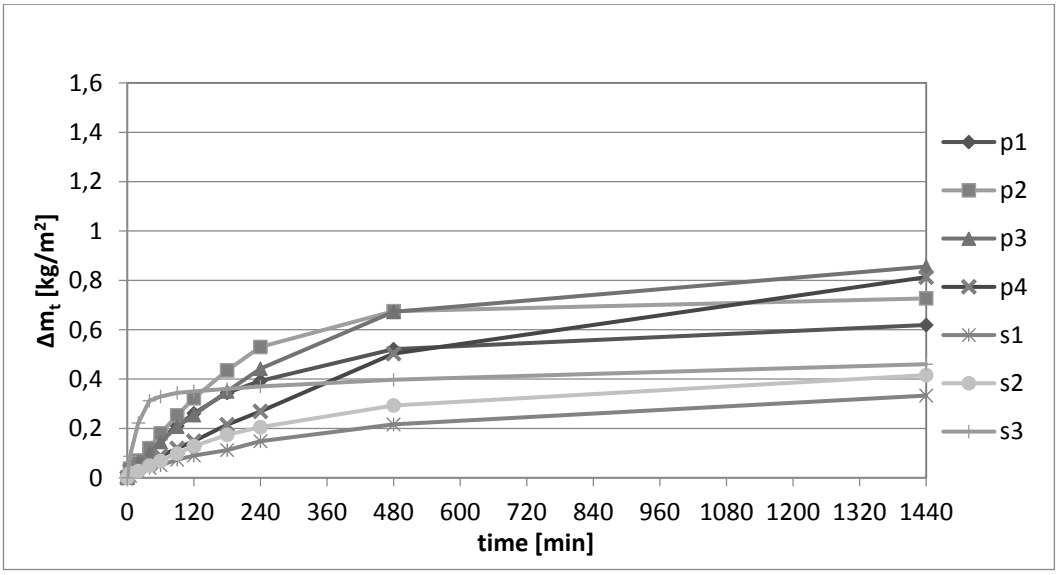

Figure 4.17 - Mass gain per surface area during 24-hour absorption (with UV) - p: photoactive, s: standard.

In the case of evaporation without UV source, the amount of mass loss in photoactive samples compare to standard ones was quite moderate (fig. 4.18). On the other hand, under UV irradiance the photoactive samples showed higher mass loss especially in the first eight hour (fig.4.19-20). This was ascribed to an increase in surface wettability due to UV illumination and consequent more diffuse spreading of water on the whole surface, therefore leading to faster evaporation.

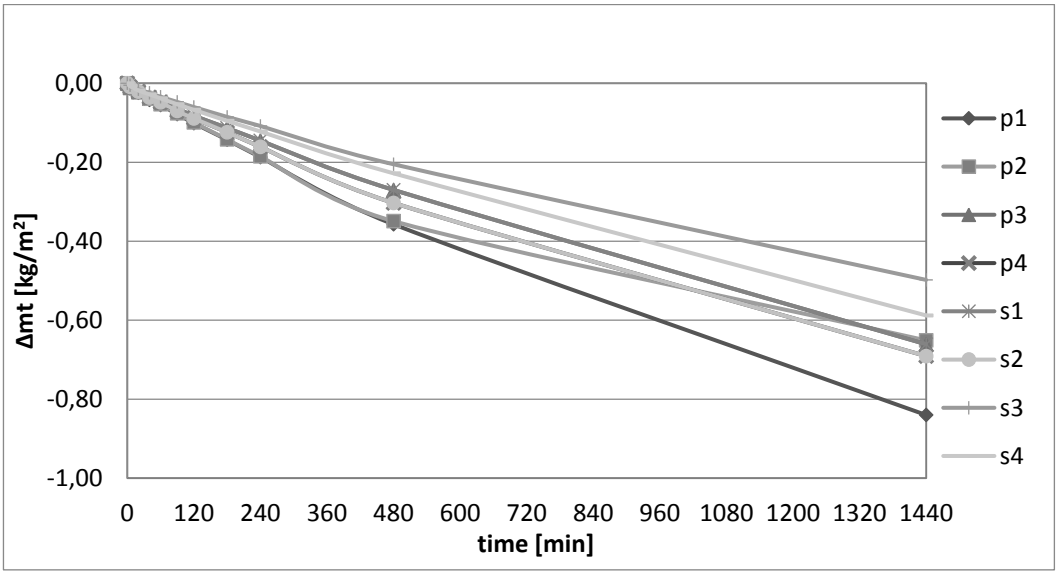

Figure 4.18 - Mass loss per surface area during 24-hour evaporation (no UV) - p: photoactive, s: standard.

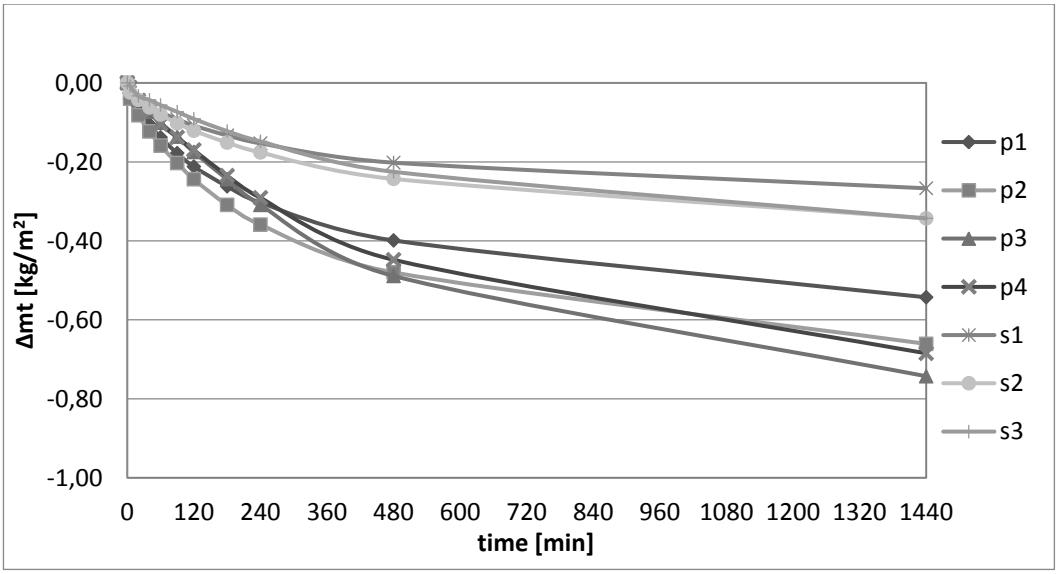

Figure 4.19 - Mass loss per surface area during 24-hour evaporation (with UV) - p: photoactive, s: standard.

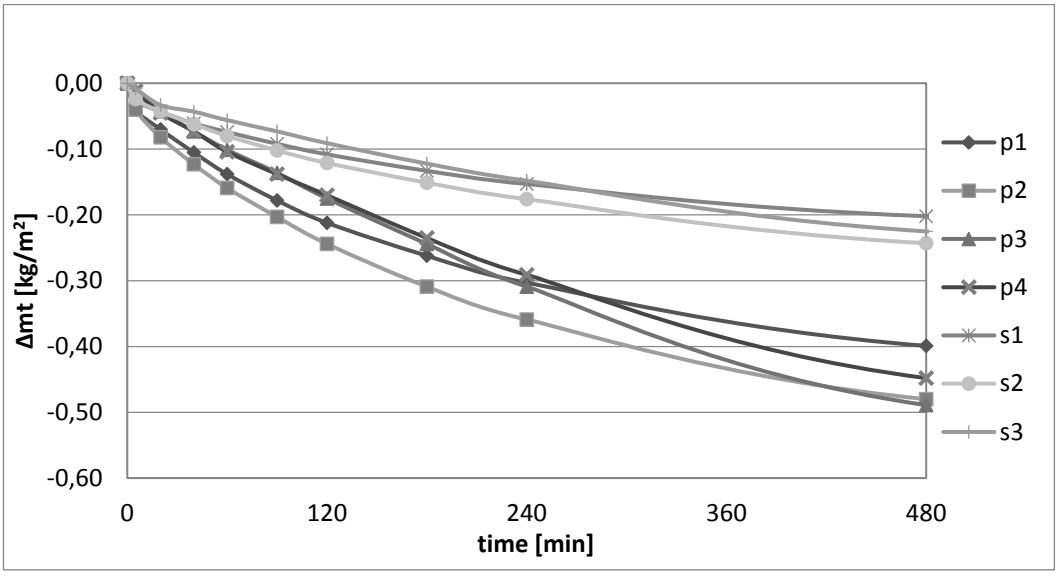

Figure 4.20 - Mass loss per surface area during 8-hour evaporation (with UV) - p: photoactive, s: standard.

Using the spray test method no significant increase in absorption or evaporation was noticed in presence of UV illumination although photoactive mortars showed higher values of mass gain in absorption compare to standard samples (without UV, standard samples gained 0.38 g, photoactive ones 0.57 g; with UV the values are 0.47 and 0.65 respectively) (table 4.5). The difference between photoactive and standard samples in absence of UV exposure, 50%, was higher compared to that observed under UV irradiation, 38%. Correspondingly, the increase in total amount of water absorbed with UV illumination was higher for the standard samples compared to the photoactive ones (24% vs. 14%, respectively). Interestingly, in presence of UV both materials lost more water by evaporation than they absorbed. This again may be related to heat generation of the lamp, which induces a partial drying of the material compared with its usual equilibrium conditions with laboratory environment.

Table 4.5 - Average mass gain and mass loss per surface area after spraying and 8-hour of evaporation - P: photoactive, S: standard, UV: irradiation, U: specimens already used.

Δm_t[kg/m^2]/Sample	P	S	P-UV	S-UV	P-U	S-U	P-UV-U	S-UV-U
Absorption	0,57	0,38	0,65	0,47	1,04	0,38	1,44	0,62
Evaporation	-0,53	-0,37	-0,71	-0,51	-0,99	-0,38	-1,28	-0,64

For the long and short term trends of evaporation there is no clear difference between the test performed with or without UV illumination (fig.4.21-24).

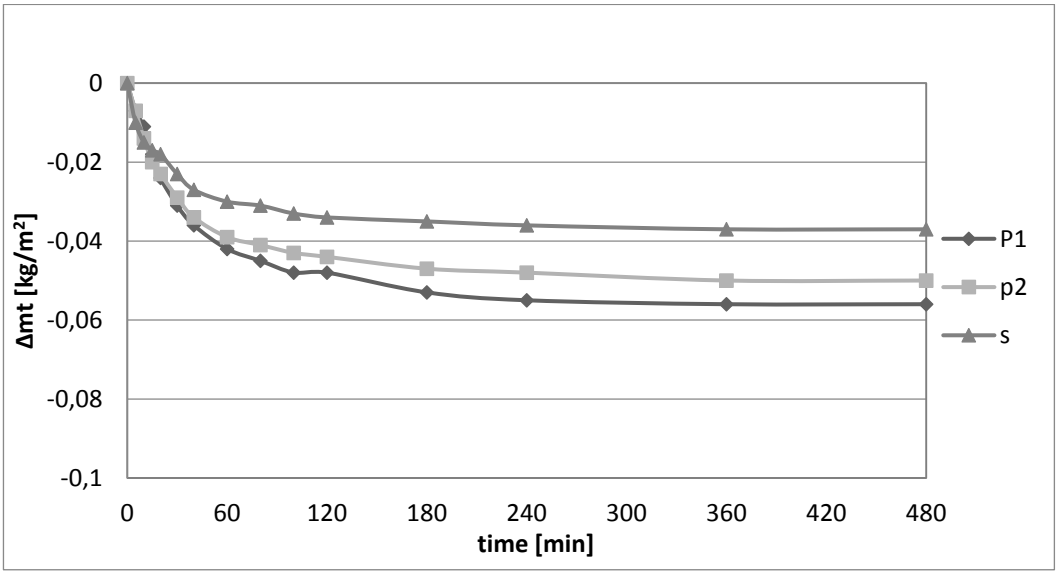

Figure 4.21 - Mass loss per surface area during 8-hour evaporation (no UV) - p: photoactive, s: standard.

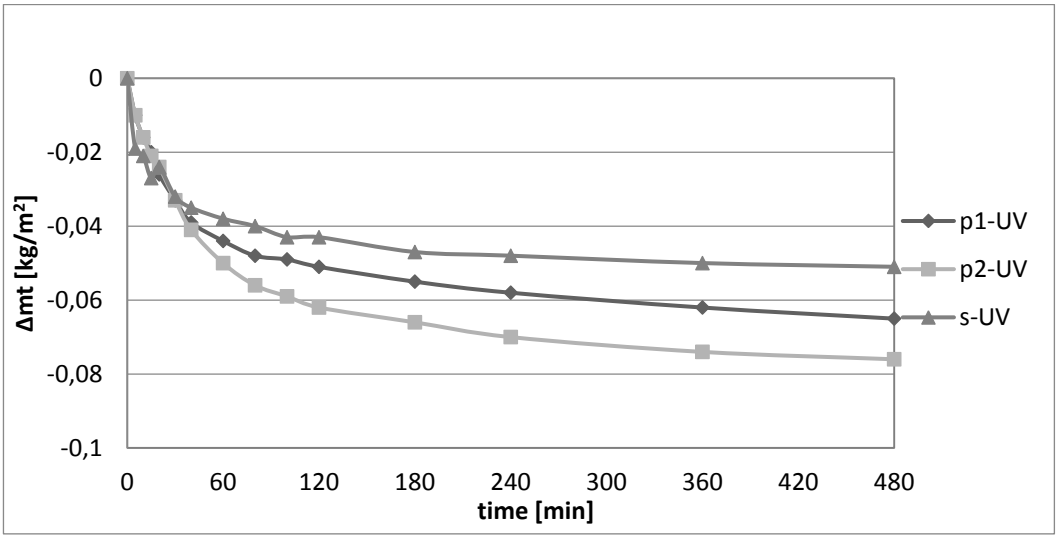

Figure 4.22 - Mass loss per surface area during 8-hour evaporation (with UV) - p: photoactive, s: standard, UV: irradiation.

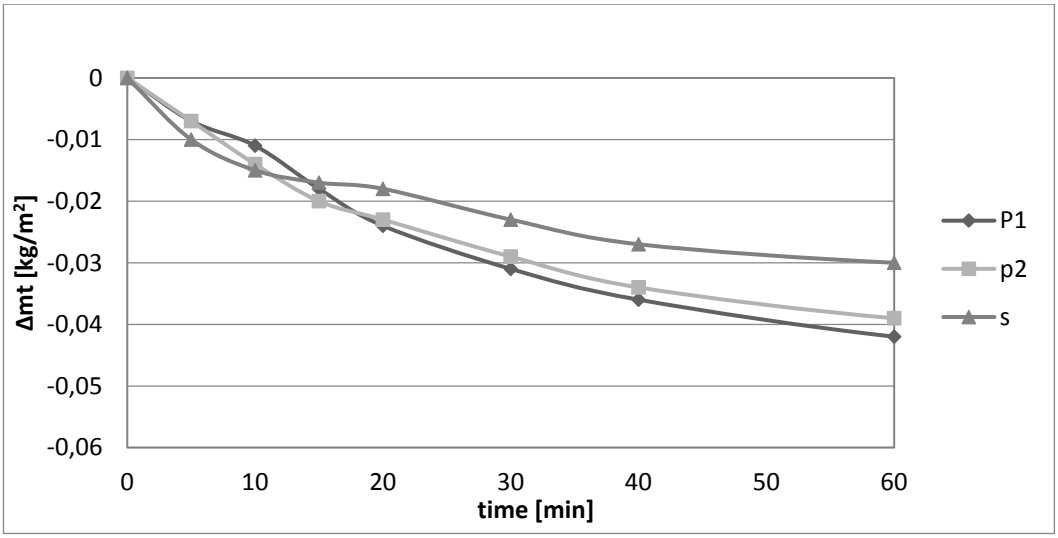

Figure 4.23 - Mass loss per surface area during 1-hour evaporation (no UV) - p: photoactive, s: standard.

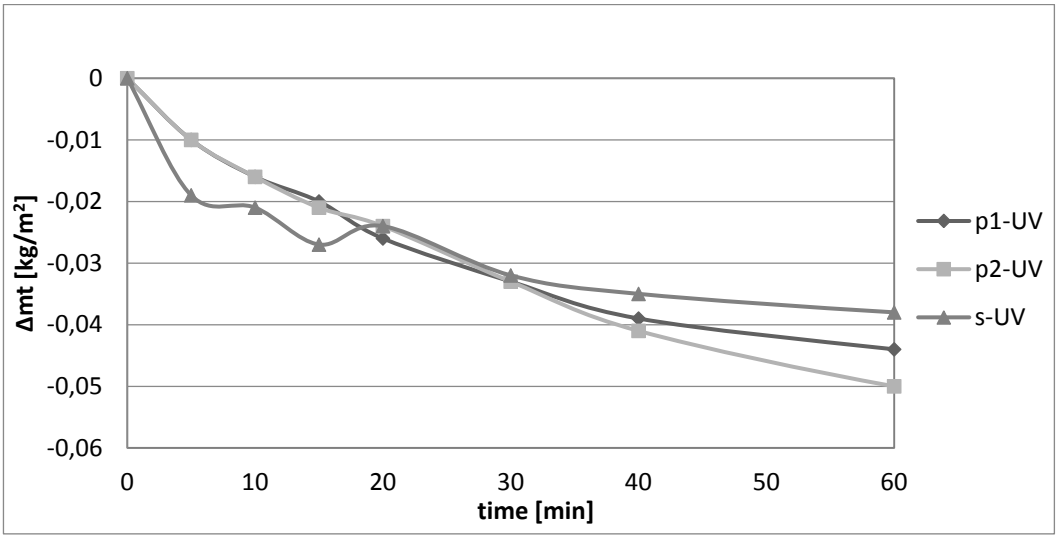

Figure 4.24 - Mass loss per surface area during 1-hour evaporation (with UV) - p: photoactive, s: standard, UV: irradiation.

On the other hand, the increase in water absorption and evaporation in photoactive samples which already used in capillary absorption test is higher compared to that of pristine ones (table 4.5, fig. 4.25-26): this behavior was noticed when performing tests both without and with UV. The increase ranged from 80 to 120 and was observed both in the absorption phase and in the evaporation one. Furthermore, the used standard samples did not show any differences in absorption extent. These increases in already used photoactive samples can be attributed to the change in surface chemistry of the photoactive mortar. Such behavior can be explained by a residual hydroxylation of the already more hydrophobic photocatalytic surface produced during the capillary absorption test.

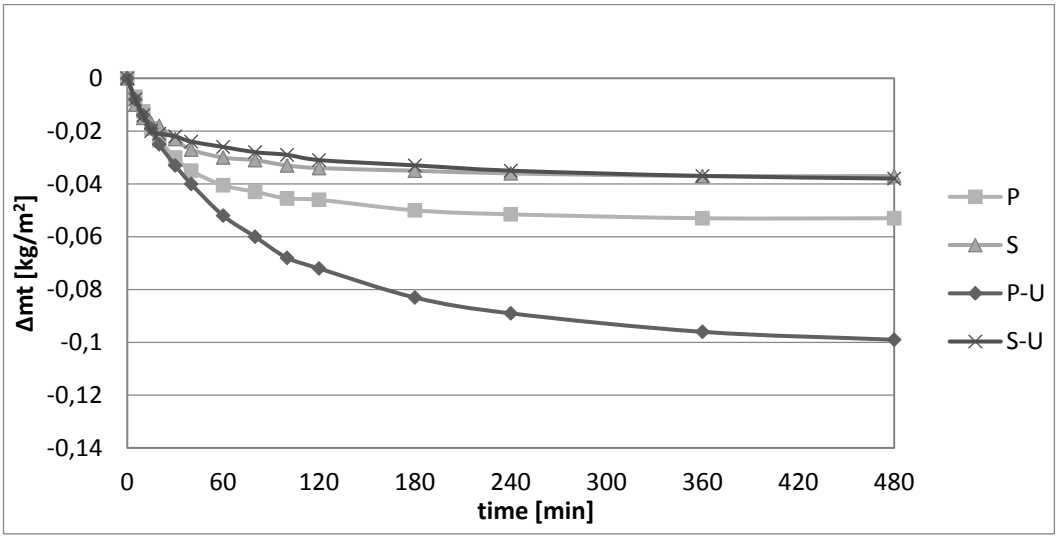

Figure 4.25 - Average mass loss per surface area during 8-hour evaporation (no UV) - P: photoactive, S: standard, U: specimens already used.

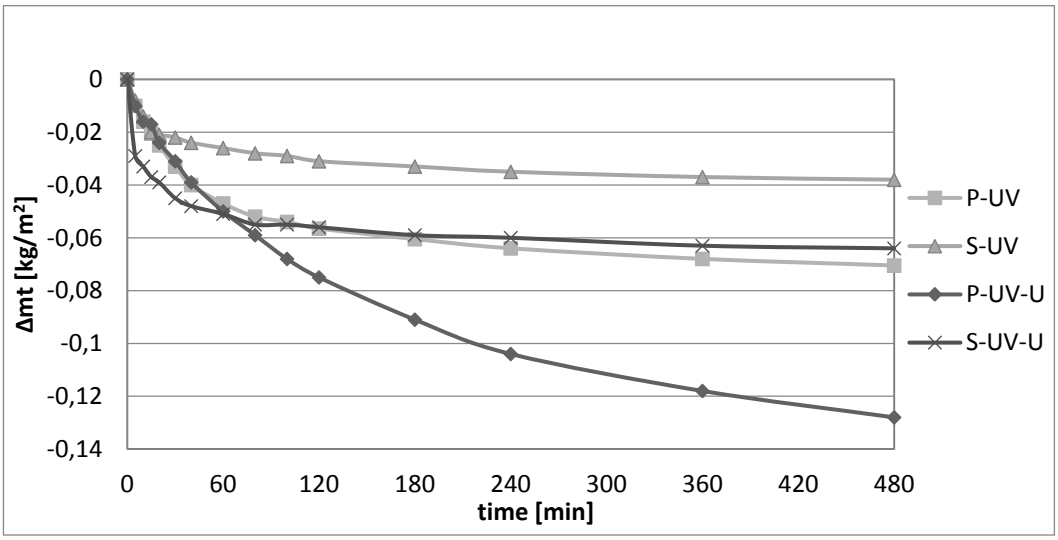

Figure 4.26 - Average mass loss per surface area during 8-hour evaporation (with UV) - P: photoactive, S: standard, UV: irradiation, U: specimens already used.

4.3 Exposure Test

The figures 4.27-30 contain the information of lightness, a*, b* and visible solar reflectance deviations from the initial values, giving an indication of photoactivity of anatase-containing mortars compared to standard ones. Since the parameters used for this experiment include the influence of finishing, orientation and inclination, information on related to these parameters can also be found in the figures. It is possible to see the effect of photoactivity in long term experiment in the form of reduced amount of lightness and visible solar reflectance variations on photoactive specimens compare to standard ones, in both orientations. Moreover, the effect is more conspicuous in samples oriented south due to atmospheric conditions. The influence of inclination on soiling can also be seen in an evident way: the variation in lightness in horizontal and inclined ones in both orientations is higher than vertical and sheltered ones. There is no noticeable change in a* (fig. 4.28), however the increase in deviation b* can be seen in figure 4.29. The variation in b* is much more evident in the case of horizontal and inclined standard samples compare to vertical and sheltered ones.

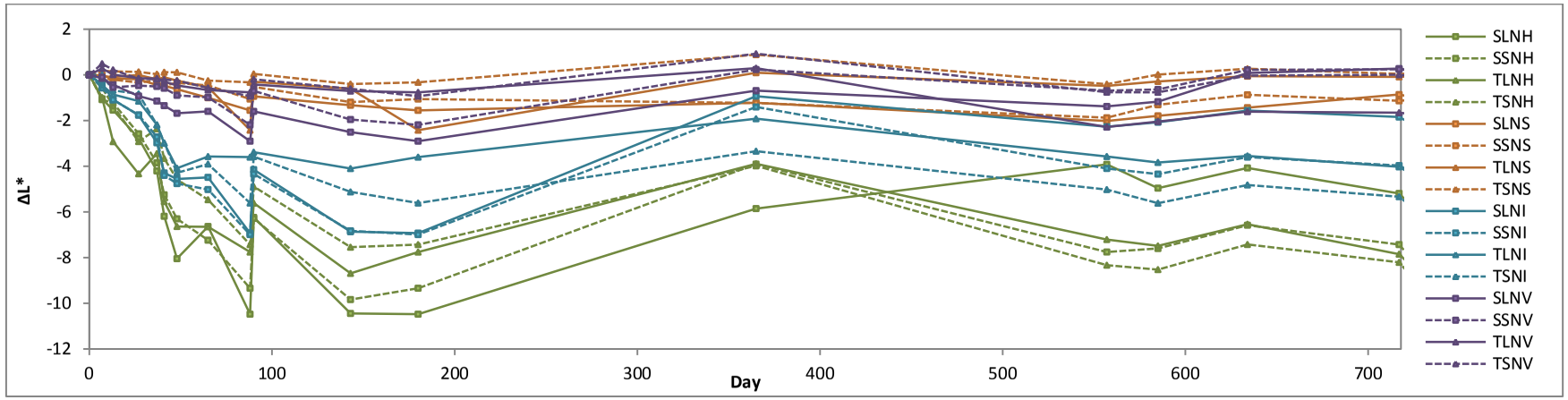

a)

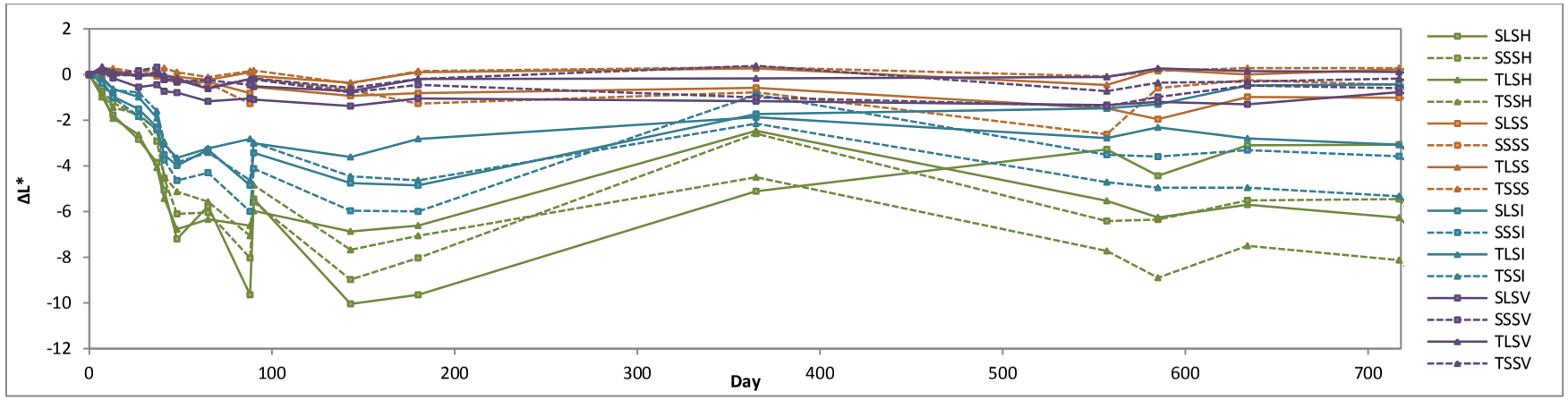

b)

Figure 4.27 - Lightness variation, ΔL* - a) samples facing north, b) samples facing south.

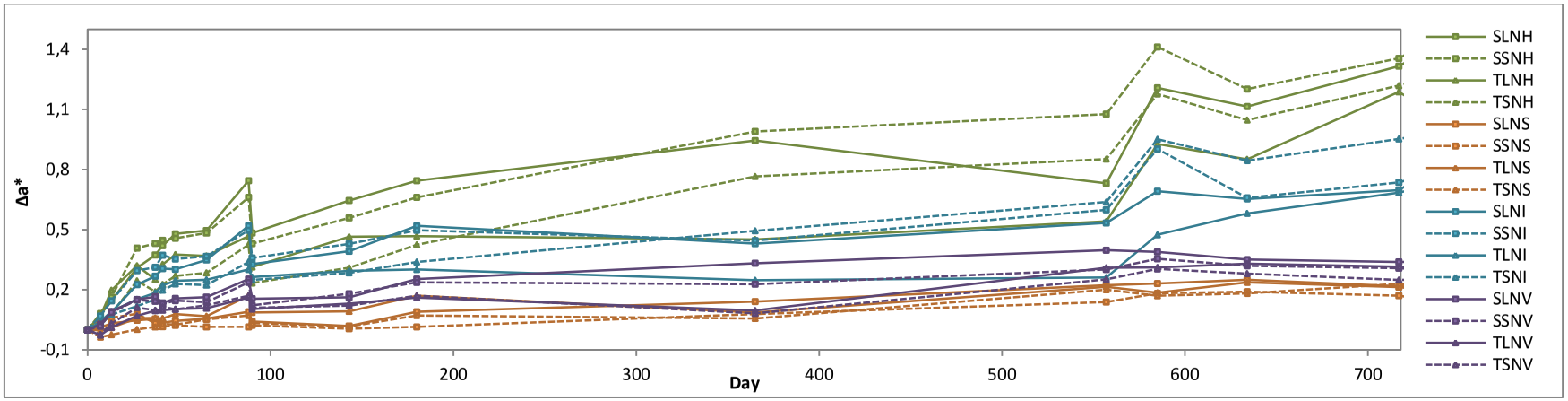

a)

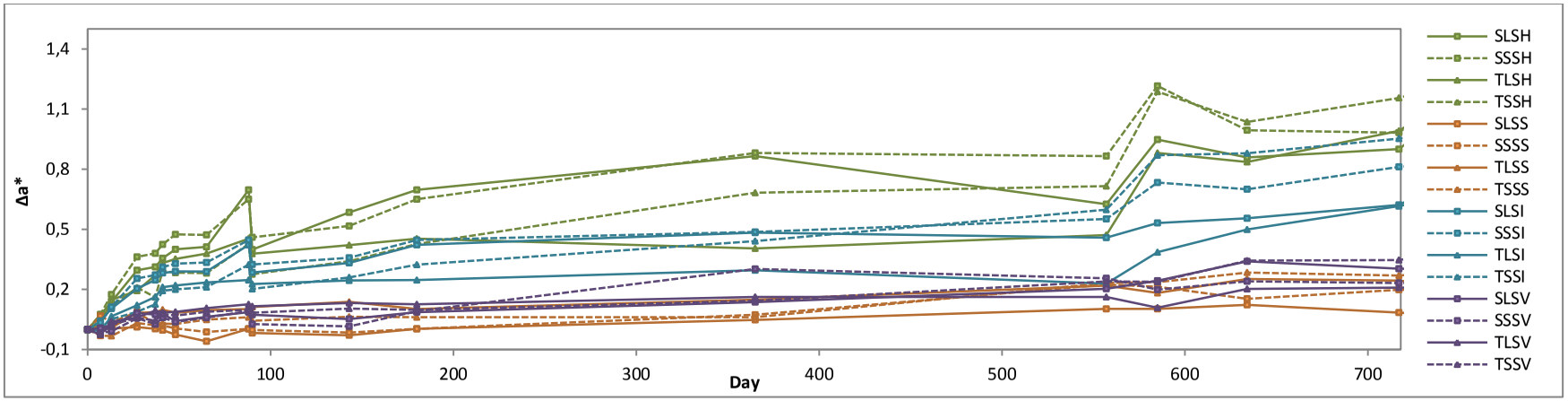

b)

Figure 4.28 - a* variation - a) samples facing north, b) samples facing south.

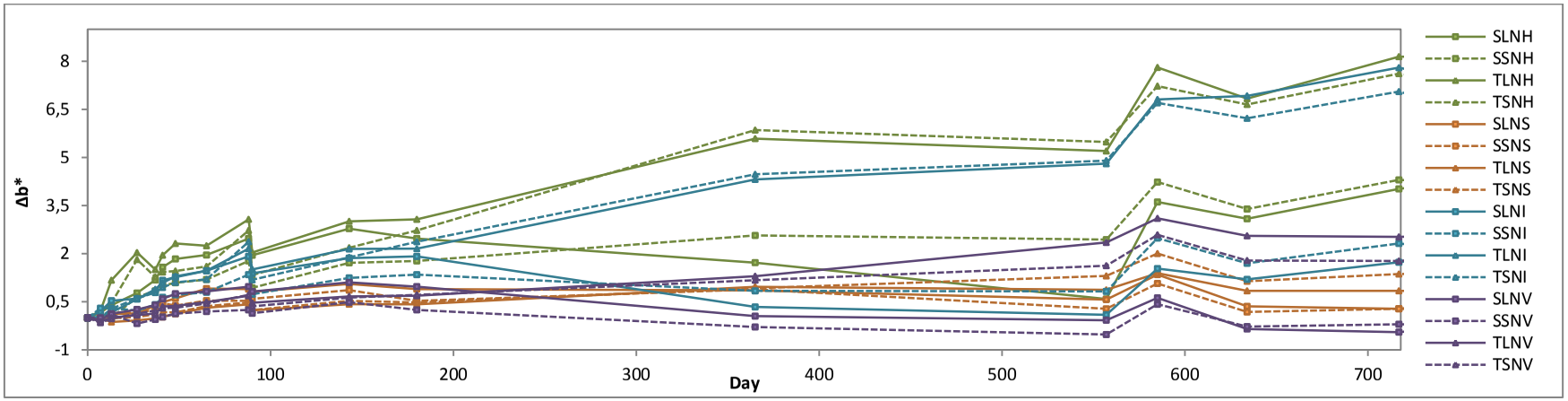

a)

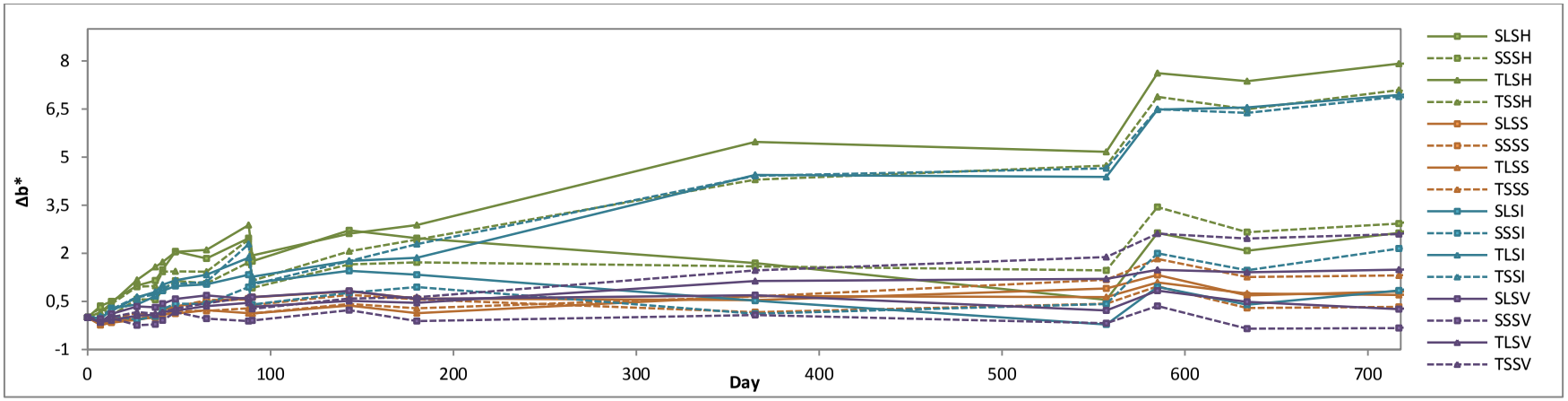

b)

Figure 4.29 - b* variation - a) samples facing north, b) samples facing south.

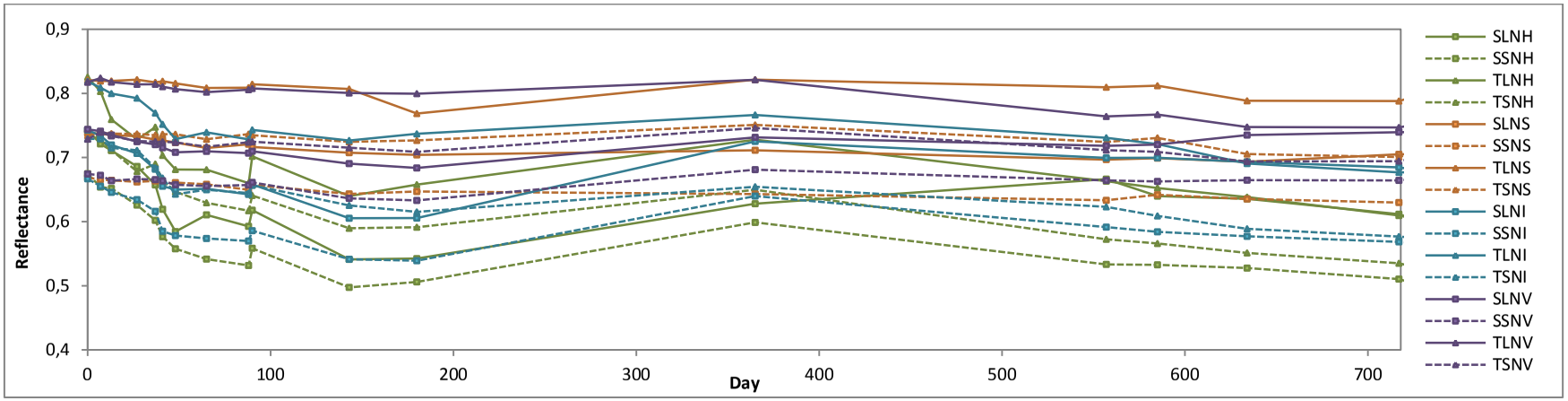

a)

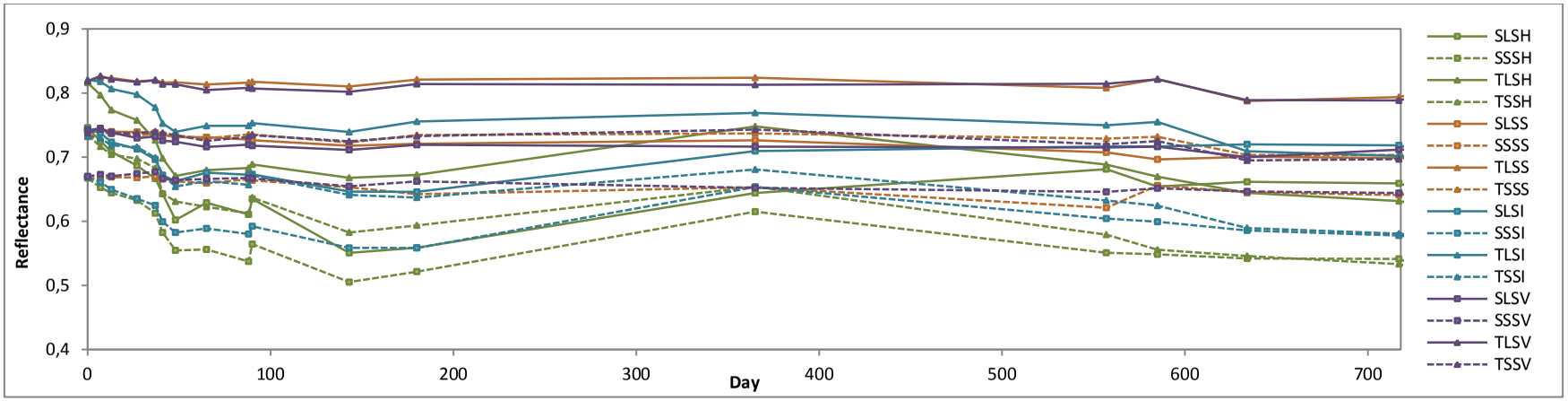

b)

Figure 4.30 - Visible solar reflectance variation - a) samples facing north, b) samples facing south.

To have better comprehension of self-cleaning a closer look was taken to vertical and sheltered samples as the most representative ones for real applications, with south orientation to limit the influence of exposure parameters. This approach gives us the possibility to understand the photoactivity of the anatase-containing samples compared to standard ones more efficiently. Results for these specific conditions are shown in figure 4.31.

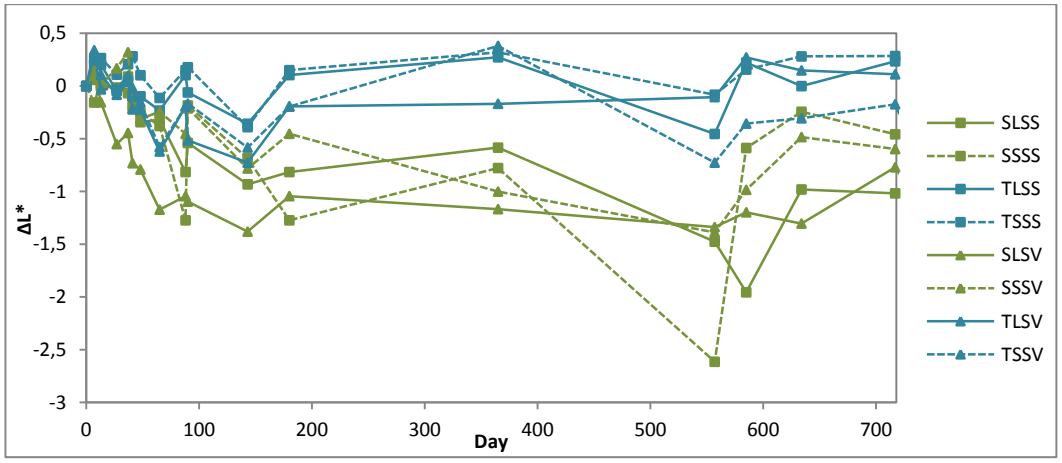

Figure 4.31 - Lightness variation of vertical and sheltered specimens facing south.

A clear effect of photoactivity in long term experiment was observed in the form of reduced amount of lightness variation. The maximum decrease in lightness for photoactive, sheltered, smooth samples is 0.19 points and for the vertical one this amount is only 0.11 points. In the case of standard samples the decrease is respectively 1.26 and 1.46 points. This difference between the two materials, as an indication of reduced soiling for anatase-containing mortars, is a consequence of photoactive mechanism. Furthermore, CIE standards defines that the maximum color variation which can be noticed by human eye for grayscale is 1[49], thus in the case of smooth photoactive samples the decrease in lightness is not noticeable with human eye after a 2 year exposure, which is a desired parameter for white mortars as a coating material.

Another consideration that can be an evidence of photoactivity is the increase in b*. As can be seen in figure 4.32, a shift from blue to yellow color is much more

evident in the case of photoactive samples. An interpretation of this effect was suggested: this shift may be owing to mineralization of organic compounds formerly adsorbed on the surface[49]. This statement explains why the lightness variation is small compare to continued increase in b* coordinate of photoactive samples, since the photoactive material degrades the pollutants continuously, and therefore partially degraded organic contaminants adsorbed on the surface, continue to accumulate and change surface color to more yellow hues.

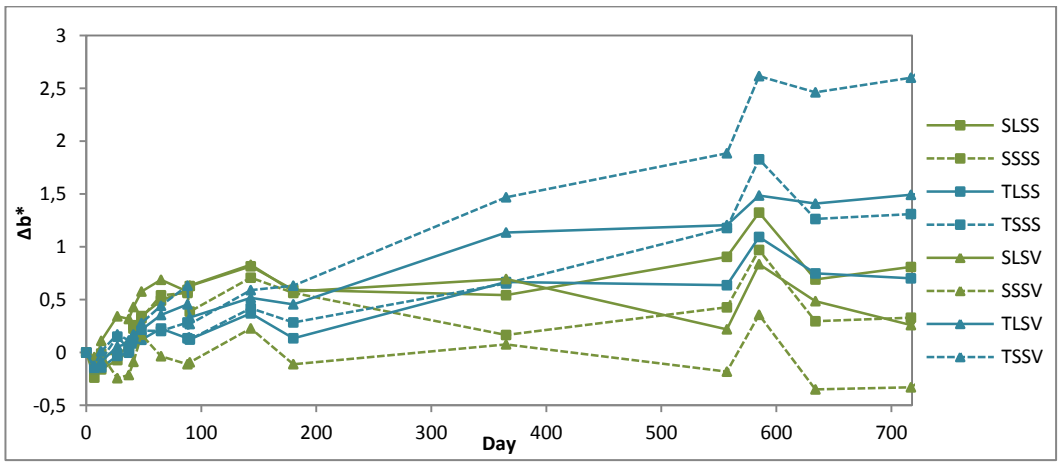

Figure 4.32 - Δb* variation of vertical and sheltered specimens facing south.

To have a better understanding of the corrosive effect of the atmospheric factors, specimens surface were roughened by sandblasting and exposed with identical samples which have smooth finishing. During setting, mortars were affected by bleeding which is the sedimentation of aggregates and simultaneous upward migration of water [90]. In the case of photoactive glass fiber reinforced mortars, the effect induced a quite glossy surface, changing its color and reflectance to higher values. Smooth samples gave a higher reflectance compare to sandblasted ones, regardless of TiO_2 content, on account of light scattering (fig.4.33).

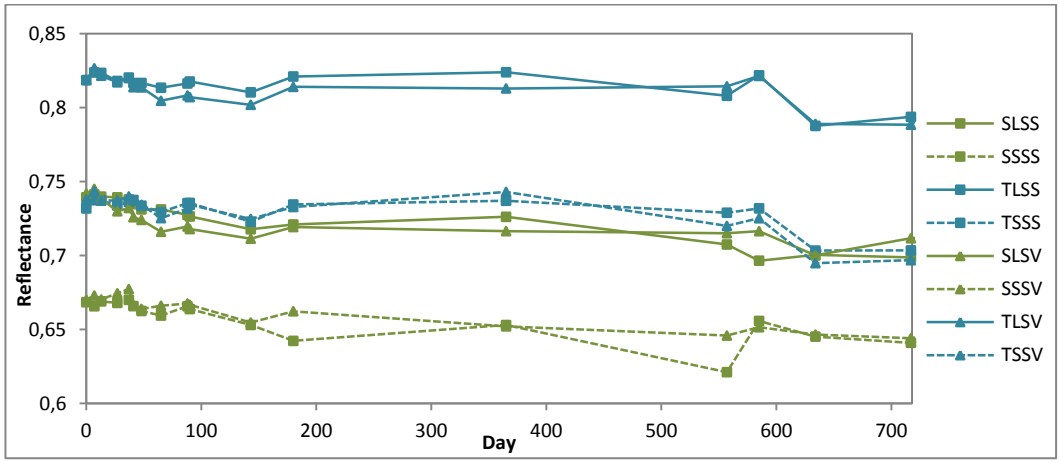

Figure 4.33 - Visible solar reflectance of vertical and sheltered specimens facing south.

Sandblasting decreased the reflectance and lightness slightly more on TiO_2-containing mortars compared to standard ones (reflectance: 10.98% vs. 9.56%; lightness: 4.05% vs. 3.85%), which may due to accumulation of photoactive component in the surface caused by bleeding. Yet, variations of lightness in sandblasted sheltered and vertical ones compared to smooth ones (fig.4.34-35) indicated that the surface of smooth samples could perceive slight corrosive effect due to the erosion of the glossy surface: in fact, in these inclinations the cleaning efficiency of the sandblasted samples is slightly higher than the standard ones.

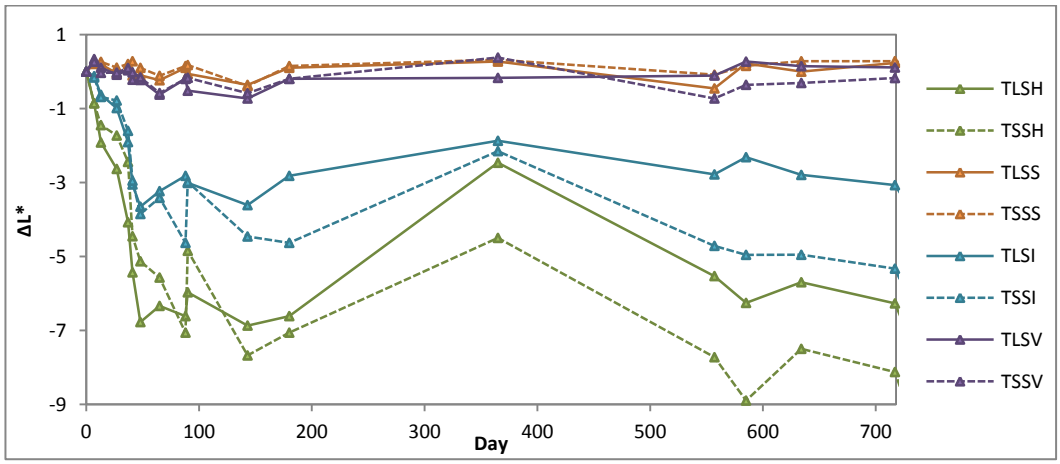

Figure 4.34 - Lightness variation of smooth and sandblasted photoactive samples facing south.

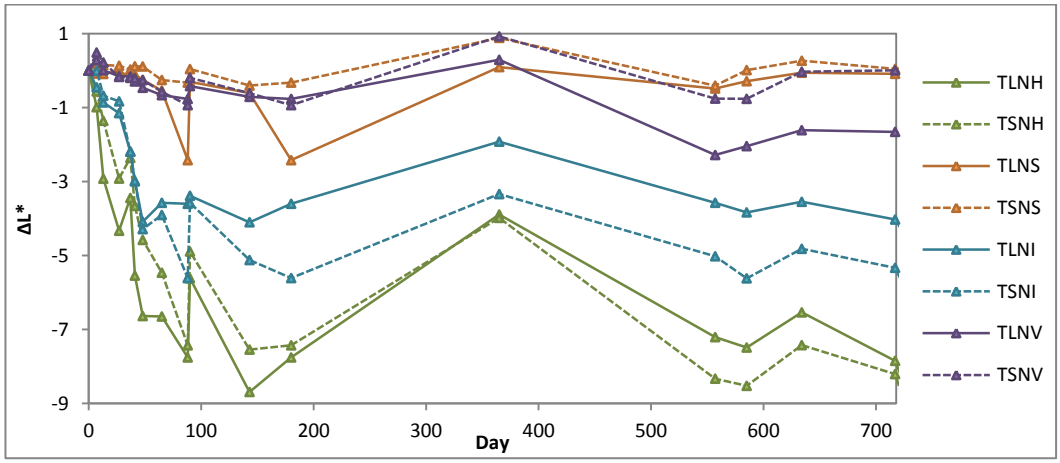

Figure 4.35 - Lightness variation of smooth and sandblasted photoactive samples facing north.

On the other hand, in inclined and horizontal specimens there is a different trend to be discussed, which is overall as a consequence of atmospheric effects.

To evaluate the influence of atmospheric agents as a function of specimens inclination which is important in light color materials[91], standard samples will be considered first (fig.4.36-37).

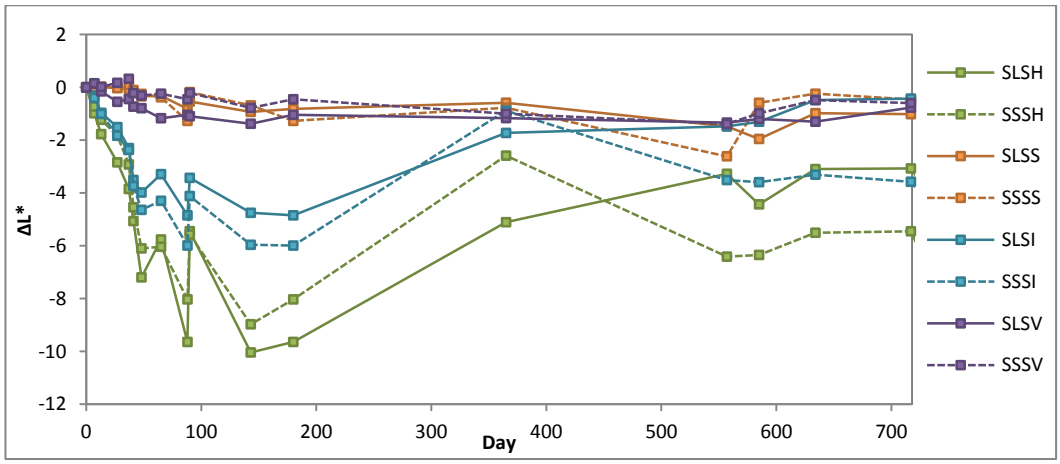

Figure 4.36 - Lightness variation of smooth and sandblasted standard samples facing south.

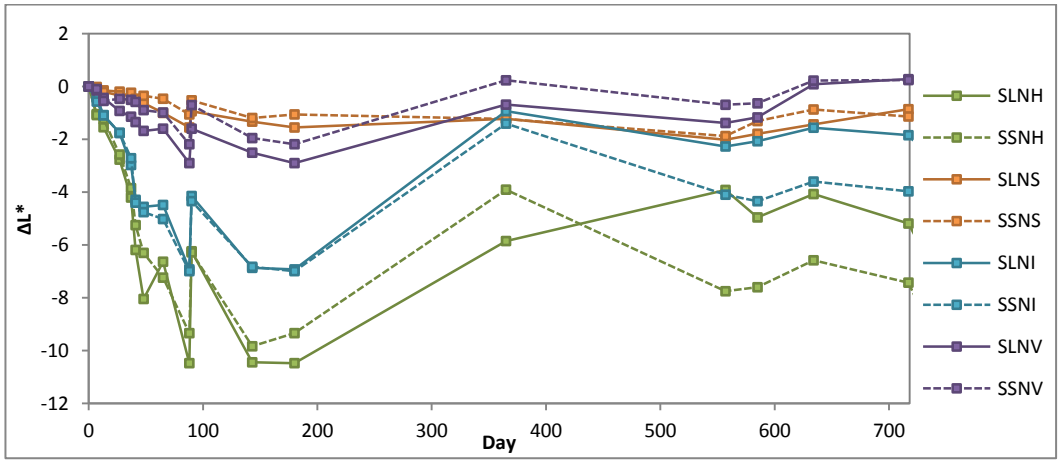

Figure 4.37 - Lightness variation of smooth and sandblasted standard samples facing north

It is known that soil deposits, even at the same location, vary with materials type and slope because these parameters affect how well the material is cleaned by rain[92] and the affinity between surface and soil, specially on account of surface hydrophilicity or oleophilicity. In this long term exposure, it is evident that horizontal specimens oriented in both directions (fig.4.36-37) were affected by climatic soiling at identical extents, since both of them experienced the same atmospheric conditions (and especially received similar radiation amounts), but more severely compared to other inclinations, since it maintains larger quantity of contaminants adhering to the surface. The difference between the lightness values of sandblasted and smooth samples indicate that sandblasted samples lost their lightness more than smooth ones, due to their surface finishing. This effect can be explained by surface roughness of the sandblasted materials, which reduces the cleaning effect of rain; however, in both materials precipitation and/or wind sweeping helps restoring the deviation from the initial lightness. The same trend can be observed on inclined mortars. On the other hand, vertical and sheltered ones experienced a less conspicuous soiling, due to smaller quantity of contaminants and better washing upon rainy events. The evident difference between north and south exposed samples can be due to wind direction, since wind direction during the exposure period was between 90-270^{o} (east-south-west)

97% of the time exposure time, samples with oriented to north should experienced the wind affect more severally.

The prolonged exposure did not allow to understand which contaminant affects more surface soiling among the ones considered (PM10, PM2.5, NO_x) since the trend of lightness and b* variations in time and related to the pollutant amount was similar for all (fig. 4.38-40), and the number of color measurements was not adequate to establish a reliable correlation.

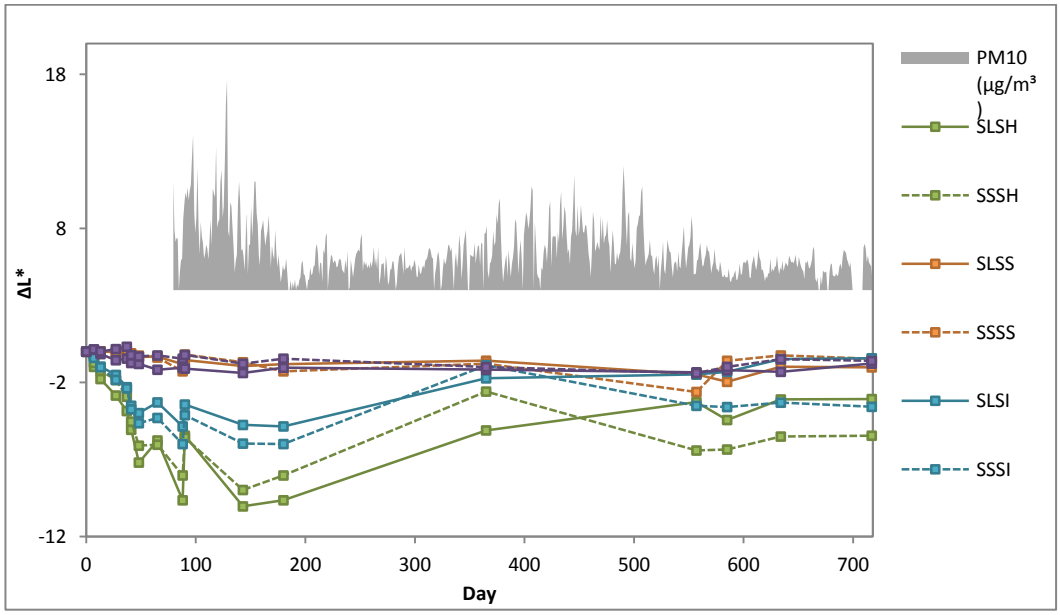

Figure 4.38 - Lightness variation of smooth and sandblasted standard samples facing south and PM10 variation.

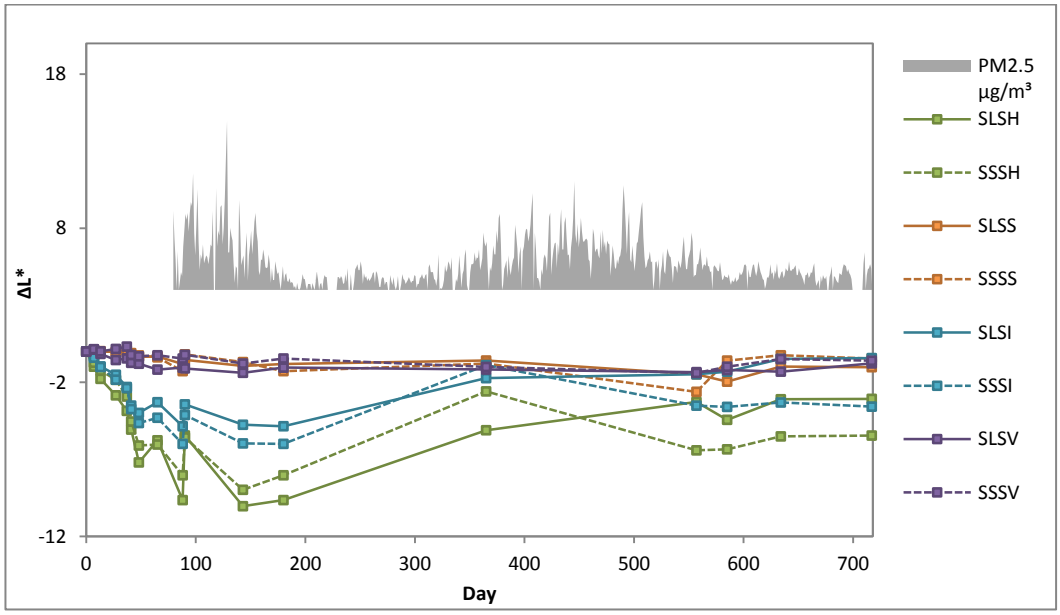

Figure 4.39 - Lightness variation of smooth and sandblasted standard samples facing south and PM2.5 variation.

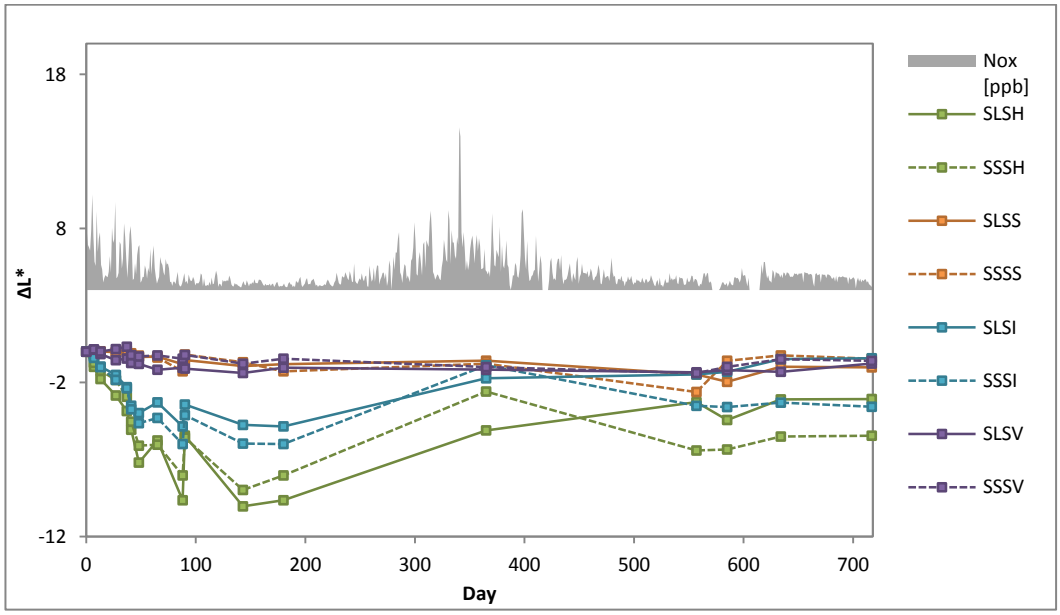

Figure 4.40 - Lightness variation of smooth and sandblasted standard samples facing south and NO_x variation.

On the other hand, a clear influence of rainy events can be seen especially during the last six months (fig. 4.41). Evident examples are between the days 180-365 (fig. 4.41 (b)) and 557-585 (fig. 4.41 (c)) in which the contamination amount slightly increased but the variation in surface lightness decreased: this can be explained by a heavy precipitation before the measurement. However, in the case of particularly high amount of contamination, it is not possible to establish a clear relationship with rainy events and the overall lightness variation; conversely, this is possible in the case of low amounts of contamination, as suggested by evident examples between the days between 65 and 143 (fig. 4.41 (a)).

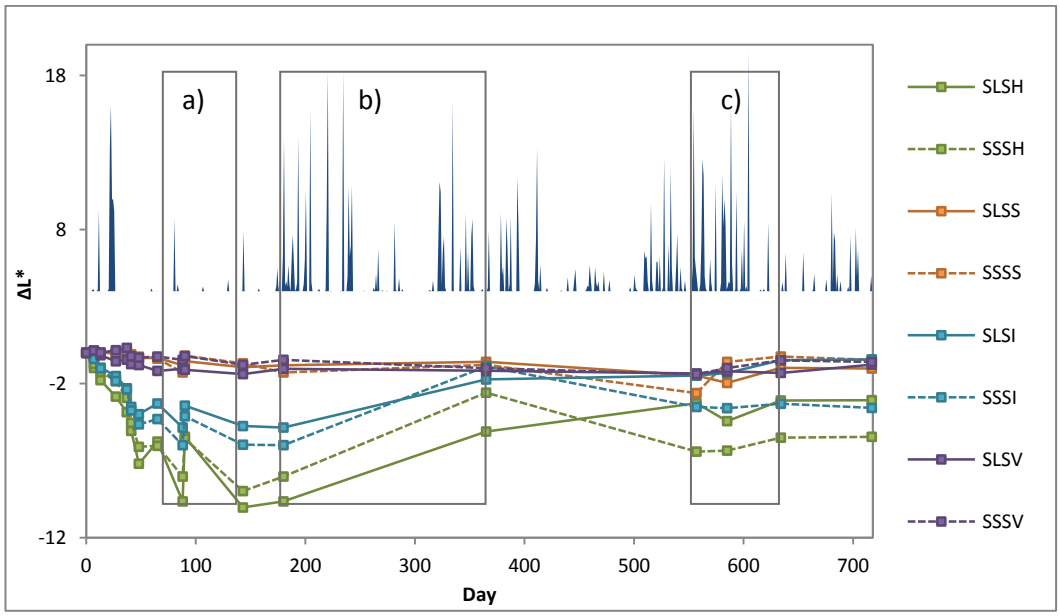

Figure 4.41 - Lightness variation of smooth and sandblasted standard samples facing south and precipitation variation - a) between days 65-143, b) between days 180-365, c) between days 557-585.

The previously reported considerations apply to both photoactive and sandblasted mortars to correlate seasonal atmospheric conditions with self-cleaning effect. The self-cleaning effect was then evaluated by comparing standard and photoactive samples. Horizontal samples can rely on a good light harvesting in the hours of higher irradiation (close to midday), which would make this inclination optional to study photoinduced effects. Yet, these mortars are subject to complex

mechanisms of the effect of rainy events, specially on sandblasted samples account of their surface roughness, therefore the evaluation continued with smooth samples inclined vertical and sheltered (fig. 4.42).

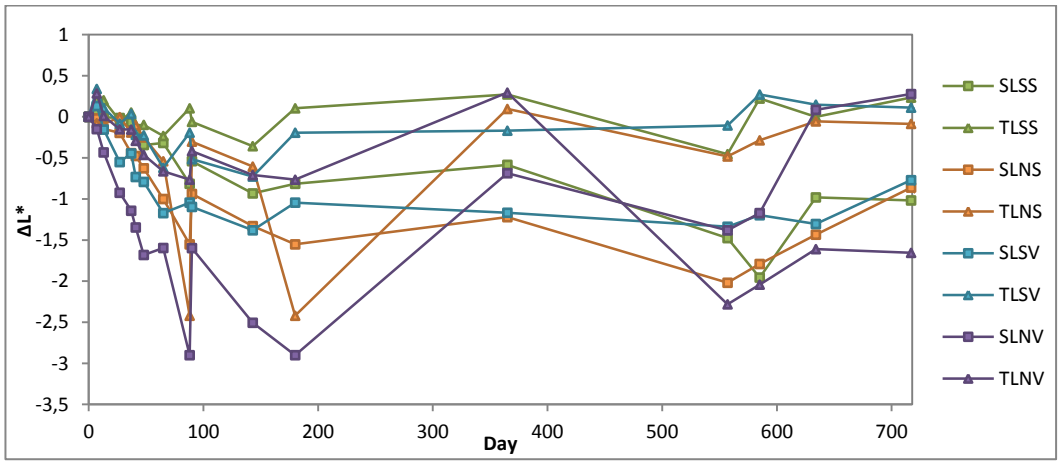

Figure 4.42 - Lightness variation of smooth samples, inclined vertical and sheltered.

In general, TiO_2-containing specimens actually showed an increase in lightness, maintaining the surface cleaner and closer to initial white color. The trend of lightness variations depends mostly on irradiance and rainy events. The variation in irradiance has same trends with temperature (fig. 4.43) on the other hand it is inversely correlated with amount of contaminants (fig. 4.44) and relative humidity (fig. 4.45): while the irradiance increases, the pollutants amount and relative humidity decrease.

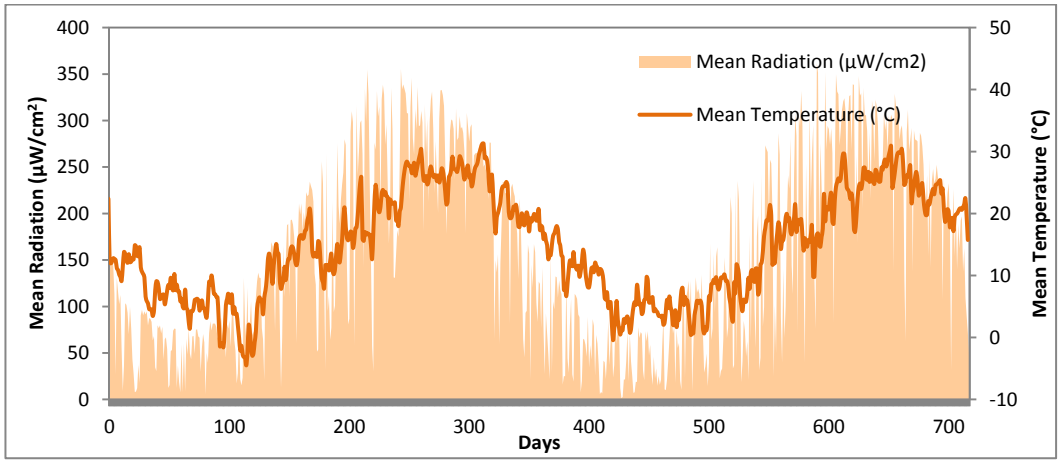

Figure 4.43 - Mean radiation and mean temperature variations.

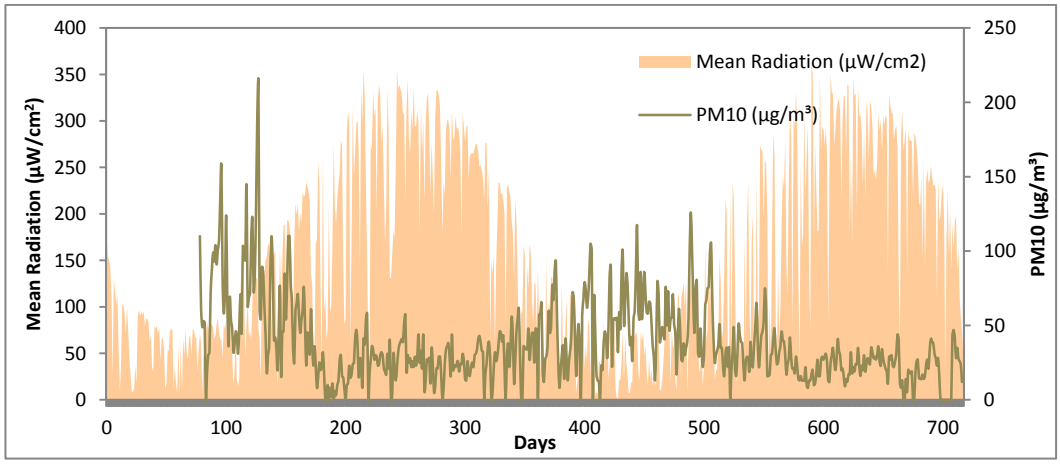

Figure 4.44 - Mean radiation and PM10 variations.

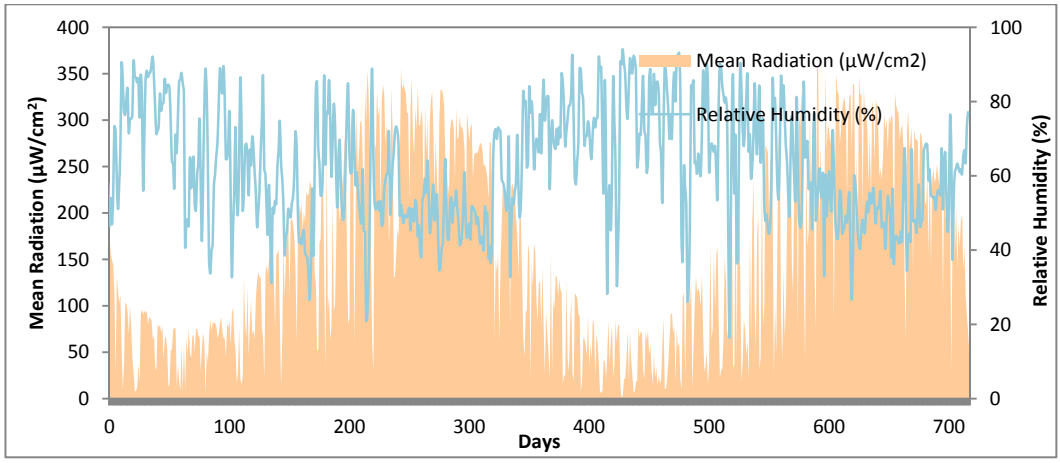

Figure 4.45 - Mean radiation and relative humidity variations.

Keeping these considerations in mind, it can be seen from the figures 4.46-7, specially considering the specimens oriented south, which can exploit sunlight more efficiently, it has been shown that in absence of rain, if the contamination level is high and irradiation is low the surface lightness decreases; on the other hand in presence of high irradiance and low concentration level there is an increase in lightness. In case of rainy events, even the irradiation is low, there is an increase in lightness, and this increase is more noticeable in low contaminant concentrations. Also with in consideration of the cleaning ability of rain itself, it has seen that the increase in lightness is more evident in photoactive samples.

In general, it has been shown that rainy events have more influence on demonstrating the actual onset of self-cleaning compared to irradiance regardless of contaminant concentration, and irradiation itself is only effective in low contaminant levels.

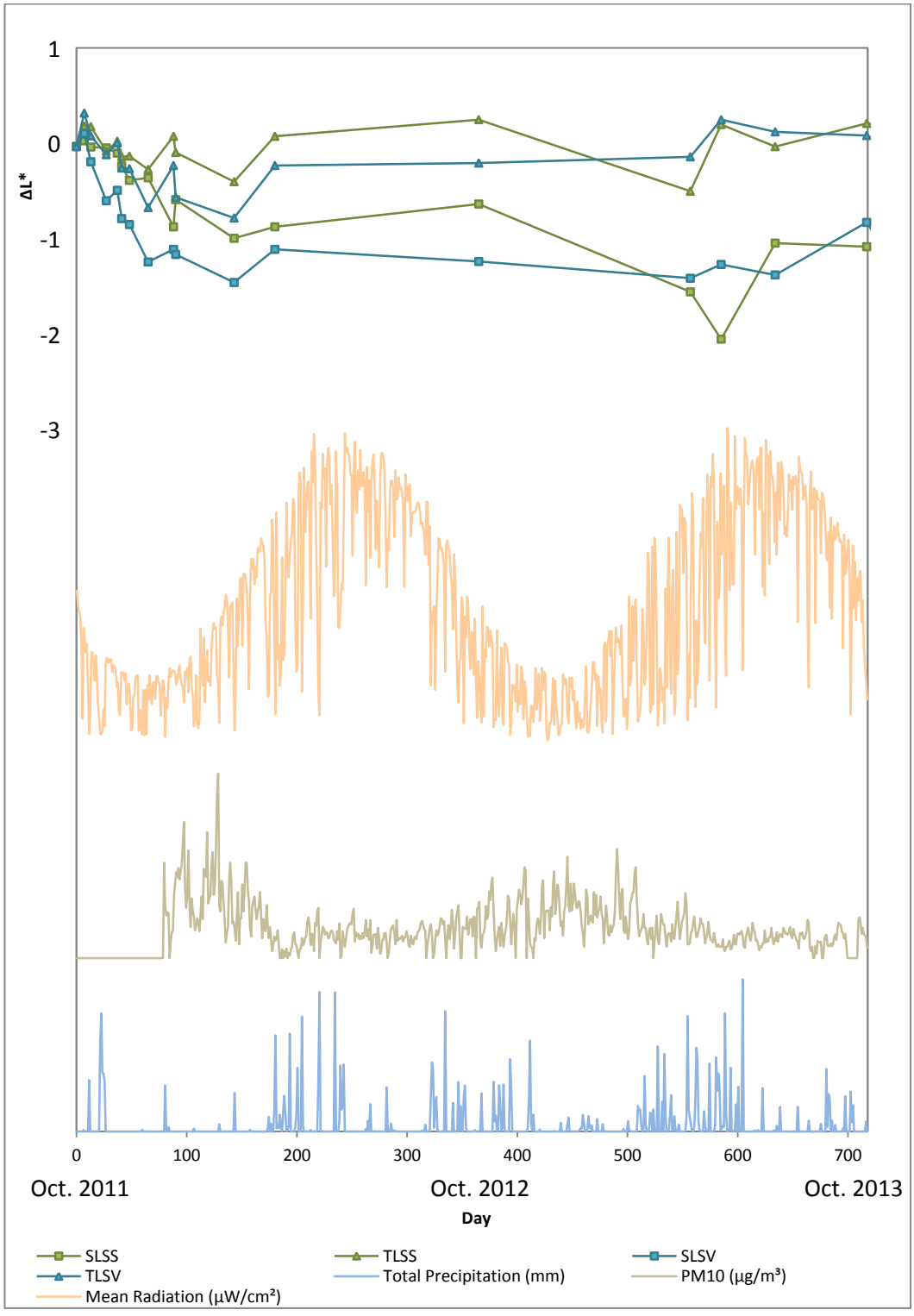

Figure 4.46 - Lightness variation of smooth finishing, vertical and sheltered, oriented to south samples - total precipitation, PM10 and mean radiation variations.

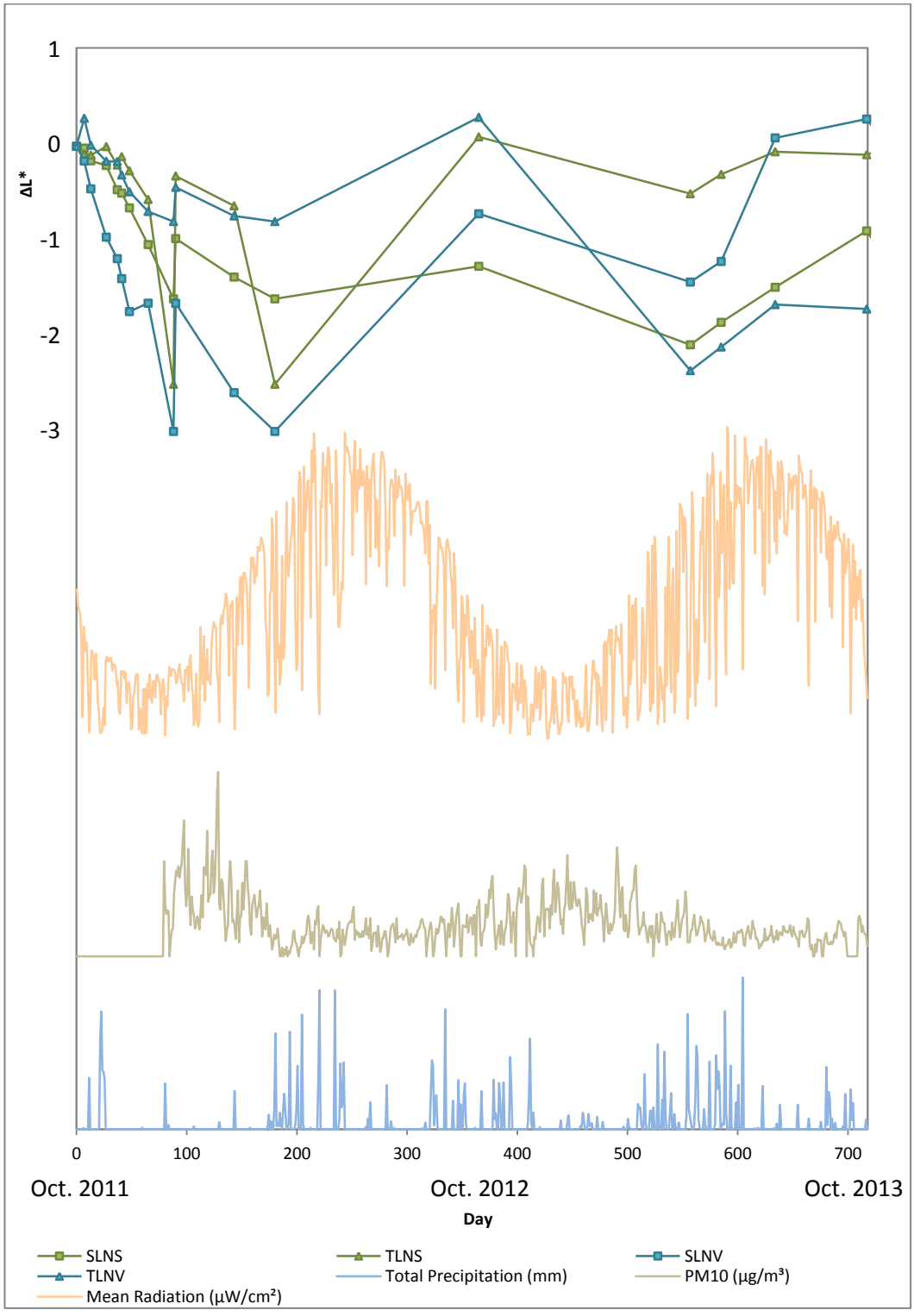

Figure 4.47 - Lightness variation of smooth finishing, vertical and sheltered, oriented to north samples - total precipitation, PM10 and mean radiation variations.

Conclusion

The application of TiO_2 photocatalysis to construction materials provides an efficient strategy to obtain self-cleaning surfaces, simply with the support of sunlight, atmospheric oxygen and water present as humidity and/or rain water.

In this master thesis work, the performances of photoactive materials in degrading organic contaminants and to express photoinduced hydrophilicity are presented, together with an insight into their ability to retard natural ageing, caused by processes such as soiling and erosion in presence of atmospheric effects. This analysis focused in particular on the behaviour of commercial glass fiber reinforced mortars containing anatase-phase TiO_2.

Colorimetric measurements were performed to estimate the degradation extent of an organic dye in contact with the material surface. Such tests showed that for different substrates the methodology chosen to evaluate the photoactivity should depend on the materials properties, in particular substrates color and porosity. For thin porous samples, immersion-drying or ring tests i.e., all tests that involve the maintaining of the sample in contact with the liquid contaminant, gave better evaluations; on the other hand, for white mortars the stain method is more useful. Yet in all cases rhodamine B degradation test confirmed that the photoactivity of mortars can be evidenced, but this method can be used for a precise quantification of degradation efficiency only in particular cases.

Absorption-evaporation tests gave a better understanding of the material hydrophilicity and its variations upon UV irradiation. Under UV irradiation the increase in mass gain during absorption and its decrease during evaporation was more evident in photoactive mortars compared to standard ones; furthermore, the trend of absorption in time also changed in presence of UV. In the case of evaporation under UV illumination, an initial faster evaporation was observed in photoactive mortars related to a more diffuse spreading of water on the whole surface, which in turn was ascribed to an increase in surface wettability. Moreover, photoactive samples that were already used in capillary absorption tests showed higher water absorption compared to pristine ones. This was attributed to the change in surface chemistry of the photoactive mortar, explained by a residual hydroxylation of the photocatalytic surface produced during the capillary absorption test.

The use of TiO_2 containing materials was proved to provide self-cleaning behavior during the long-lasting environmental exposure test. Photoactive materials not only maintain the surface cleaner and closer to its initial white color while the non-photoactive samples present a decrease in lightness, but also they prevent the accumulation of dirth without showin deactivation during the years. Exposure was performed on multiple sample inclinations and orientations to evidence the possible effect of environmental parameters on the self-cleaning behavior. The detailed mechanisms causing the differences between different inclanations due to environmental effects, still need further investigation. No clear correlation of surface soiling with specific pollutants could be observed, as the concentration of these pollutants show the same trend during the long term experiment, which is inversely correlated to irradiance.

The most significant correlations were found with irradiation and rainy events. In fact, it has been shown that in absence of rain, if the contamination level is high and irradiation is low the surface lightness decreases; on the other hand in presence of high irradiance and low pollutants concentration there is an increase in lightness. In case of rainy events, even the irradiation is low, there is an

increase in lightness, and this increase is more noticeable in low contaminant concentrations. In general, it has been shown that rainy events have more influence on demonstrating the actual onset of self-cleaning compared to irradiance regardless of contaminant concentration, and irradiation itself is only effective in low contamination levels.

BIBLIOGRAPHY

1 Fujishima A., Honda K. (1972). 'Electrochemical photolysis of water at a semiconductor electrode', *Nature,* 238, 37–38.

2 Lackhoff M., Prieto X., Nestle N., Dehn F., Niessner R. (2003). 'Photocatalytic activity of semiconductor-modified cement-influence of semiconductor type and cement ageing', *Applied Catalysis B: Environmental*,, 43(3), 205—216.

3 Berto A. M., (2007). 'Ceramic tiles: Above and beyond traditional applications', *J Eur Ceram Soc,* 27 (2-3), 1607—1613.

4 Lee J. H. (2002). 'Environmental construction materials fixing titanium dioxide decomposing nitrogen oxide (NO_x)', *KR Patent,* KR2002058946-A.

5 Diebold, U. (2003). 'The surface science of titanium dioxide', *Surface Science Reports,* 48 (5-8), 53-229.

6 Chen J., Poon C.S. (2009). 'Photocatalytic construction and building materials: From fundamentals to applications', *Build. Environ.,* 44, 1899-1906.

7 Diamanti M. V., Paolini R., Zinzi M., Ormellese M., Fiori M., Pedeferri M.P. (2013). 'Self-cleaning ability and cooling effect of TiO_2-containing mortars', *Nanotech,* 3, 716 – 719.

8 Reyes-Coronado D., Rodríguez-Gattorno G., Espinosa-Pesqueira M. E., Cab C., Coss R.d., Oskam G. (2008). 'Phase-pure TiO_2 nanoparticles: anatase, brookite and rutile', *Nanotechnology,* 19, 145605.

9 Lucasa S.S., Ferreiraa V.M., Barroso de Aguiarb J.L. (2013). 'Incorporation of titanium dioxide nanoparticles in mortar-Influence of microstructure in the hardened state properties and photocatalytic activity', *Cement and Concrete Research*, 43, 112-120.

10 Chen X., Mao S. S., (2007). 'Titanium Dioxide Nanomaterials: Synthesis, Properties, Modifications, and Applications', *Chem. Rev.*, 107, 2891-2959.

11 Austin R., Lim S.-f. (2008). 'The Sackler Colloquium on Promises and Perils in Nanotechnology for Medicine', *PNAS,* 105 (45), 17217-17221.

12 Zhang H., Banfield J. F. (2000). ‘Understanding polymorphic phase transformation behavior during growth of nanocrystalline aggregates: Insights from TiO_2.’, *Journal of Physical Chemistry*, 104B, 3481-3487.

13 Fujishima A., Zhang X.T., Tryk D.A. (2008). ‘TiO_2 photocatalysis and related surface phenomena, *Surface Science Reports*, 63 (12), 515–582.

14 Linsebigler A.L., Lu G.Q., Yates J.T. (1995). ‘Photocatalysis on TiO_2 surfaces - principles, mechanisms, and selected results’, *Chem. Rev.*, 95, 735–758.

15 Diamanti M. V., Pedeferri M.P. (2013). ‘Photocatalytic based materials: Concrete, mortars and plasters using nanoparticles’, *Nanotechnology in Eco-Efficient Construction*, Woodhead Publishing.

16 Fujishima A., Rao T.N., Tryk D.A. (2000). ‘Titanium dioxide photocatalysis’, J *Photoch Photobiol C*, 1, 1–21.

17 Herrmann, J-M. (1999). ‘Heterogeneous photocatalysis: fundamentals and applications to the removal of various types of aqueous pollutants’, *Catalysis Today*, 53 (1), 115-129.

18 Schiavello M. (1988). *Photocatalysis and Environment: Trends and Applications*, Springer, Palermo, Italy.

19 Devahasdin S., Fan C. Jr, Li K., Chen D. H. (2003). ‘TiO_2 photocatalytic oxidation of nitric oxide: transient behavior and reaction kinetics’, *Journal of Photochemistry and Photobiology*, 156, 161–170.

20 Szczepankiewicz S. H., Colussi A. J., Hoffmann M. R. (2000). ‘Infrared spectra of photoinduced species on hydroxylated titania surfaces’, *Journal of Physical Chemistry B.*, 104, 9842-9850.

21 Zhang Z., Wang C. C., Zakaria R., Ying, J. Y. (1998). ‘Role of Particle Size in Nanocrystalline TiO_2-Based Photocatalysts’, *Journal of Physical Chemistry B*, 102, 10871–10878.

22 Wang R., Hashimoto K., Fujishima A., Chikuni M., Kojima E., Kitamura A., Shimohigoshi M., Watanabe T. (1997). ‘Light-induced amphiphilic surfaces’, *Nature*, 388, 431–432.

23 Guan K. (2005). 'Relationship between photocatalytic activity, hydrophilicity and selfcleaning effect of TiO_2/SiO_2 films', *Surface and Coatings Technology*, 191 (2), 155–160.

24 Sakai N., Fujishima A., Watanabe T., Hashimoto K. (2003). 'Quantitative evaluation of the photoinduced hydrophilic conversion properties of TiO_2 thin film surfaces by the reciprocal of contact angle', *Journal of Physical Chemistry B*, 107 (4), 1028–1035.

25 Frank S. N., Bard A.J., (1997). 'Heterogeneous photocatalytic oxidation of cyanide ion in aqueous solutions at titanium dioxide powder', *Journal of American Chemistry Society*, 99 (1), 303–304.

26 Matsunaga T., Tomoda R., Nakajima T., Wake H. (1985). 'Photoelectrochemical sterilization of microbial cells by semiconductor powders' *FEMS Microbiol Lett*, 29, 211—214.

27 Poon C. S., Cheung E. (2007). 'NO removal efficiency of photocatalytic paving blocks prepared with recycled materials', *Constr. Build Mater.*, 21 (8), 1746—1753.

28 Guo S., Wu Z.B., Zhao W. (2009). 'TiO_2-based building materials: Above and beyond traditional applications', *Chinese Science Bulletin*, 54 (7), 1137-1142.

29 Chen J., Kou S-C., Poon C-S. (2012). 'Hydration and properties of nano-TiO_2 blended cement composites', *Cement & Concrete Composites*, 34, 642–649.

30 Fujishima A., Zhang X. T. (2006). 'Titanium dioxide photocatalysis: present situation and future approaches' *CR Chim*, 9, 750–760.

31 Fujishima A., Zhang X. T, Tryk D.A. (2007). 'Heterogeneous photocatalysis: from water photolysis to applications in environmental cleanup' *Int J Hydrogen Energy*, 32, 2664–2672.

32 Toma F.L., Bertrand G., Klein D., Coddet C. (2004). 'Photocatalytic removal of nitrogen oxides via titanium dioxide', *Environ Chem Lett*, 2, 117–121.

33 Jo W.K., Park J.H., Chun H.D. (2002). 'Photocatalytic destruction of VOCs for in-vehicle air cleaning', *J Photochem Photobiol A*, 148, 109–119.

34 Harrison R.M. (2001). *Pollution: causes, effects and control*, The Royal Society of Chemistry, Cambridge.

35 Elsom D. M. (1992). *Atmospheric Pollution: a global problem*, 2 ed., Oxford Blackwell, New York.

36 Folli A., Pade C., Hansen T. B., De Marco T., Macphee D. E. (2012). 'TiO$_2$ photocatalysis in cementitious systems: Insights into self-cleaning and depollution chemistry', *Cement and Concrete Research*, 42, 539-548.

37 Dalton J.S., Janes P.A., Jones N.G., Nicholson J.A., Hallam K.R., Allen G.C.(2002). 'Photocatalytic oxidation of NOx gases using TiO$_2$: a surface spectroscopic approach', *Environmental Pollution.*, 120, 415–422.

38 Lim T.H., Jeong S.M., Kim S.D., Gyenis J. (2000). 'Photocatalytic decomposition of NO by TiO$_2$ particles', *Journal of Photochemistry and Photobiology*, 134 (3), 209–217.

39 Serpone N., Pelizzetti E. (1989). *Photocatalysis: fundamentals and applications*, Wiley.

40 Zinzi M., Carnielo E., Agnoli S. (2012). 'Characterization and assessment of cool coloured solar protection devices for Mediterranean residential buildings application', *Energy & Buildings.*, 50, 111-119.

41 Bekbolet M. (1997). 'Photocatalytic bactericidal activity of TiO$_2$ in aqueous suspensions of E. coli.', *Water Science and Technology*, 35 (11–12), 95–100.

42 Polo A., Diamanti M.V., Bjarnsholt T., Hoiby N., Villa F., Pedeferri M.P. et al. (2007). 'Effects of photoactivated titanium dioxide nanopowders and coating on planktonic and biofilm growth of Pseudomonas aeruginosa', *Photochem Photobiol,* 87, 1387–1394.

43 Ame´zaga-Marid P., Neva´ rez-Moorillo´n G.V., Orrantia-Borunda E., Miki-Yoshida M. (2002). 'Photoinduced bactericidal activity against Pseudomonas aeruginosa by TiO$_2$ based thin films', *FEMS Microbiology Letters*, 211 (2), 183–188.

44 Fujishima A., Hashimoto K., Watanabe T. (1999). *TiO$_2$ Photocatalysis: Fundamentals and Applications*, BKC, Tokyo.

45 Hashimoto K., Irie H., Fujishima A. (2005). 'TiO$_2$ photocatalysis: A historical overview and future prospects', *Jpn J Appl Phys*, 44 (12), 8269—8285.

46 Lackhoff M., Prieto X., Nestle N., Dehn F., Niessner R. (2003). 'Photocatalytic activity of semiconductor-modified cement — influence of semiconductor type and cement ageing' *Appl. Catal. B,* 43, 205–216.

47 Hunter, R. J.(2001). *Foundations of colloid science*. 2nd ed.; Oxford University Press: Oxford, UK ; New York.

48 Laufs S., Burgeth G., Duttlinger W., Kurtenbach R., Maban M., Thomas C., Wiesen P., Kleffmann J. (2010). 'Conversion of nitrogen oxides on commercial photocatalytic dispersion paints', *Atmos Environ*, 44, 2341-2349.

49 Diamanti M.V., Del Curto B., Ormellese M., Pedeferri M.P. (2013). 'Photocatalytic and self-cleaning activity of colored mortars containing TiO_2', *Construction and Building Materials*, 46, 167-174.

50 Diamanti M.V., Ormellese M., Pedeferri M.P. (2008). 'Characterization of photocatalytic and superhydrophilic properties of mortars containing titanium dioxide', *Cement and Concrete Research*, 38, 1349–1353.

51 Diamanti M.V., Lollini F., Pedeferri M.P., Bertolini L., (2008). 'Mutual interactions between carbonation and titanium dioxide photoactivity in concrete' *Building and Environment*, 62, 174-181.

52 Nazari A., Riahi S. (2010). 'The effects of TiO_2 nanoparticles on properties of binary blended concrete' , *Journal of Composite Materials*, 45 (11), 1181-1188.

53 Irie H., Sunada K., Hashimoto K. (2004). 'Recent developments in TiO_2 photocatalysis: novel applications to interior ecology materials and energy saving systems', *Electrochemistry*, 72, 807-812.

54 Sanchez F., Sobolev K. (2010). 'Nanotechnology in concrete – A review', *Construction and Building Materials, 24*, 2060-2071.

55 Mills A., Le Hunte S. (1997). 'An overview on semiconductor photocatalysis', *J. Photochem. Photobiol.*, A 108, 1-35.

56 Bertolini L. (2008). 'Steel corrosion and service life of reinforced concrete structures', *Struct Infrastruct Eng*, 4,123-137.

57 Karatasios I., Katsiotisa M. S., Likodimosb V., Kontos A.I., et al. (2010). 'Photo-induced carbonation of lime-TiO_2 mortars', *Applied Catalysis B: Environmental,* 95 (1-2), 78-86.

58 Berdahl P., Akbari H., Levinson R., Miller W. A. (2008). 'Weathering of roofing materials – An overview', *Construction and Building Materials,* 22, 423–433.

59 Hüsken G., Hunger M., Brouwers H. J. H. (2007). 'Comparative study on cementitious products containing titanium dioxide as photo-catalyst', *International RILEM Symposium on Photocatalysis, Environment and Construction Materials - TDP 2007*, RILEM Publications, 147–154.

60 Markham M. M., Laidler K. J. (1953). 'A Kinetic Study of Photo-oxidations on the Surface of Zinc Oxide in Aqueous Suspensions', *Journal of Physical Chemistry,* 57, 363-369.

61 Schwarz P.F., Turro N.J., Bossmann S.H., Braun A.M., Wahab A.A.A., Dürr H. (1997). 'A new method to determine the generation of hydroxyl radicals in illuminated TiO_2 suspensions', *Journal of Physical Chemistry B,* 101 (36), 7127–7134.

62 Shapovalov V., Stefanovich E.V., Truong T.N. (2002). 'Nature of the excited states of the rutile TiO_2(1 1 0) surface with adsorbed water', *Surfice Science Lett.,* 498 (1–2), L103-L108.

63 Chen J., Poon C.S.(2009). 'Photocatalytic cementitious materials: Influence of the microstructure of cement paste on photocatalytic pollution degradation', *Environ. Sci. Technol*., 43 (23), 8948–8952.

64 Rachel A., Subrahmanyam M., Boule P. (2002). 'Comparision of photocatalytic efficiencies of TiO_2 in suspended and immobilised form for the photocatalytic degradation of nitrobenzenesulfonic acids', *Applied Catalysis B: Environemntal*, 37 (4), 301–308.

65 Sugrañez R., Álvarez J.I., Cruz-Yusta M., Mármol I., Morales J., Vila J., Sánchez L. (2013). 'Enhanced photocatalytic degradation of NOx gases by regulating the microstructure of mortar cement modified with titanium dioxide', *Building and Environment*, 69, 55-63.

66 Hoffmann M. R., Martin S. T., Choi W., Bahnemann D.W. (1995). 'Environmental applications of semiconductor photocatalysis', *Chem. Rev.*, 95, 69–96.

66 Yu J. C-M. (2003). '*Deactivation and Regeneration of Environmentally Exposed Titanium Dioxide (TiO_2) Based Products*' Environmental Protection Department, HKSAR, Departmental Order Ref. No.: E183413.

67 Iavicoli I., Leso V., Fontana L., Bergamaschi A. (2011). 'Toxicological effects of titanium dioxide nanoparticles: a review of in vitro mammalian studies', *Eur Rev Med Pharmacol Sci*. 15 (5), 481-508.

68 Cassar L. (2004). 'Photocatalysis of cementitious materials: clean buildings and clean air.', *MRS Bull*, 29 (5), 328–331.

69 UNI 11259 - February 2008, Determination of the photocatalytic activity of hydraulic binders: Rodammina test method., MillanUNI.

70 Camarillo R., Rincón J. (2011). 'Photocatalytic Discoloration of Dyes: Relation between Effect of Operating Parameters and Dye', *Chemical Engineering & Technology*, 34 (10), 1675-1684.

71 Zhang K., Oh W-C. (2009). 'The Photocatalytic Decomposition of Different Organic Dyes under UV Irradiation with and without H_2O_2 on Fe-ACF/TiO_2 Photocatalysts', *Journal of the Korean Ceramic Society,* 46 (6), 561-567.

72 Wu T., Liu G., Zhao J., Hidaka H., Serpone N. (1998). 'Photoassisted Degradation of Dye Pollutants. V. Self-Photosensitized Oxidative Transformation of Rhodamine B under Visible Light Irradiation in Aqueous TiO_2 Dispersions.', J., *Phys. Chem.*, B 102, 5845–5851.

73 Folli A., Jakobsen U.H., Guerrini G.L., Macphee D.E. (2009). 'Rhodamine B Discolouration on TiO_2 in the Cement Environment: A Look at Fundamental Aspects of the Self-cleaning Effect in Concretes', *J. Adv. Oxid. Technol.*, 12, 126–133.

74 ISO 10678:2010 – Determination of photocatalytic activity of surfaces in an aqueous medium by degradation of methylene blue.

75 Ruot B., Plassais A., Olive F., Guillot L., Bonafous L. (2009). 'TiO_2-containing cement pastes and mortars: Measurements of the photocatalytic efficiency using a rhodamine B-based colourimetric test', *Solar Energy*, 83, 1794–1801.

76 Martys N. S., Ferraris C. F. (1997). ‘Capillary transport in mortars and concrete’, *Cem Concr Res*, 27 (5), 747–760.

77 ISO 15148:2002 - Hygrothermal performance of building materials and products — Determination of water absorption coefficient by partial immersion.

78 Hanzic L., Kosec L., Anzel I. (2010). ‘Capillary absorption in concrete and the Lucas–Washburn equation’, *Cement & Concrete Composites*, 32, 84–91.

79 Shah R. A., Pitroda J. (2013). ‘Effect of Water Absorption and Sorptivity on Durability of Pozzocrete Mortar’, *IJESE*, 1 (5), 73-77.

80 Assouline S., Or D., (2008).‘Air entry–based characteristic length for estimation of permeability of variably compacted earth materials’, *Water Resources Research*, 44, 11.

81 Buenfeld N.R, Okundi E., (1998). ‘Effect of cement content on transport in concrete’, *Magazine of Concrete Research*, 50, 339-351.

82 Zhang S. P., Zong L. (2014). ‘Evaluation of Relationship between Water Absorption and Durability of Concrete Materials’, *Advances in Materials Science and Engineering*, 2014.

83 Minabe T., Tryk D. A., Sawunyama P., Kikuchi Y., Hashimoto K., Fujishima A. (2000). ‘TiO_2-mediated photodegradation of liquid and solid organic compounds’, *Journal of Photoc. and Photob. A: Chem.*, 137 (1), 53–62.

84 Herrmann J.M., Peruchon L., Puzenat E., Guillard C. (2007). ‘Photocatalysis: from fundamentals to self-cleaning glass application’, *Proceedings international RILEM symposium on photocatalysis, environment and construction materials-TDP*, RILEM Publications SARL, 41–48.

85 Cheng M-D., Miller W., New J., Berdahl P. (2012). ‘Understanding the long-term effects of environmental exposure on roof reflectance in California’ *Construction and Building Materials*, 26, 516-526.

86 Obee T.N., Hay S.O. (1997). ‘Effects of moisture and temperature on the photooxidation of ethylene on titania’, *Environ. Sci. Technol.*, 31 (7), 2034-2038

87 Costacurta S, Dal Maso G, Gallo R, Guglielmi M, Brusatin G, Falcaro P. (2010). 'Influence of temperature on the photocatalytic activity of sol-gel TiO_2 films.', *ACS Appl Mater Interfaces*, 2 (5), 1294-1298.

88 Beeldens A., (2007). 'Air purification by roadmaterials: results of the test project in Antwerp' *Proceedings international RILEM symposium on photocatalysis, environment and construction materials TDP*, RILEM Publications SARL, 187–194.

89 Hunger M., Hüsken G., Brouwers H.J.H. (2010). 'Photocatalytic degradation of air pollutants — From modeling to large scale application', *Cement and Concrete Research*, 40, 313–320.

90 Kosmatka S.H. (2006). 'Bleed Water', *Significance of Tests andProperties of Concreteand Concrete-Making Materials,* Lamond J. F., Pielert J. H., ASTM International, USA. 99-122.

91 Cheng M-D., Pfiffner S. M.,Miller W. A., Berdahl P. (2011). 'Chemical and microbial effects of atmospheric particles on the performance of steep-slope roofing materials', *Building and Environment*, 46, 999-1010.

92 Berdahl P., Akbari H., Rose L. S. (2002). 'Aging of reflective roofs: soot deposition', Applies Optics, 41 (12), 2355-2360.